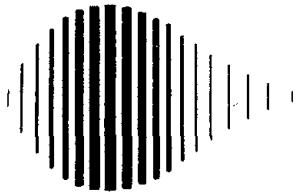

NATIONAL CENTER FOR EARTHQUAKE ENGINEERING RESEARCH

State University of New York at Buffalo

VISCOUS DAMPERS: TESTING, MODELING AND APPLICATION IN VIBRATION AND SEISMIC ISOLATION

by

N. Makris and M. C. Constantinou

Department of Civil Engineering
State University of New York at Buffalo
Buffalo, New York 14260

Technical Report NCEER-90-0028

December 20, 1990

This research was conducted at the State University of New York at Buffalo and was partially supported by the National Science Foundation under Grant No. ECE 86-07591.

NOTICE

This report was prepared by the State University of New York at Buffalo as a result of research sponsored by the National Center for Earthquake Engineering Research (NCEER). Neither NCEER, associates of NCEER, its sponsors, State University of New York at Buffalo, nor any person acting on their behalf:

a. makes any warranty, express or implied, with respect to the use of any information, apparatus, method, or process disclosed in this report or that such use may not infringe upon privately owned rights; or

b. assumes any liabilities of whatsoever kind with respect to the use of, or the damage resulting from the use of, any information, apparatus, method or process disclosed in this report.

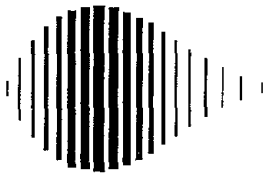

VISCOUS DAMPERS: TESTING, MODELING AND APPLICATION IN VIBRATION AND SEISMIC ISOLATION

by

N. Makris[1] and M.C. Constantinou[2]

December 20, 1990

Technical Report NCEER-90-0028

NCEER Project Number 89-2101

NSF Master Contract Number ECE 86-07591

and

NSF Grant Number BSC-8857080

1 Research Assistant, Department of Civil Engineering, State University of New York at Buffalo

2 Associate Professor, Department of Civil Engineering, State University of New York at Buffalo

NATIONAL CENTER FOR EARTHQUAKE ENGINEERING RESEARCH
State University of New York at Buffalo
Red Jacket Quadrangle, Buffalo, NY 14261

PREFACE

The National Center for Earthquake Engineering Research (NCEER) is devoted to the expansion and dissemination of knowledge about earthquakes, the improvement of earthquake-resistant design, and the implementation of seismic hazard mitigation procedures to minimize loss of lives and property. The emphasis is on structures and lifelines that are found in zones of moderate to high seismicity throughout the United States.

NCEER's research is being carried out in an integrated and coordinated manner following a structured program. The current research program comprises four main areas:

- Existing and New Structures
- Secondary and Protective Systems
- Lifeline Systems
- Disaster Research and Planning

This technical report pertains to Program 2, Secondary and Protective Systems, and more specifically, to a passive protective systems. Protective Systems are devices or systems which, when incorporated into a structure, help to improve the structure's ability to withstand seismic or other environmental loads. These systems can be passive, such as base isolators or viscoelastic dampers; or active, such as active tendons or active mass dampers; or combined passive-active systems.

Passive protective systems constitute one of the important areas of research. Current research activities, as shown schematically in the figure below, include the following:

1. Compilation and evaluation of available data.
2. Development of comprehensive analytical models.
3. Development of performance criteria and standardized testing procedures.
4. Development of simplified, code-type methods for analysis and design.

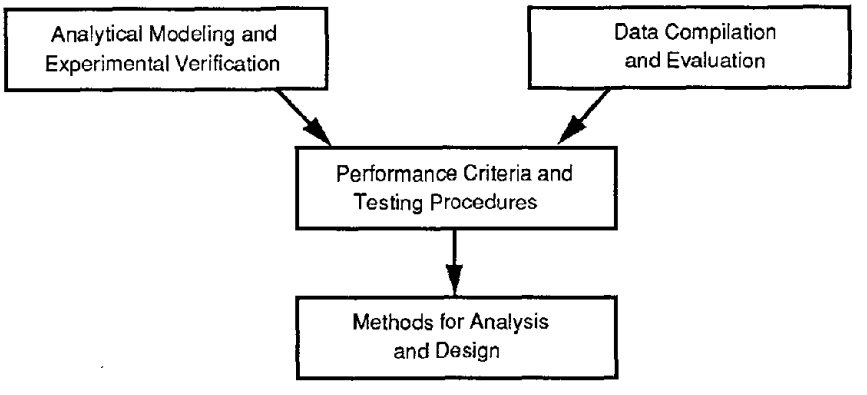

Considered in this report is the modeling of viscous dampers for vibration and seismic isolation of building structures. A fractional derivative Maxwell model is proposed and validated by experimentally observed dynamic characteristics. It is also used in the analysis of a base-isolated model structure which has been tested on a shaking table.

ABSTRACT

A fractional derivative Maxwell model is proposed for viscous dampers which are used for vibration isolation of piping systems, forging hammers and other industrial equipment, as well as for vibration and seismic isolation of building structures. The development and calibration of the model is based on experimentally observed dynamic characteristics. The proposed model is validated by dynamic testing and very good agreement between predicted and experimental results is obtained. Some analytical results for a single-degree-of-freedom viscodamper system are presented. These results are useful to the design of vibration isolation systems. Furthermore, an equivalent viscous oscillator is defined whose response is essentially the same as that of the viscodamper isolator. Finally, the model is employed in the analysis of a base-isolated model structure which has been tested on a shake table.

ACKNOWLEDGEMENTS

Financial support for this project has been provided by the National Center for Earthquake Engineering Research (Contract No. 89-2101) and the National Science Foundation (Grant No. BSC-8857080). GERB Vibration Control, Germany donated the viscous dampers and helical steel springs used in the experiments. Watson Bowman Acme, Corp. of Amherst, N.Y. donated the sliding Teflon disc bearings.

TABLE OF CONTENTS

LIST OF ILLUSTRATIONS

LIST OF TABLES

SECTION 1

INTRODUCTION

Viscous dampers are devices for dissipating energy. They are used in the reduction of vibration in pipework systems and together with helical steel springs in vibration isolation of massive industrial equipment like presses and forging hammers. More recently they have been proposed for seismic isolation of buildings (Huffmann, 1985). Two residential buildings have been very recently constructed in Los Angeles, California on isolation systems, consisting of helical steel springs and viscous dampers, for earthquake protection.

Viscous dampers typically consist of a moving part immersed in highly viscous fluid. In the applications described above, the moving part is in the form of a hollow cylinder (piston). Figure 1-1 shows the construction of an experimental cylindrical damper which has been used in the experiments described in this report. The damper piston can move in all directions and damping forces develop as a result of shearing action and displacement in the fluid. Dampers of different geometry than the one shown in Figure 1-1 have been used in combination with elastomeric bearings in a seismic isolated building in Japan (Higashino et al 1988, Kelly 1988). The dampers consisted of circular plates which were positioned on top of viscous fluid within a container. Damping forces develop by shearing of the fluid during motion of the plate.

The dynamic characteristics of a viscous damper depend primarily on the properties of the viscous fluid and secondarily on the geometry of the device. Two types of damper fluid are used: temperature-dependent fluids which can be adapted to the operating temperature of a particular application, and nearly temperature-independent fluids. The fluid used in the tests reported herein is a form of silicon gel with nearly temperature-independent properties in the range of -40 to 130^{o} C. It was supplied by a manufacturer of viscous dampers (GERB, 1986). It is known that viscous dampers exhibit viscoelastic behavior, that is behavior which incorporates both elastic and viscous characteristics. Furthermore, the properties of viscous dampers are strongly frequency dependent,

e.g. for the tested dampers the damping coefficient showed a ten-fold decrease within the frequency range of 0 to 50 Hz. Nevertheless, mathematical models used for these devices have been limited to that of the simple linear viscous dashpot (GERB 1986, Higashino et al 1988).

Herein, the concept of fractional derivative (Oldham and Spanier, 1974) is employed in the development of a force-displacement relationship for viscous dampers. Fractional derivatives within the context of viscoelasticity have been used as early as 1936 by Gemant, 1936 and very recently by Koh and Kelly, 1990, who proposed a fractional Kelvin model for elastomeric bearings. Earlier experiments with viscous dampers (Schwahn et al, 1988) have demonstrated that the classical two- and three-parameters models of viscoelasticity were incapable of describing the behavior of the dampers with sufficient degree of accuracy. The authors of this report observed that the frequency dependency of the mechanical properties of the tested dampers varied as frequency was raised to fractional rather than integer powers. This suggests that differentials of fractional order could be used in modeling of the dampers. Similar observations have prompted Gemant, 1936 to first propose fractional derivative models for viscoelastic materials. The above reasons motivated the study reported herein.

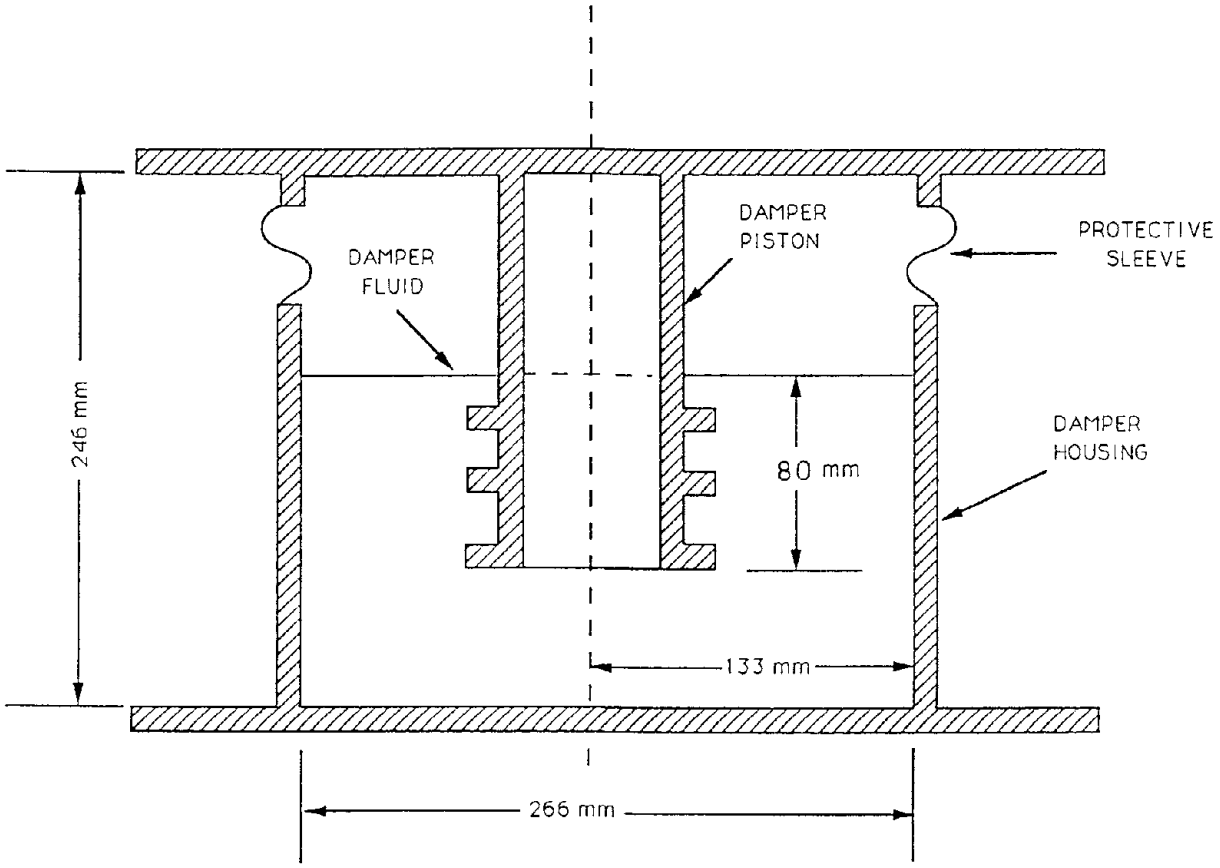

Figure 1-1 Geometry of Tested Damper.

SECTION 2

FRACTIONAL DERIVATIVE MAXWELL MODEL

2.1 Model of Viscous Fluid

The dynamic characteristics of the viscous damper of Figure 1-1 depend primarily on the properties of the viscous fluid. The fluid used in the tested damper is a form of silicon gel with mass density of 0.93 g/cm^3, which is slighly less than that of water. The rate-dependent and frequency-dependent properties of the fluid were determined in tests employing the cone-and-plate method (Bird et al, 1987).

First, the cone-and-plate method in steady shear flow was used to obtain measurements of the dynamic viscosity of the fluid. Figure 2-1 depicts measured values of viscosity as function of rate of strain for two samples of the fluid. The viscosity has a value of about 1900 Pa-sec (19,000 poise) in the range of shear strain rate of 0 to 2 sec^{-1}. Beyond the limit of 2 sec^{-2}, the viscosity reduces.

Oscillatory shear flow experiments using the cone-and-plate method were used to measure the storage and loss shear moduli of the fluid. In this test, oscillatory shear flow is imposed and measurements of the induced shear stresses are made (see Bird et al, 1987 for details). The relation between amplitude of shear stress, $\bar{\tau}(\omega)$, and amplitude of shear strain, $\bar{\gamma}(\omega)$ is expressed as

$$\bar{\tau}(\omega)=[G_1(\omega) + iG_2(\omega)]\bar{\gamma}(\omega) \qquad (2\text{-}1)$$

where G_1 and G_2 are the storage and loss shear modulus, respectively, i is the imaginary unit and ω is the frequency of oscillation. Figures 2-2 and 2-3 show measured values of moduli G_1 and G_2 as function of frequency for two values of amplitude of shear strain, 5% and 10%. It may be observed that the amplitude of strain has an insignificant effect on the measured values of the shear moduli.

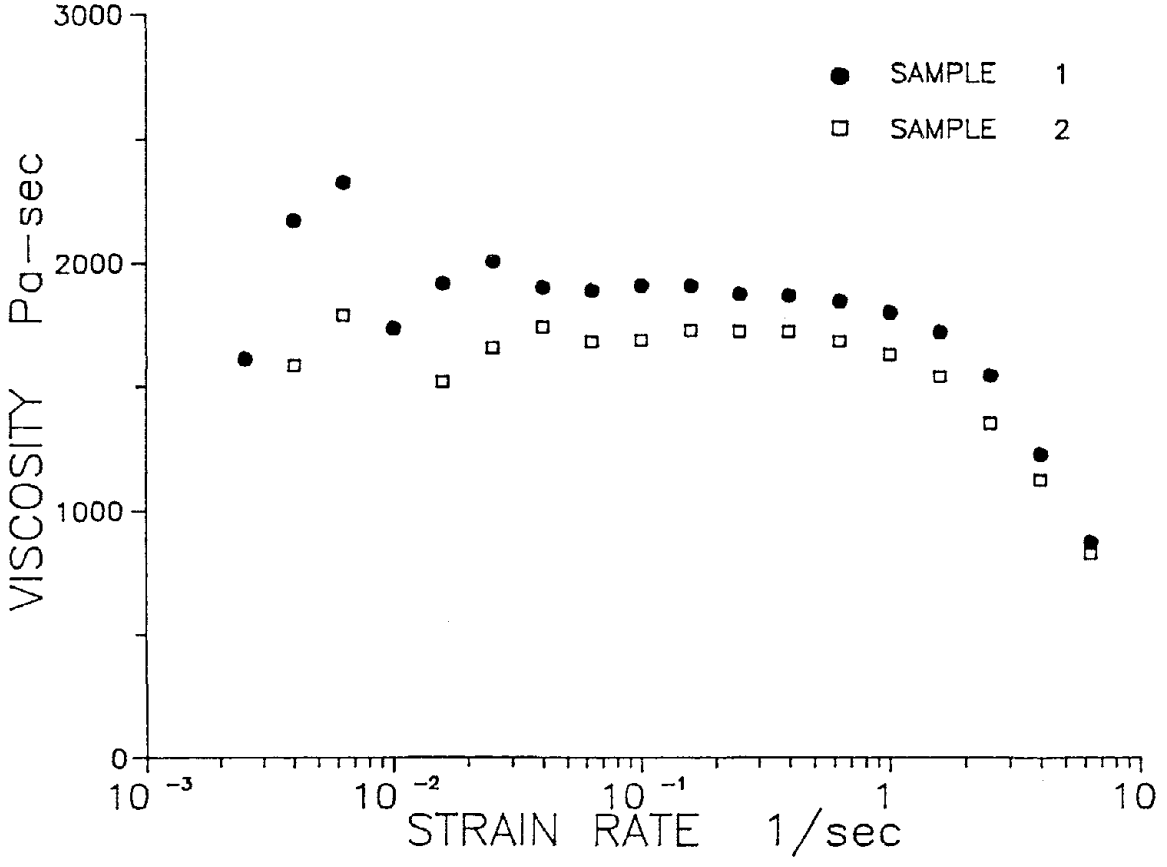

Figure 2-1 Viscosity of Damper Fluid as Function of Strain Rate.

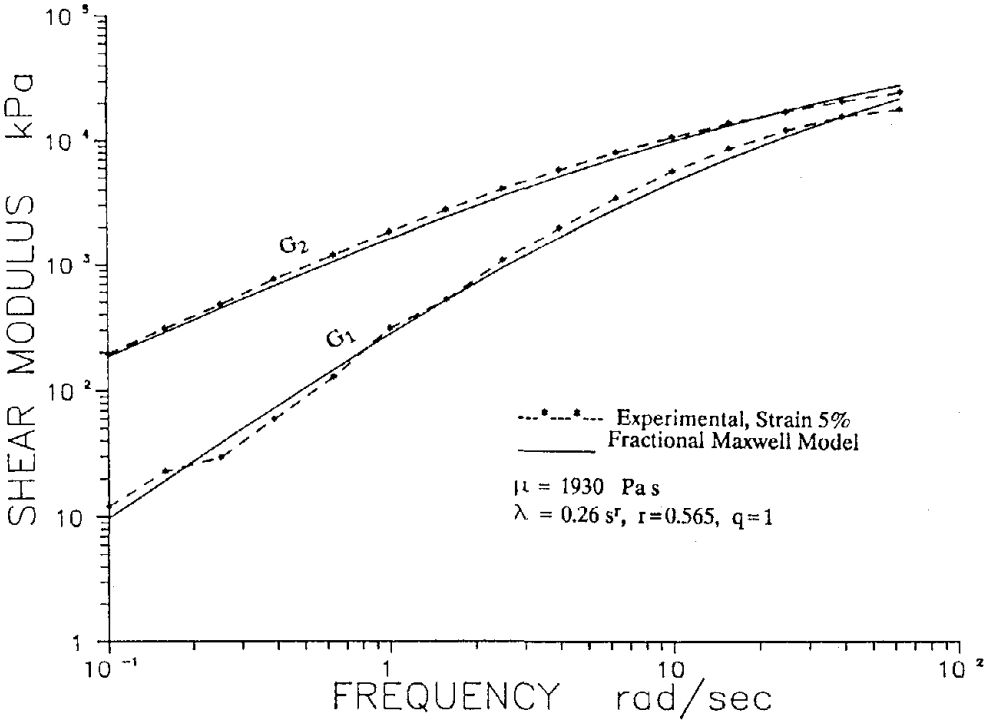

Figure 2-2 Measured Frequency Dependent Properties of Damper Fluid at 5% Strain and Comparison to Predictions of Fractional Maxwell Model.

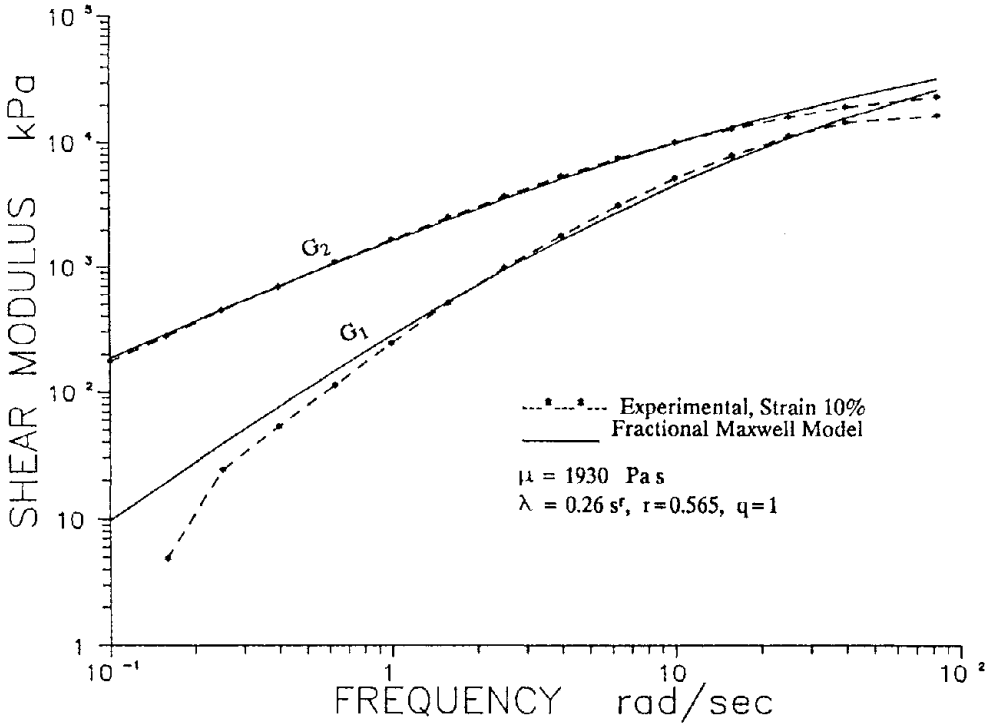

Figure 2-3 Measured Frequency Dependent Properties of Damper Fluid at 10% Strain and Comparison to Predictions of Fractional Maxwell Model.

The authors observed that the frequency dependency of the shear moduli of the fluid varied as frequency was raised to fractional rather than integer powers. This suggests that fractional differentials could be used in modeling the shear stress-strain relationship of the fluid. The simplest model of viscoelasticity which is capable of describing fluid behavior is the Maxwell model. It was natural to consider as candidate model the Maxwell model with the first order derivatives replaced by fractional order derivatives.

The shear stress-strain relationship in the fractional derivative Maxwell model is

$$\tau + \lambda D^{r}[\tau] = \mu D^{q}[\gamma] \tag{2-2}$$

in which τ and γ are the shear stress and strain, respectively and λ and μ are generalized material constants. $D^{r}[f(t)]$ is the fractional derivative of order r of the time dependent function f. A definition of the fractional derivative of a function satisfying the condition $f(t)=0$ for $t<0$ is via the following series which was given by Grunwald (Oldham and Spanier, 1974)

$$D^{r}[f(t)] = \frac{d^{r}f(t)}{dt^{r}} = \lim_{N\to\infty}\left\{ \frac{[\frac{t}{N}]^{-r}}{\Gamma(-r)} \sum_{j=0}^{N-1} \frac{\Gamma(j-r)}{\Gamma(j+1)} f(t-j\frac{t}{N}) \right\} \tag{2-3}$$

where Γ is the Gamma function. The authors prefer the above definition to the more commonly used integral representation of Riemann-Liouville (Oldham and Spanier, 1974) because equation 2-3 involves only evaluations of the function itself and not of its derivatives and integrals.

The model of equation 2-2 is a special case of the more general model of Bagley and Torvik, 1983. It may be seen that the model of equation 2-2 collapses to the conventional Maxwell model when r=q=1, in which case λ and μ become the relaxation time and dynamic viscosity, respectively.

Equation 2-2 may be written in the form of equation 2-1 by taking Fourier transform and noting the property of the Fourier transform of a fractional derivative,

$$F[D^r[f(t)]] = (i\omega)^r F[f(t)] \tag{2-4}$$

in which i^r is represented by its principal value

$$i^r = \cos\left(\frac{\pi r}{2}\right) + i \sin\left(\frac{\pi r}{2}\right) \tag{2-5}$$

and F [ ] is the Fourier transform of the expression in the brackets. The storage and loss shear moduli are given by

$$G_1 = \frac{\mu\,\omega^q \cos\left(\frac{q\pi}{2}\right)[1+\lambda\omega^r \cos\left(\frac{r\pi}{2}\right)] + \mu\,\lambda\omega^{q+r}\sin\left(\frac{r\pi}{2}\right)\sin\left(\frac{q\pi}{2}\right)}{d} \tag{2-6}$$

$$G_2 = \frac{\mu\,\omega^q \sin\left(\frac{q\pi}{2}\right)[1+\lambda\omega^r \cos\left(\frac{r\pi}{2}\right)] - \mu\,\lambda\omega^{q+r}\sin\left(\frac{r\pi}{2}\right)\cos\left(\frac{q\pi}{2}\right)}{d} \tag{2-7}$$

$$d = 1 + \lambda^2\omega^{2r} + 2\lambda\omega^r \cos\left(\frac{r\pi}{2}\right) \tag{2-8}$$

The four parameters of the model were determined by the following procedure. Based on the fact that the viscosity is independent of the rate of strain in a wide range of values, parameter q was set equal to unity. Accordingly, parameter μ becomes the viscosity. It should be equal to about 1900 Pa-sec. Parameters λ and r were determined in a least square fit of the experimental data on the storage modulus at 5% strain and parameter μ was found by fitting the loss modulus experimental data. The results was $\lambda=0.26(\text{sec})^{0.565}$, r=0.565, q=1 and μ=1930 Pa-sec. The value of μ is in very good agreement with the experimental results on the viscosity. The values of moduli G_1 and G_2 predicted by equations 2-6 to 2-8 are plotted against the experimental results in Figures 2-2 and 2-3. The agreement is seen to be very good.

Attempts have been made to fit the viscoelastic properties of the viscous fluid with conventional models of viscoelasticity. It was found that conventional models were worst than the proposed fractional derivative model and valid only in a small range of frequencies. For example, the conventional Maxwell model could fit well only the data on the loss modulus within a frequency range 50 times smaller than that in the fractional derivative Maxwell model. Figures 2-4 and 2-5 compare the experimental values of shear moduli of the fluid at 5% strain to values predicted by the conventional Maxwell model (q=r=1). Evidently, the conventional Maxwell model is incapable of describing the behavior of the fluid.

2.2 Model of Viscous Damper in Vertical Motion

Dynamic tests of the viscous damper of Figure 1-1 were conducted by imposing sinusoidal motion of specified amplitude and frequency to the piston of the damper and measuring the force needed to maintain the motion. Figure 2-6 shows a schematic representation of the testing arrangement. A hydraulic actuator was used to impose the motion. A load cell was placed below the damper to measure the reaction force. Figure 2-7 shows a photograph of the testing arrangement together with a close-up of the damper with the protective sleeve lowered to reveal the piston. It should be noted that the reaction force is the force needed to maintain the motion, whereas the force imposed by the actuator differs from the reaction force by the inertia force of the moving part. This inertia force is larger than the reaction force in the tests at large frequency of motion. For example, in a test at 45 Hz frequency, the peak reaction force was 463.7N (104 lbs) and the peak inertia force was about 758N (170 lbs). This large inertia force was a result of the almost 8.5g acceleration of the moving part which weighed about 90N (20 lbs).

The recorded force-displacement loops had an almost precise elliptical shape (see Section 3 for graphs of the loops). These loops were used in obtaining the frequency dependent properties of the damper. Under steady-state conditions, the force and displacement are

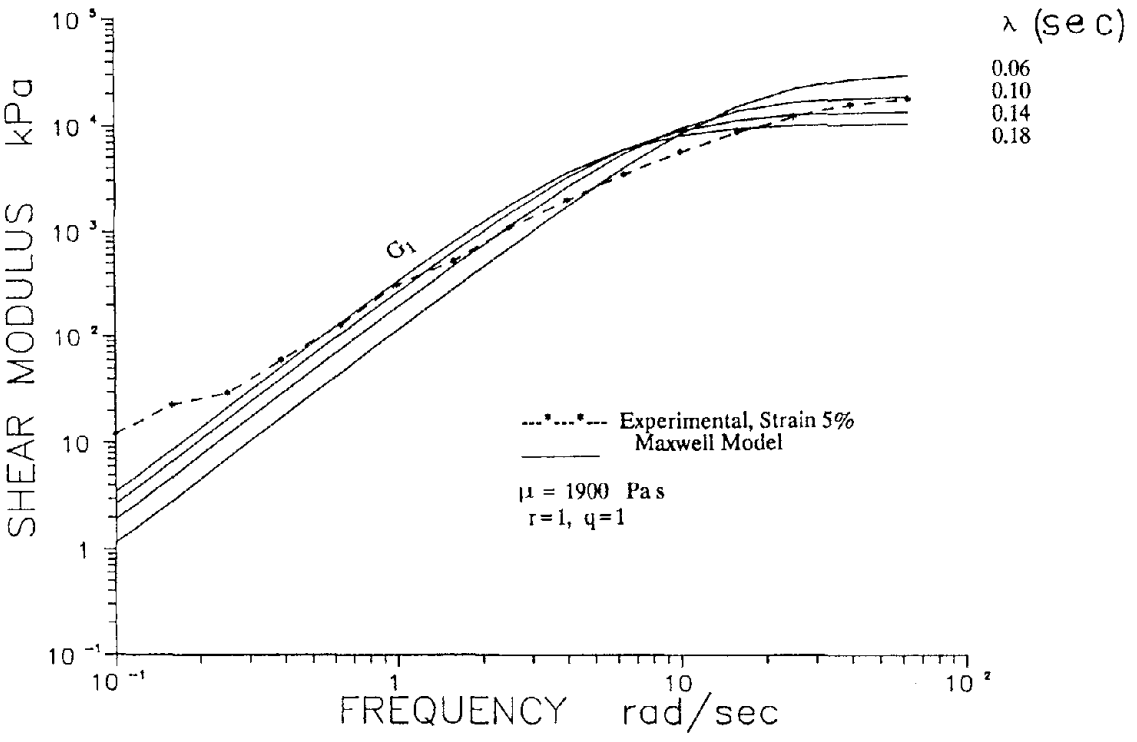

Figure 2-4 Storage Shear Modulus of Damper Fluid and Comparison to Prediction of Conventional Maxwell Model.

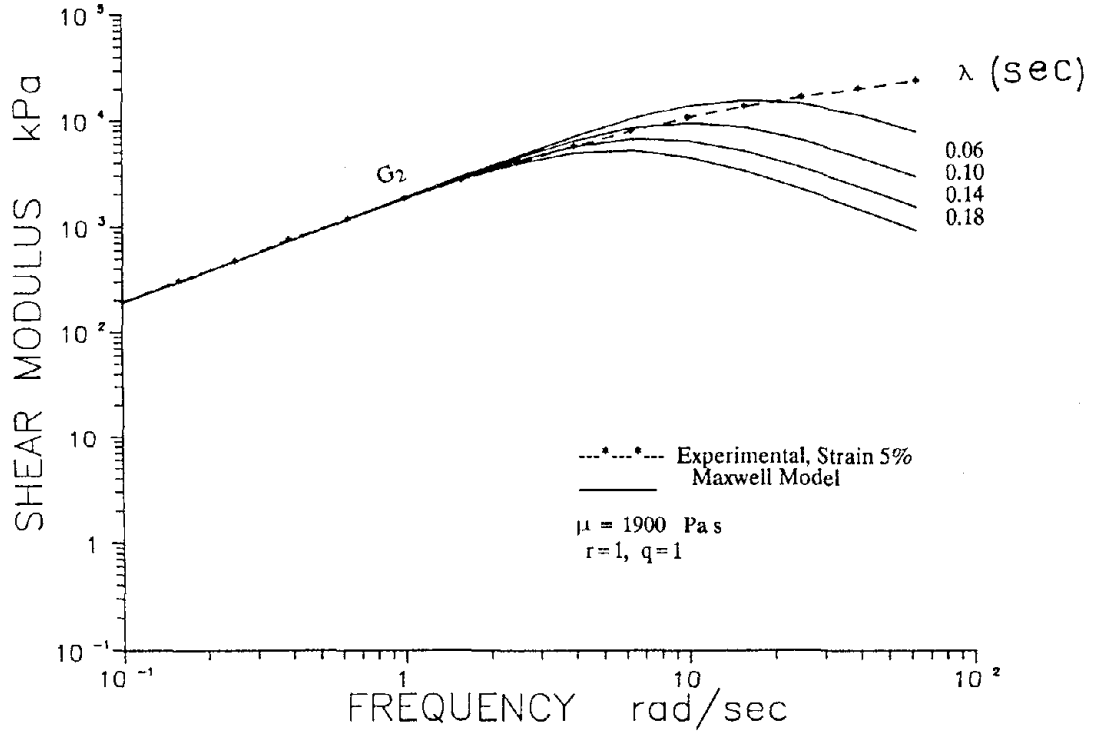

Figure 2-5 Loss Shear Modulus of Damper Fluid and Comparison to Prediction of Conventional Maxwell Model.

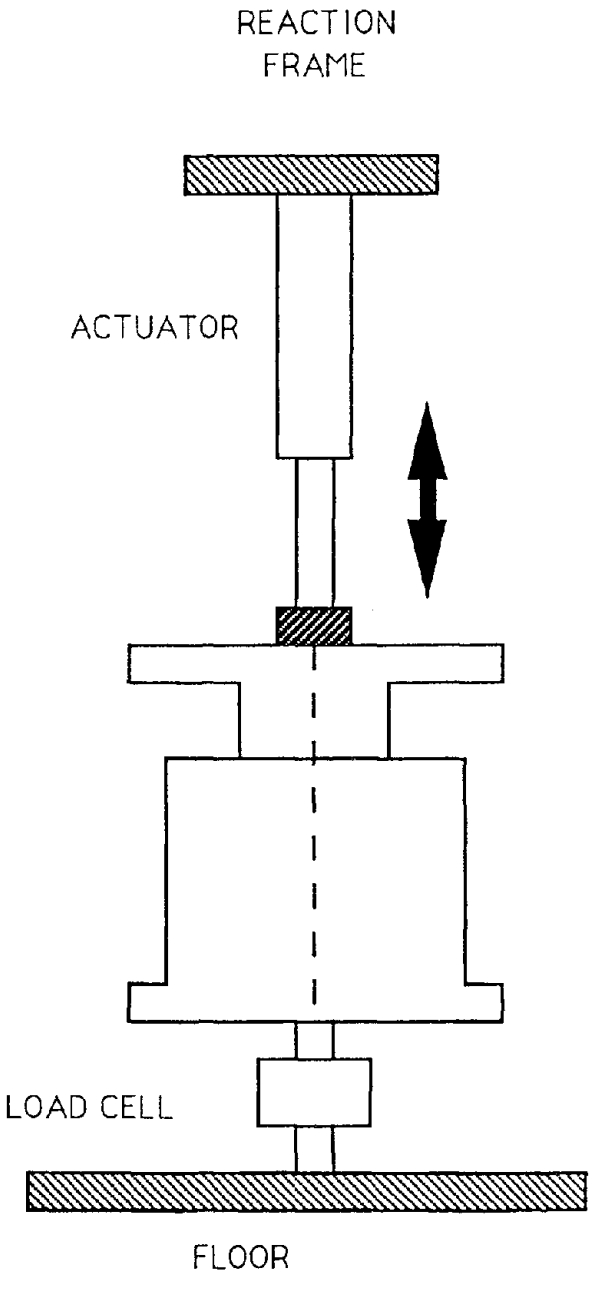

Figure 2-6 Testing Arrangement of Damper for Vertical Motion.

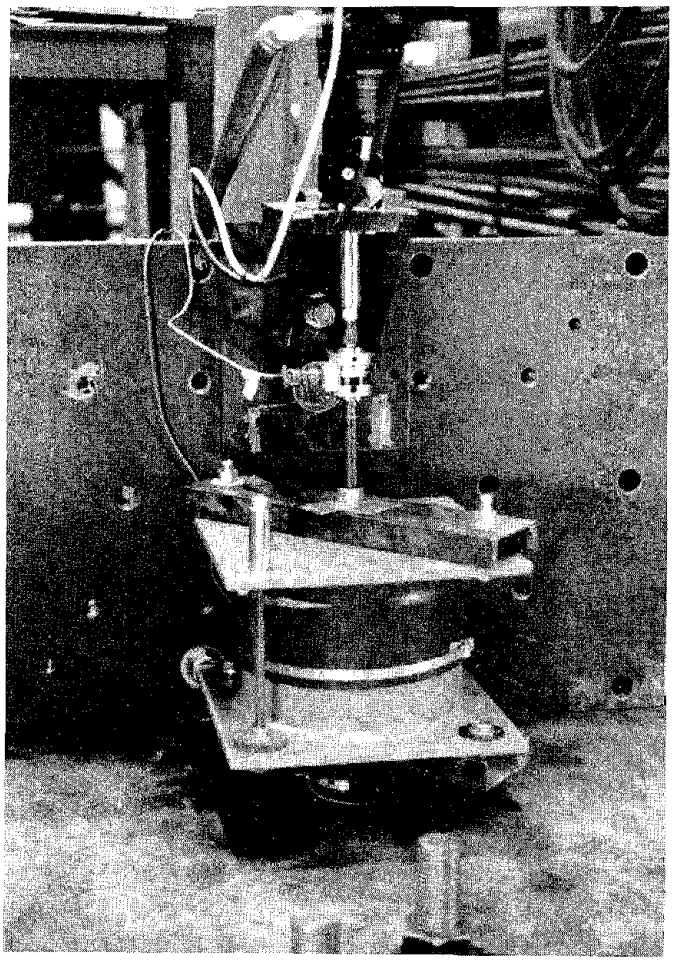

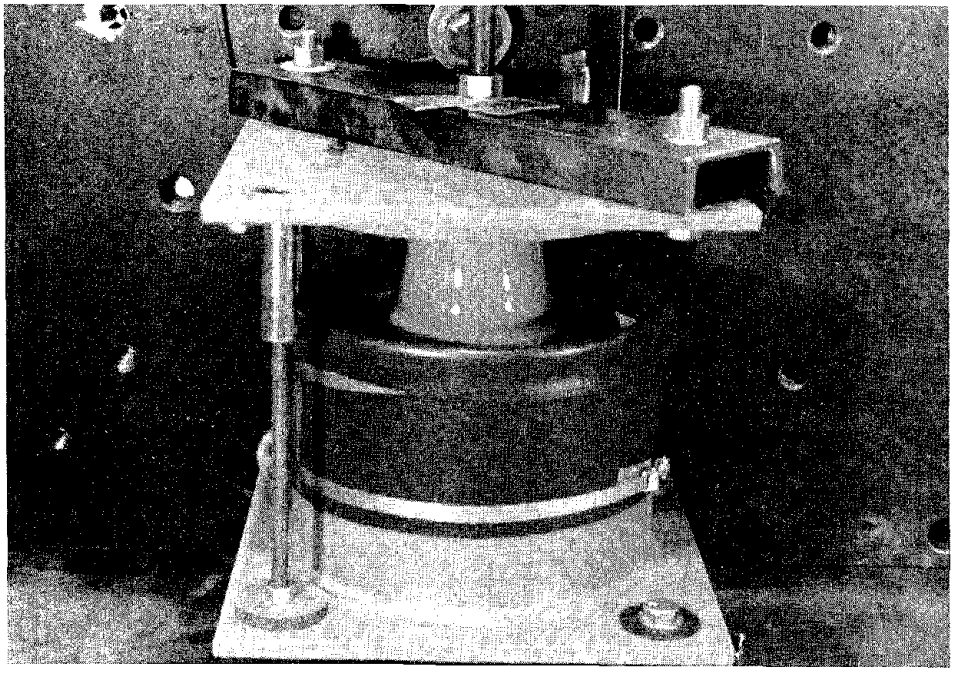

Figure 2-7 Photographs of Testing Arrangement for Vertical Motion.

$$u=U_o \sin\omega t \tag{2-9}$$

$$P=P_o \sin(\omega t+\delta) \tag{2-10}$$

where P_o is the recorded amplitude of the force, U_o is the recorded amplitude of displacement, ω is the frequency of motion and δ is the phase difference. The energy dissipated in a cycle of steady-state motion is

$$W_d = \oint Pdu = \pi \sin\delta \; P_o U_o \tag{2-11}$$

Furthermore, equation 2-10 may be written as

$$P = K_1 U_o \sin \omega t + K_2 U_o \cos \omega t \tag{2-12}$$

where

$$K_1 = \frac{P_o}{U_o} \cos\delta, \; K_2 = \frac{P_o}{U_o} \sin\delta \tag{2-13}$$

K_1 and K_2 are the storage and loss stiffnesses of the damper. Quantity $P_o/U_o = K_o$ represents the elastic stiffness. It should be noted that the two parts of equation 2-12 represent respectively the in-phase and 90^o out-of-phase parts of the force. Accordingly, using equation 2-9 and its time derivative (velocity),

$$P = K_1 \, u + \frac{K_2}{\omega} \, \dot{u} \tag{2-14}$$

Quantity K_2/ω is the damping coefficient of the damper,

$$C = \frac{K_2}{\omega} \tag{2-15}$$

Returning to equation 2-13 and using equation 2-11,

$$K_2 = \frac{W_D}{\pi U_o^2} \tag{2-16}$$

Equations 2-11 to 2-16 are used to extract the frequency-dependent properties of the damper from the measured quantities P_o, U_o and W_D. First, equation 2-16 is used to obtain the loss stiffness. Equation 2-15 is used to obtain the damping coefficient. Finally, equations 2-13 are used to obtain the phase difference and storage stiffness.

Table 2-I summarizes the experimental results for motion in the vertical direction. The results are presented in units of lbs and in., the units in which measurements were made. The strong dependency of the mechanical properties of the damper on frequency is evident. In some of the tests the amplitude of displacement was varied while the frequency was kept constant. The properties were practically unaffected by the value of displacement amplitude. This indicates that for the range of parameters used in these tests, the properties are frequency-dependent but rate-independent (i.e. independent of velocity of motion).

A mathematical model of the device is written in a form analogous to that of the shear stress-strain relationship of the damper fluid. This is based on the assumption that the fluid is primarily subjected to shearing action while the piston moves in vertical motion. The force-displacement relationship in vertical motion is expressed as

$$P + \lambda D^r[P] = C_o D^q[u] \tag{2-17}$$

in which P and u are the force and displacement, respectively. The expectation is that q equals to unity and λ and r are very close to the values obtained for the stress-strain relationship of the fluid. For q=1, constant C_o attains physical interpretation. It is the damping coefficient at zero frequency which could be measured in an oscillatory test at very low frequency (0.01 Hz in this study).

Table 2-I: Experimental Results for Vertical Motion (1 lb = 4.46 N, 1 in.= 25.4 mm)

Frequency (Hz)	Amplitude U_o(in)	Force P_o(lbs)	Energy W_D(lb-in)	Stiffness K_1(lb/in)	Stiffness K_2(lb/in)	Damping Coef. C (lb-sec/in)	Phase (degrees)
0.01	0.2	0.97	0.60	0.85	4.77	75.99	79.89
0.05	0.2	4.57	2.52	10.95	20.05	63.83	61.36
0.10	0.2	8.57	5.00	15.91	39.79	63.33	68.21
0.20	0.2	16.42	10.00	20.19	79.58	63.33	75.76
0.50	0.2	36.78	21.84	60.11	173.79	55.32	70.92
1	0.2	62.50	35.60	131.91	283.29	45.09	65.03
2	0.2	102.80	56.08	255.03	446.27	35.51	60.25
4	0.2	157.00	76.00	500.46	604.79	24.06	50.39
6	0.2	200.00	93.60	667.27	744.85	19.76	48.15
8	0.1	118.00	27.20	801.74	865.80	17.22	47.20
8	0.2	220.99	100.80	752.71	802.14	15.96	46.82
10	0.1	118.00	24.40	888.35	776.68	12.36	41.16
10	0.2	245.00	108.00	872.92	859.44	13.68	44.55
12	0.1	143.00	31.60	1016.44	1005.86	13.34	44.70
15	0.1	154.30	33.60	1112.19	1069.52	11.35	43.88
15	0.2	291.50	120.00	1101.10	954.93	10.13	40.93
18	0.055	89.30	10.20	1218.28	1073.31	9.49	41.38
18	0.1	164.30	35.20	1201.68	1120.45	9.91	42.99
18	0.2	300.00	124.40	1126.95	989.94	8.75	41.30
20	0.055	89.30	10.00	1236.50	1052.26	8.37	40.40
25	0.055	90.00	10.30	1225.97	1083.83	6.90	41.47
25	0.1	181.50	37.60	1364.47	1196.84	7.62	41.25
30	0.055	108.50	11.40	1613.09	1451.49	7.70	41.98
35	0.038	79.70	6.60	1510.72	1454.88	6.62	43.92
40	0.044	109.00	10.00	1853.00	1644.16	6.54	41.58
40	0.018	50.00	1.67	2241.48	1640.67	6.52	36.20
45	0.041	104.00	7.61	2087.52	1441.01	5.09	34.62
50	0.035	65.00	5.88	1055.72	1527.89	4.86	55.36

The relationship between force amplitude, $\bar{P}(\omega)$, and displacement amplitude, $\bar{u}(\omega)$ is obtained by employing Fourier transform to equation 2-17

$$\bar{P}(\omega) = [K_1(\omega) + i\ K_2(\omega)]\ \bar{u}(\omega) \qquad (2\text{-}18)$$

where K_1 and K_2 are the storage and loss stiffnesses. The mathematical expressions for stiffnesses K_1 and K_2 are identical to those for moduli G_1 and G_2 (equations 2-6 to 2-8) except that μ is replace by C_o.

In the calibration of the model, parameter q was set equal to unity and parameters λ and r were determined in a least square fit of the elastic stiffness curve (defined as the square root of the sum of squares of K_1 and K_2). Constant C_o was then found by fitting the damping coefficient curve. The parameters of the model are q=1, C_o=15,000 Ns/m, r=0.6 and λ=0.3(sec)$^{0.6}$. Indeed, parameters λ and r are very close to those of the stress-strain relationship of the fluid.

Figures 2-8 to 2-12 compare predictions of the calibrated model of equation 2-17 with experimental results on the elastic stiffness, damping coefficient, storage and loss stiffness and phase difference (calculated as $\tan^{-1}(K_2/K_1)$). The agreement between the two sets of results is very good. Comparison of experimental and analytical force-displacement loops are presented in section 3.

2.3 Model of Viscous Dampers in Horizontal Motion

Tests with motion in the horizontal direction were conducted with the arrangement of Figure 2-13. The damper was placed on top of very low friction roller bearings and a load cell mounted on the damper housing was used to measure the reaction force. Roller bearings were also used to support the moving piston and prevent it from tilting. The friction force from the roller bearings was estimated to be extremely low and accordingly the measured force in

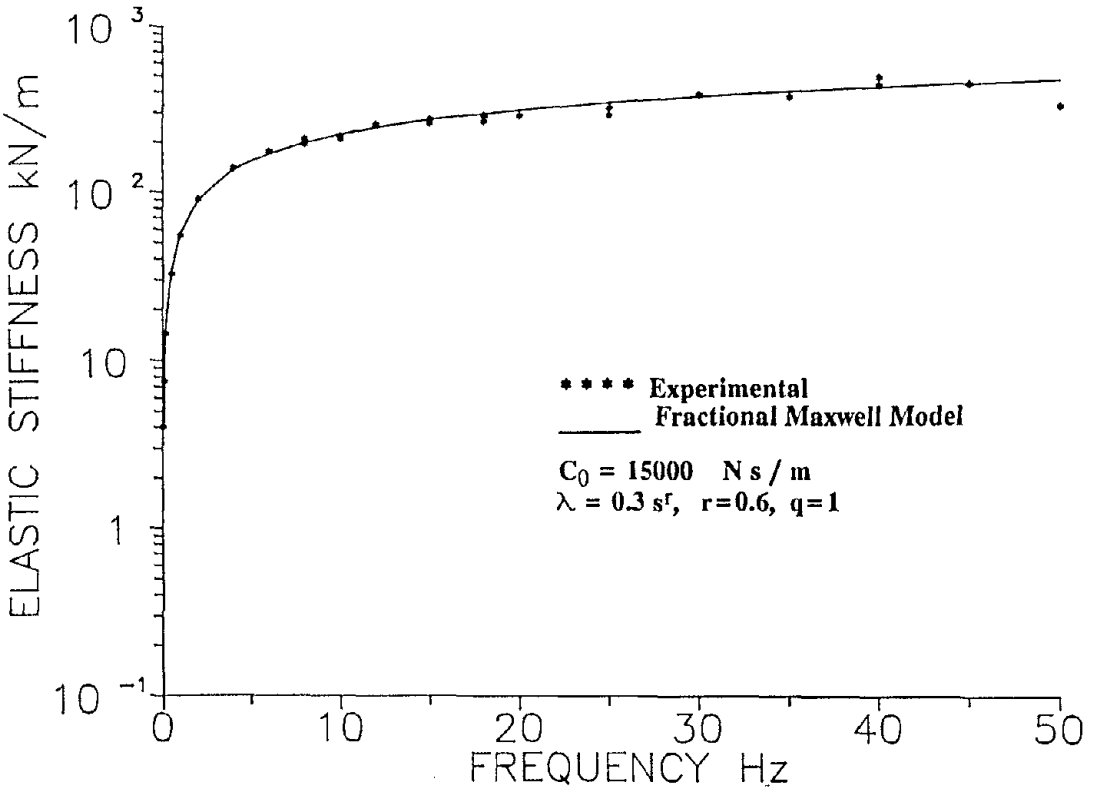

Figure 2-8 Fitting of Elastic Stiffness of Tested Damper in Vertical Motion by Fractional Maxwell Model.

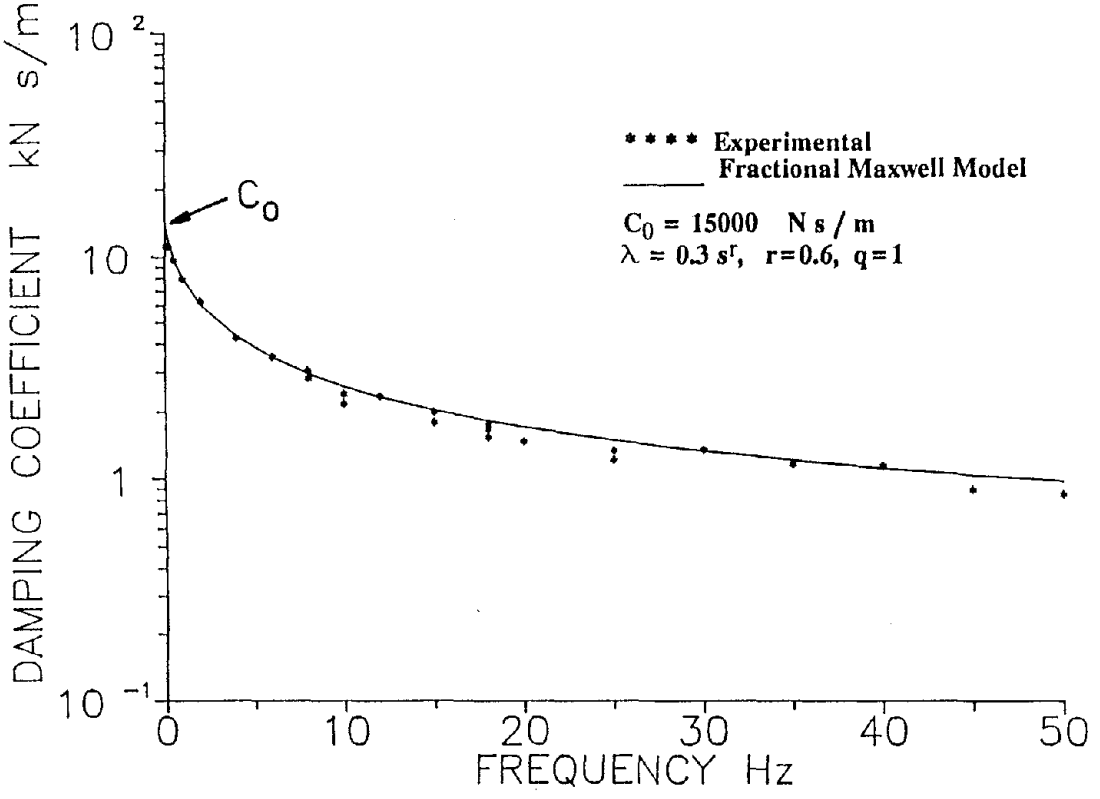

Figure 2-9 Fitting of Damping Coefficient of Tested Damper in Vertical Motion by Fractional Maxwell Model.

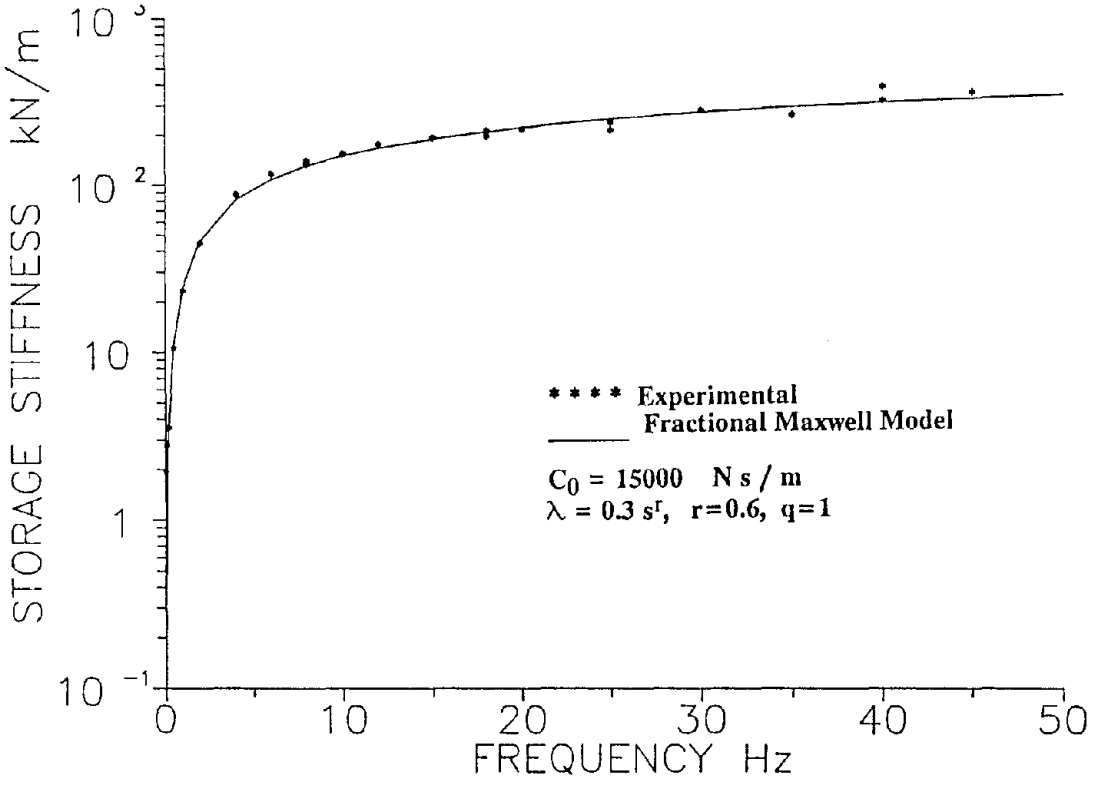

Figure 2-10 Fitting of Storage Stiffness of Tested Damper in Vertical Motion by Fractional Maxwell Model.

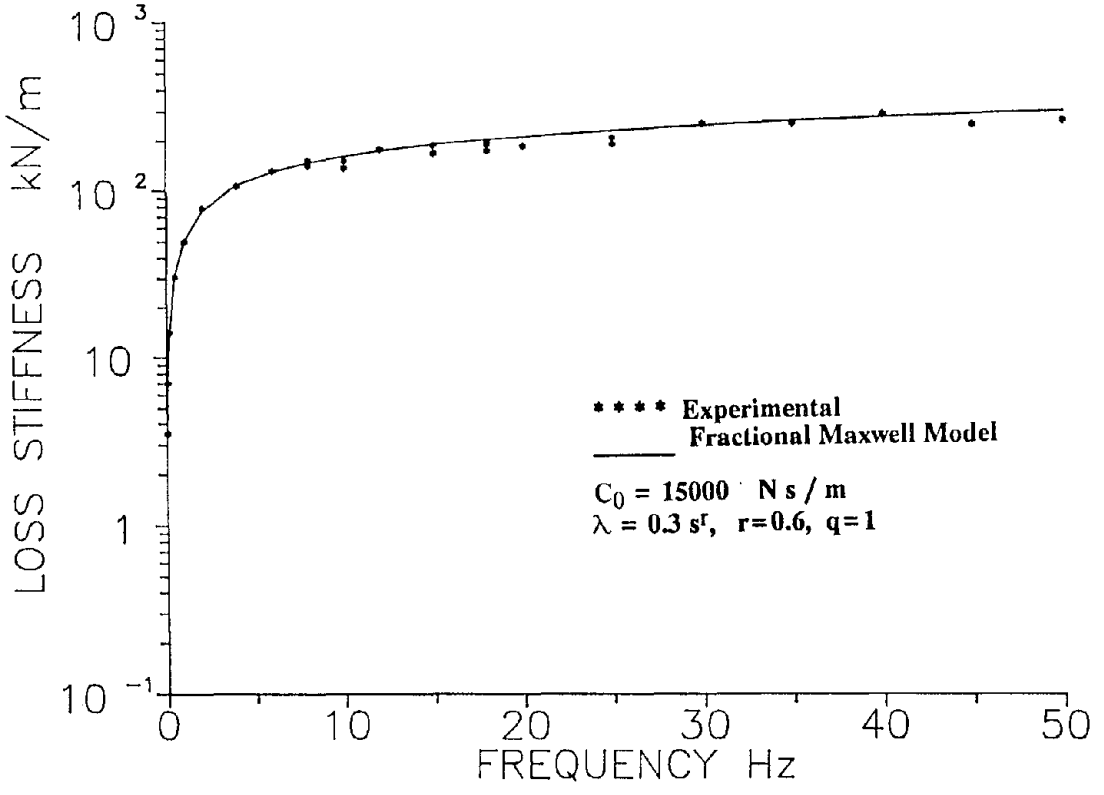

Figure 2-11 Fitting of Loss Stiffness of Tested Damper in Vertical Motion by Fractional Maxwell Model.

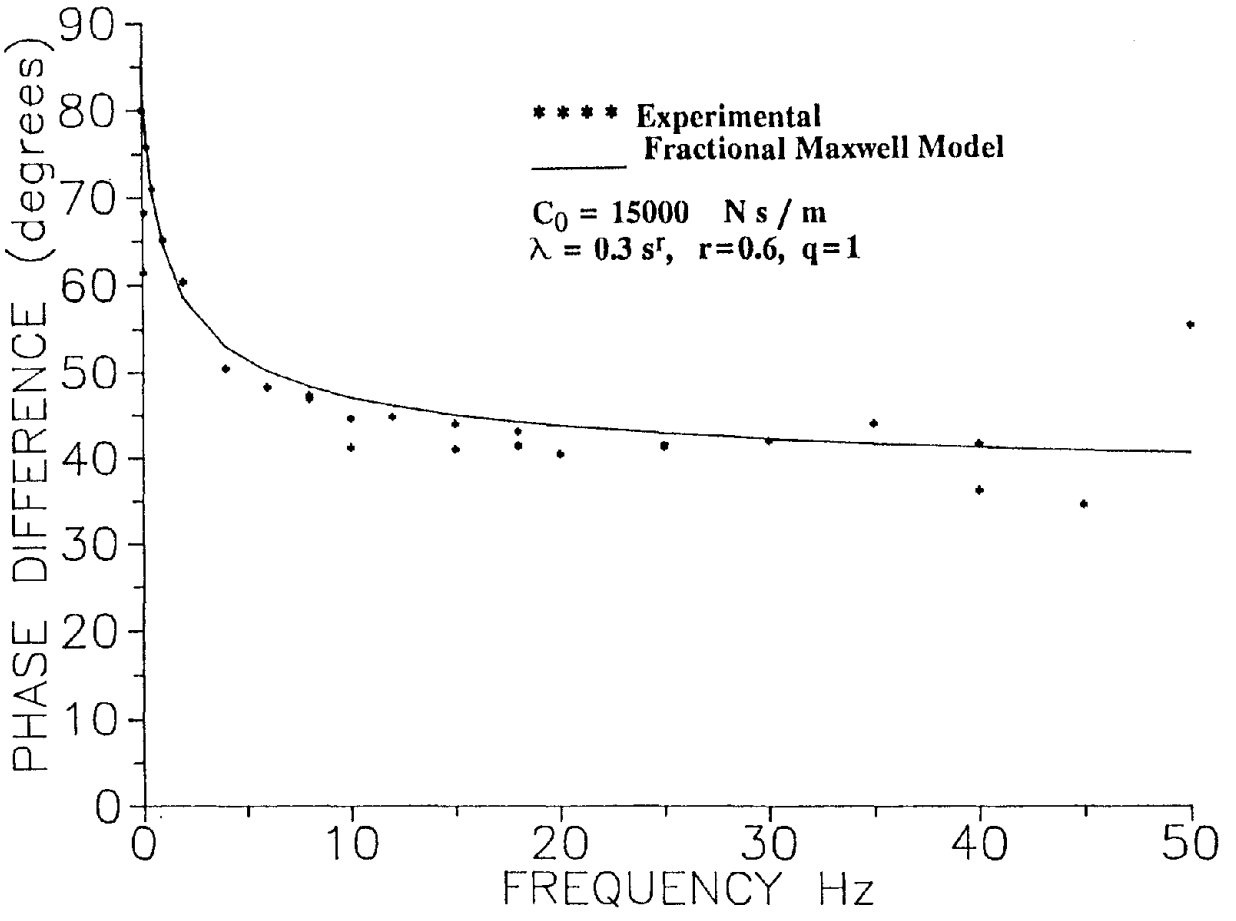

Figure 2-12 Fitting of Phase Difference of Tested Damper in Vertical Motion by Fractional Maxwell Model.

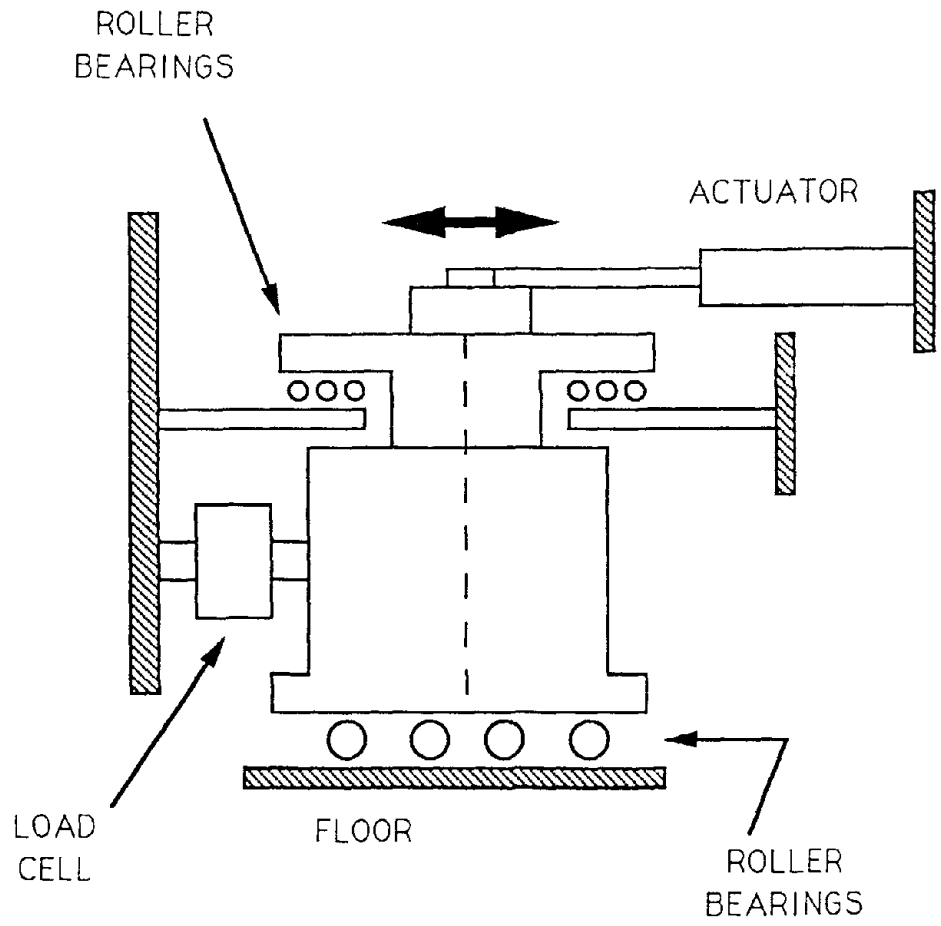

Figure 2-13 Testing Arrangement of Damper for Horizontal Motion.

the load cell was not corrected for the effect of the friction force. Photographs of the testing arrangement are shown in Figure 2-14. The top photograph shows a general view of the arrangement. The middle photograph shows the roller bearing connection for preventing tilting of the piston and the bottom photograph shows the connection of the housing to the load cell.

The recorded force-displacement loops had again elliptical shape for frequencies of motion up to 1 Hz. For frequencies of 2 Hz and above, the loops had a higher harmonic function superimposed on the basic elliptical shape. Figures 2-15 show experimental force-displacement loops for horizontal motion and for frequencies of 1 to 15 Hz. The wavy form of the loop is seen in these figures. This phenomenon is caused by standing waves that generate in the fluid during motion of the piston. In modeling the behavior of the device, only the basic elliptical shape has been accounted and the higher harmonics in the recorded force have been neglected.

Tests were conducted with the arrangement of Figure 2-13 with frequencies in the range of 0.05 to 20 Hz. The measured properties of the damper are given in Table 2-II. The properties are given in units of lbs and in., the units in which measurements were made. Three of the tests in Table 2-II (those identified by an asterisk) were conducted at large amplitude of displacement using a different testing arrangement. Four identical dampers were connected to the shake table at Buffalo with their pistons connected to a stiff base consisting of two heavy W14x90 steel sections. The weight of the base was carried by a crane. The base was connected by stiff rods to a nearby reaction wall. The rods were instrumented by load cells (see Figure 2-16). The shake table was driven in displacement-controlled mode with specified amplitude and frequency. The force transmitted through the four dampers was measured by the load cells connecting the base to the reaction wall. In this way, data from four dampers were obtained and then reduced to a single damper. The properties obtained in these tests are consistent with those obtained with the arrangement of Figure 2-13.

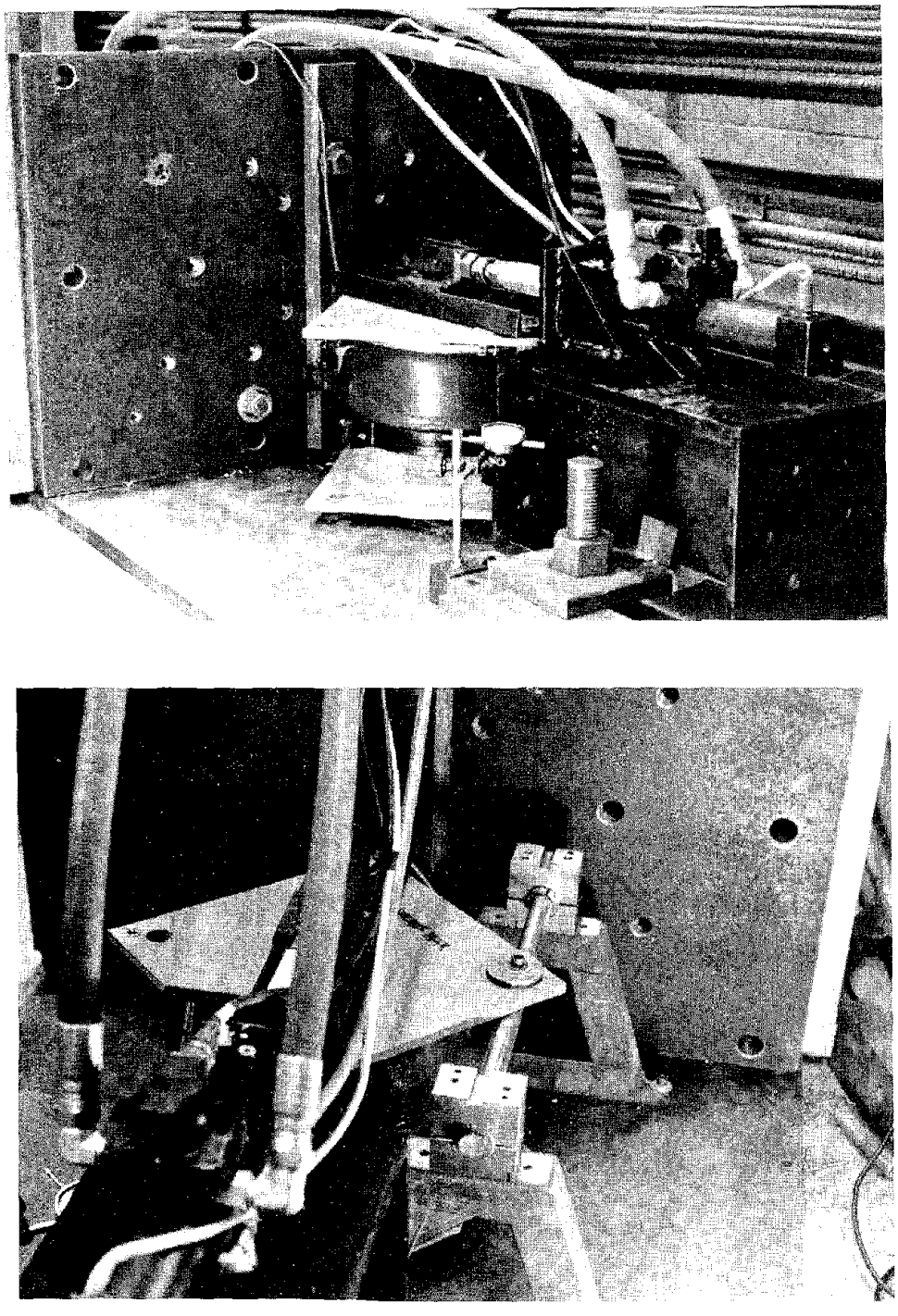

Figure 2-14 Photographs of Testing Arrangement of Damper for Horizontal Motion.

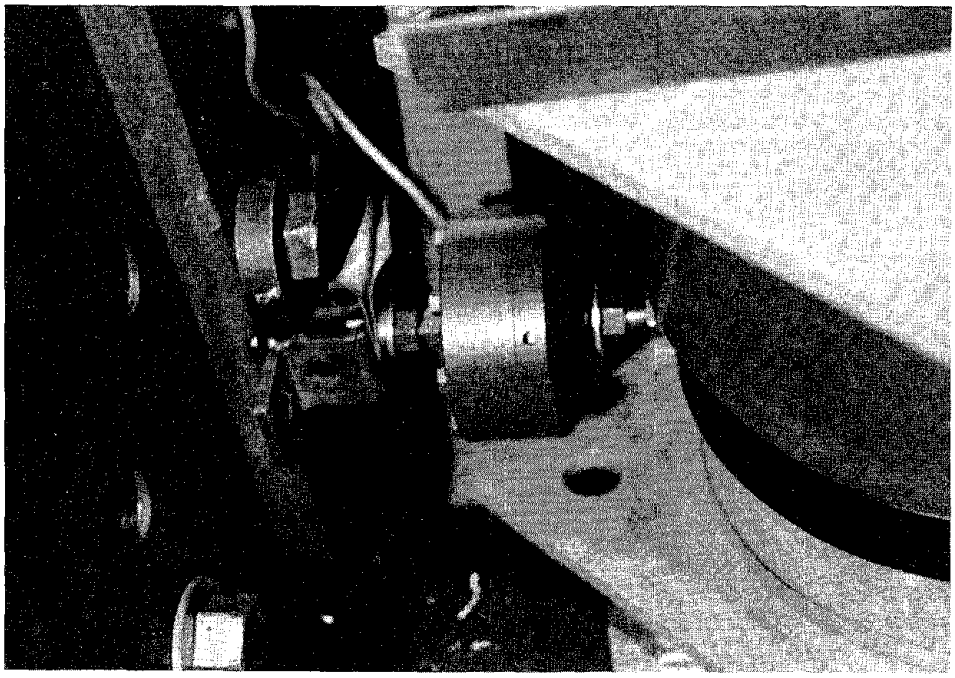

Figure 2-14 Continued.

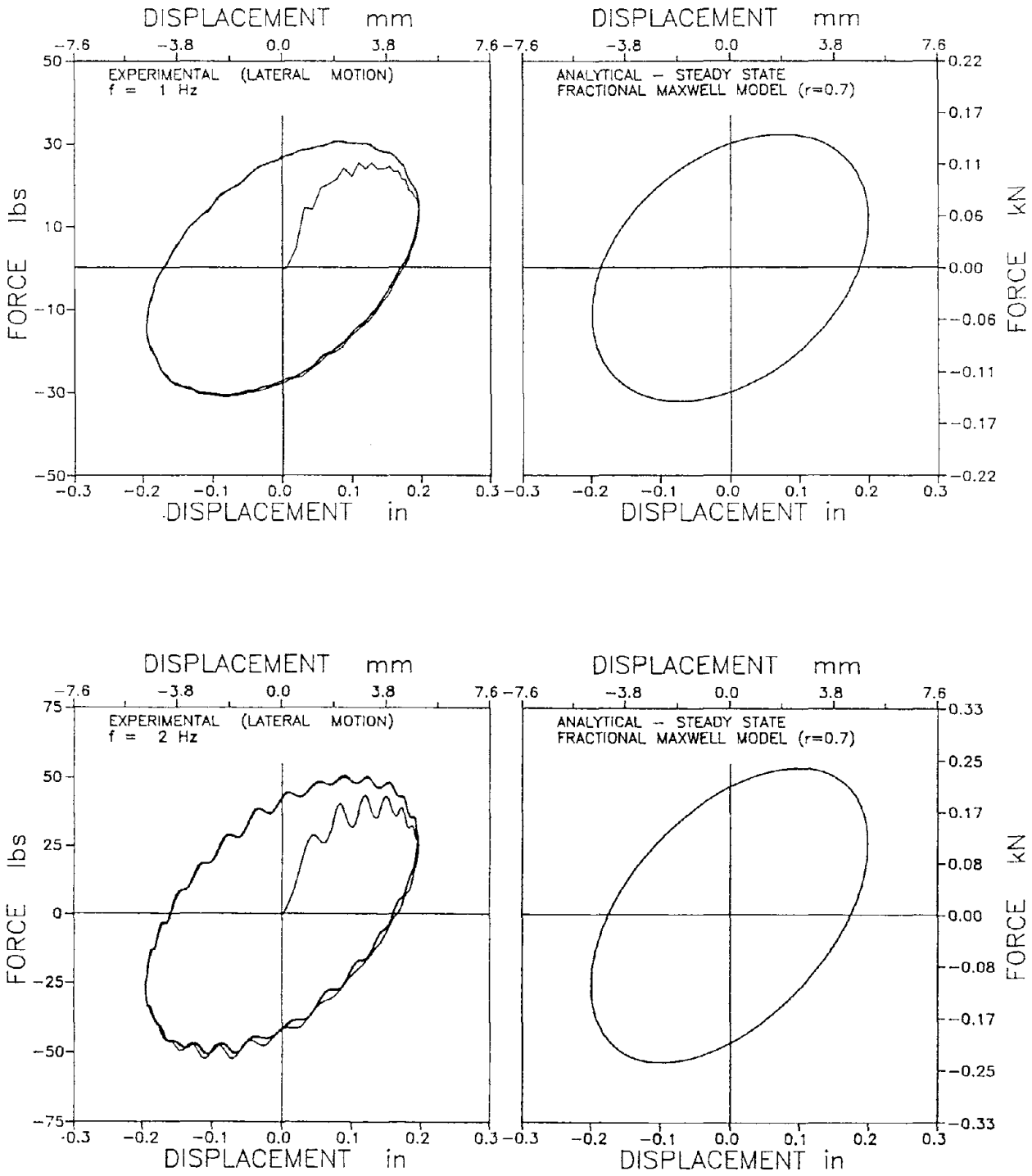

Figure 2-15 Recorded Force-Displacement Loops of Damper for Horizontal Motion for Frequency of 1 to 15 Hz.

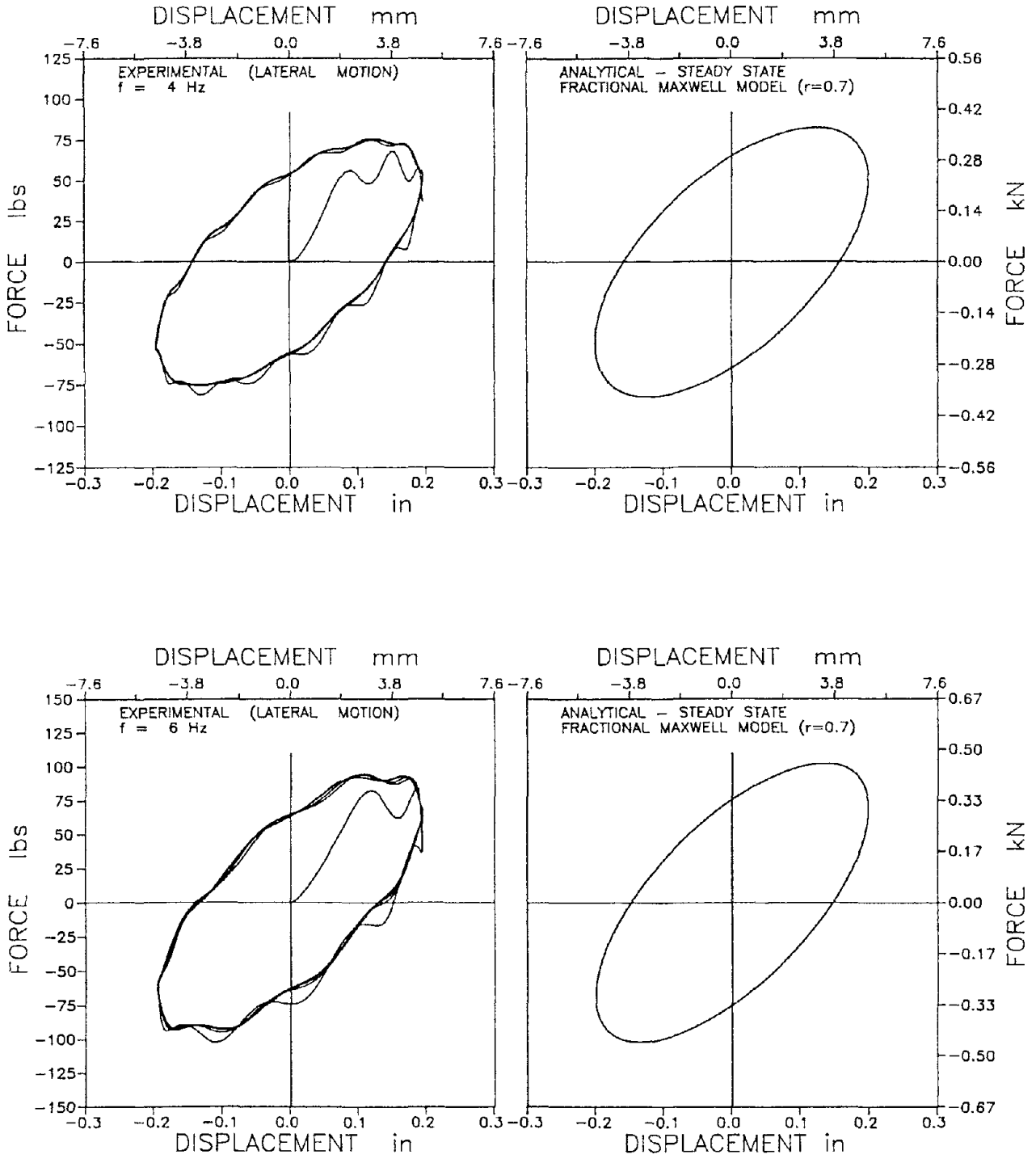

Figure 2-15 Continued.

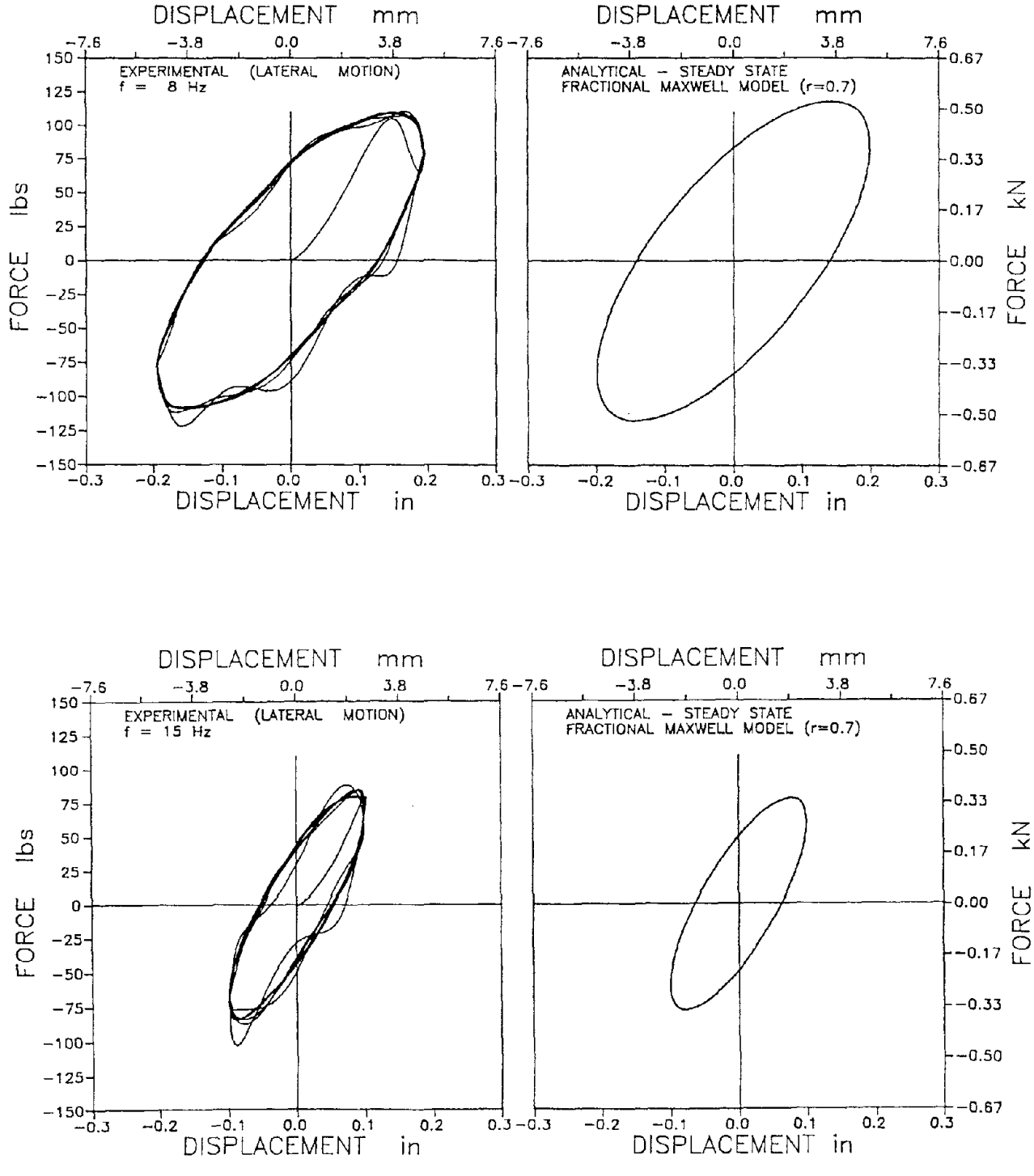

Figure 2-15 Continued.

Table 2-II: Experimental Results for Horizontal Motion (1lb = 4.46N, 1 in. = 25.4 mm)

Frequency (Hz)	Amplitude U_o(in)	Force P_o(lbs)	Energy W_D(lb-in)	Stiffness K_1(lb/in)	Stiffness K_2(lb/in)	Damping Coef. C (lb-sec/in)	Phase (degrees)
0.05	0.20	2.28	1.28	5.08	10.24	32.59	63.60
0.10	0.20	4.57	2.44	12.00	19.51	30.90	58.42
0.20	0.20	8.12	4.66	16.36	37.27	29.66	66.30
0.50	0.20	17.96	10.00	41.33	79.98	25.46	62.67
0.50	0.81	69.11	162.76	31.21	79.95	25.45	68.63 *
1	0.20	30.28	16.60	73.56	132.76	21.13	61.01
1	0.20	28.17	14.40	81.70	115.17	18.33	54.65
1	0.84	128.34	290.91	78.91	129.99	20.45	58.74 *
2	0.20	50.00	25.80	142.26	206.34	16.42	55.42
2	0.81	213.49	424.56	163.60	208.54	16.59	51.85 *
4	0.20	74.99	35.40	239.65	283.12	11.26	49.75
5	0.10	43.31	9.75	300.22	336.75	10.72	48.28
6	0.20	92.96	40.80	332.64	326.31	8.66	44.45
6	0.19	90.27	40.60	314.31	339.87	9.02	47.24
8	0.20	103.52	45.60	369.12	364.69	7.26	44.65
8	0.10	54.90	12.00	394.33	381.97	7.60	44.09
10	0.10	60.56	13.00	442.17	413.80	6.59	43.10
10	0.20	119.44	48.00	464.81	423.24	6.74	42.32
12	0.10	66.20	13.40	506.27	426.54	5.66	40.11
12	0.20	135.21	51.20	540.06	409.48	5.43	37.17
15	0.10	81.69	15.60	648.65	496.56	5.27	37.44
20	0.095	88.88	15.00	771.63	529.05	4.21	34.44
20	0.19	183.10	54.40	821.16	455.39	3.62	29.01

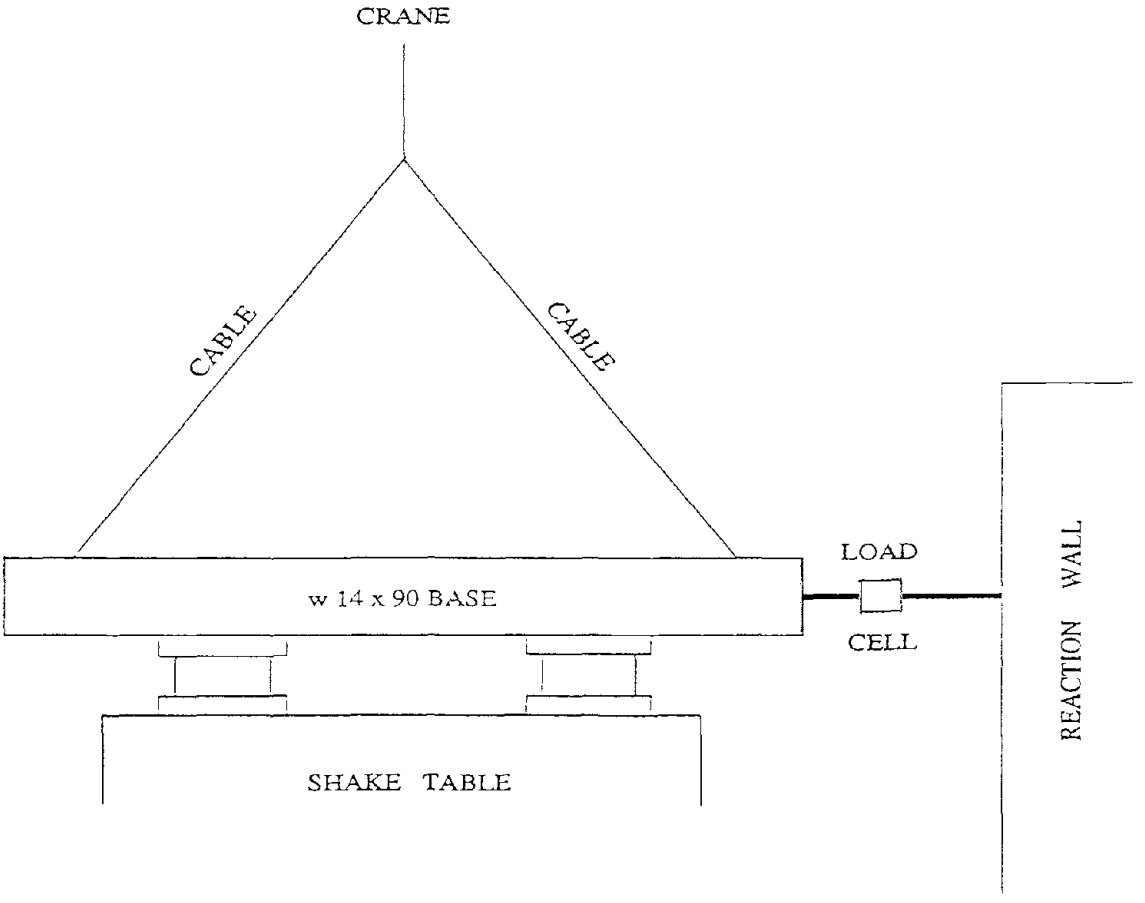

Figure 2-16 Testing Arrangement Involving Shake Table for Large Amplitude Horizontal Motion.

In modeling the behavior of the device for motion in the horizontal direction, the model of equation 2-17 is used. The calibration of the model was done in the same way as in the case of vertical motion, resulting in the following parameters: q=1, C_o = 6000 Ns/m, λ=0.15(sec)$^{0.7}$ and r=0.7. Figures 2-17 to 2-21 compare the frequency dependent properties of the damper as measured and as predicted by the fractional Maxwell model. The agreement is good. It should be noted that the model is capable of modeling only the basic behavior of the damper and not the higher harmonics observed in the loops of Figures 2-15. To demonstrate this, the steady-state force-displacement loops as predicted by the calibrated analytical model of equation 2-17 have been plotted next to the experimental loops in Figures 2-15. For the calculation of the force in steady-state motion, equation 2-12 has been used.

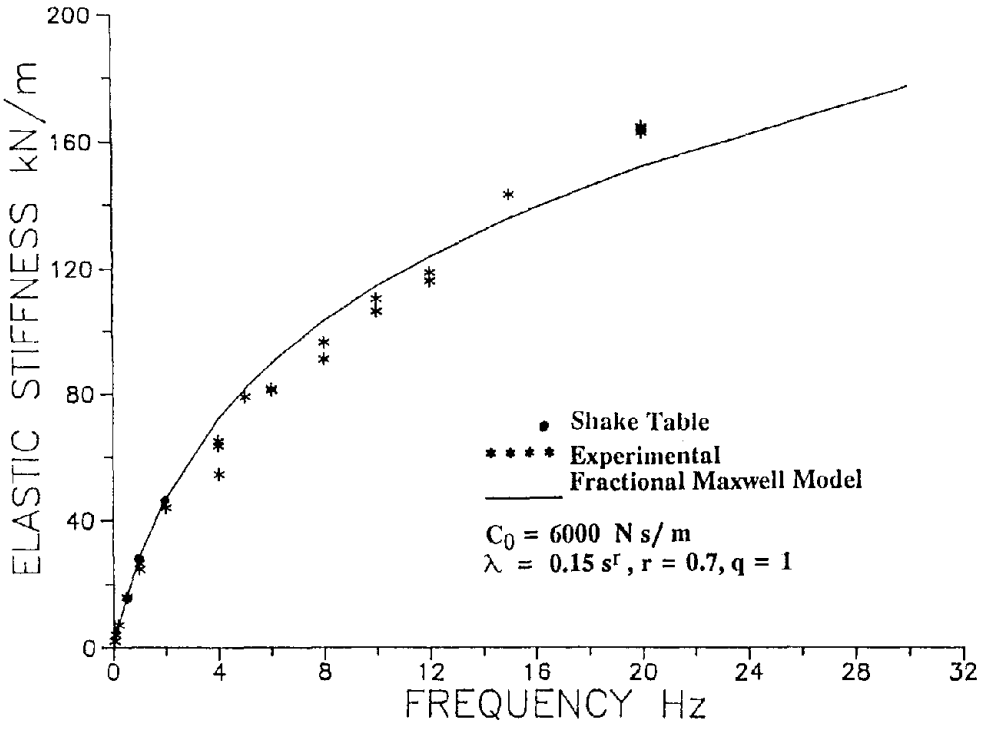

Figure 2-17 Fitting of Elastic Stiffness of Tested Damper in Horizontal Motion by Fractional Maxwell Model.

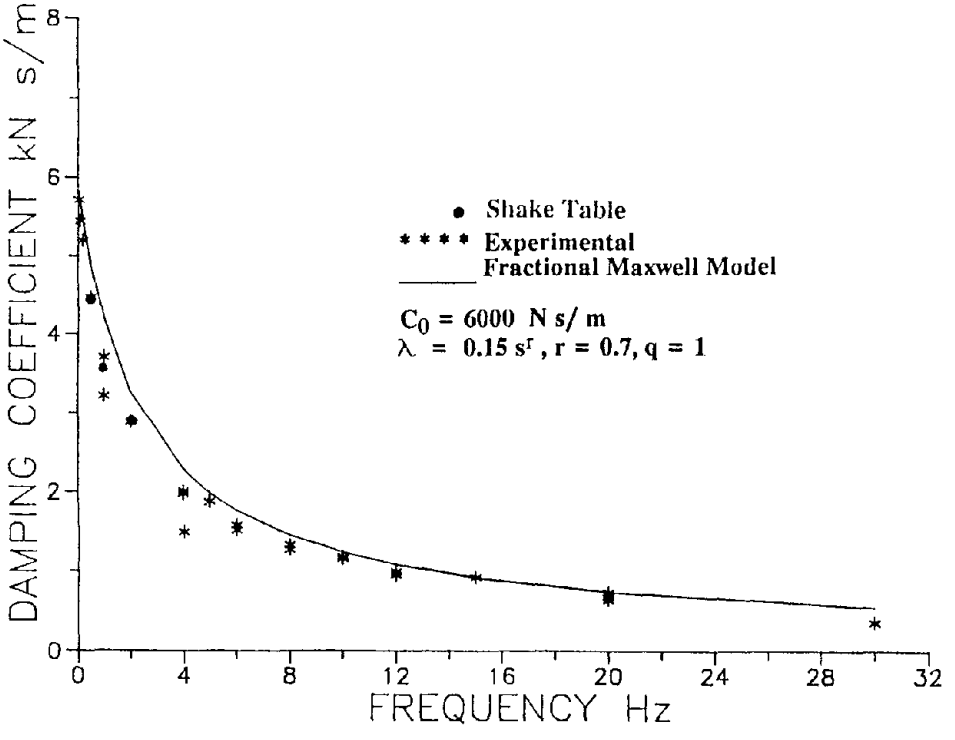

Figure 2-18 Fitting of Damping Coefficient of Tested Damper in Horizontal Motion by Fractional Maxwell Model.

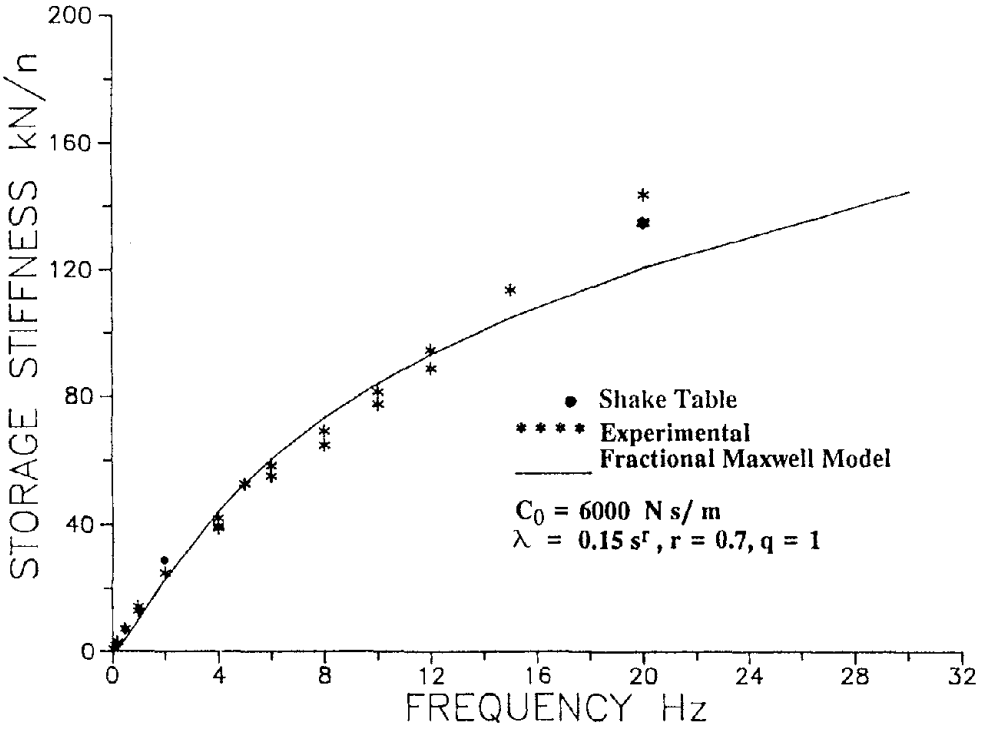

Figure 2-19 Fitting of Storage Stiffness of Tested Damper in Horizontal Motion by Fractional Maxwell Model.

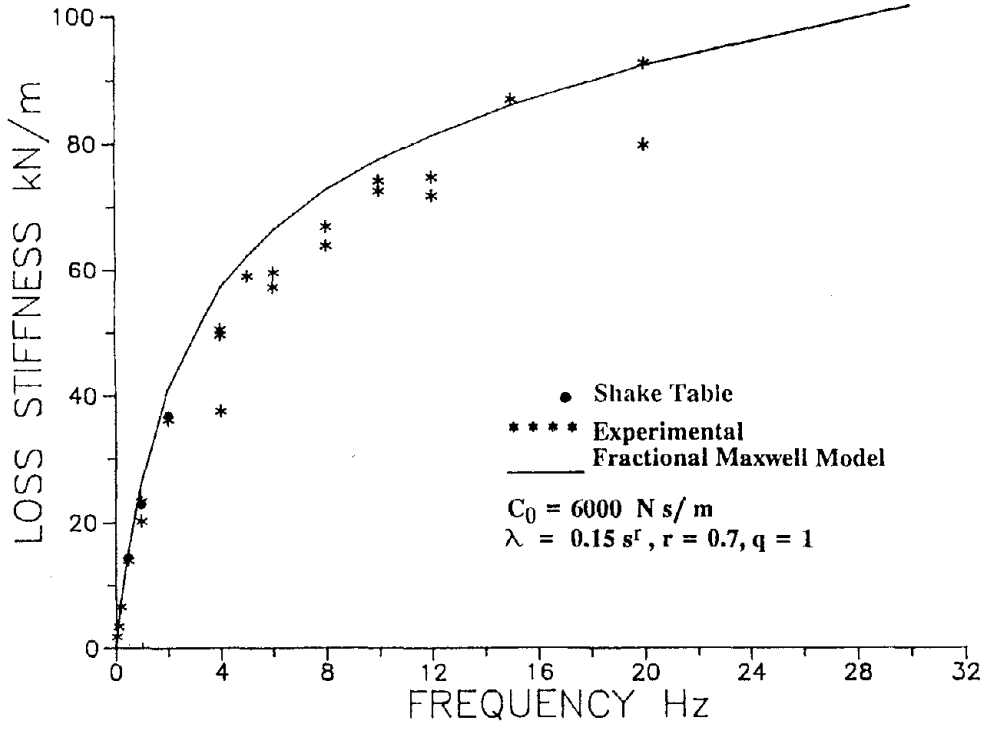

Figure 2-20 Fitting of Loss Stiffness of Tested Damper in Horizontal Motion by Fractional Maxwell Model.

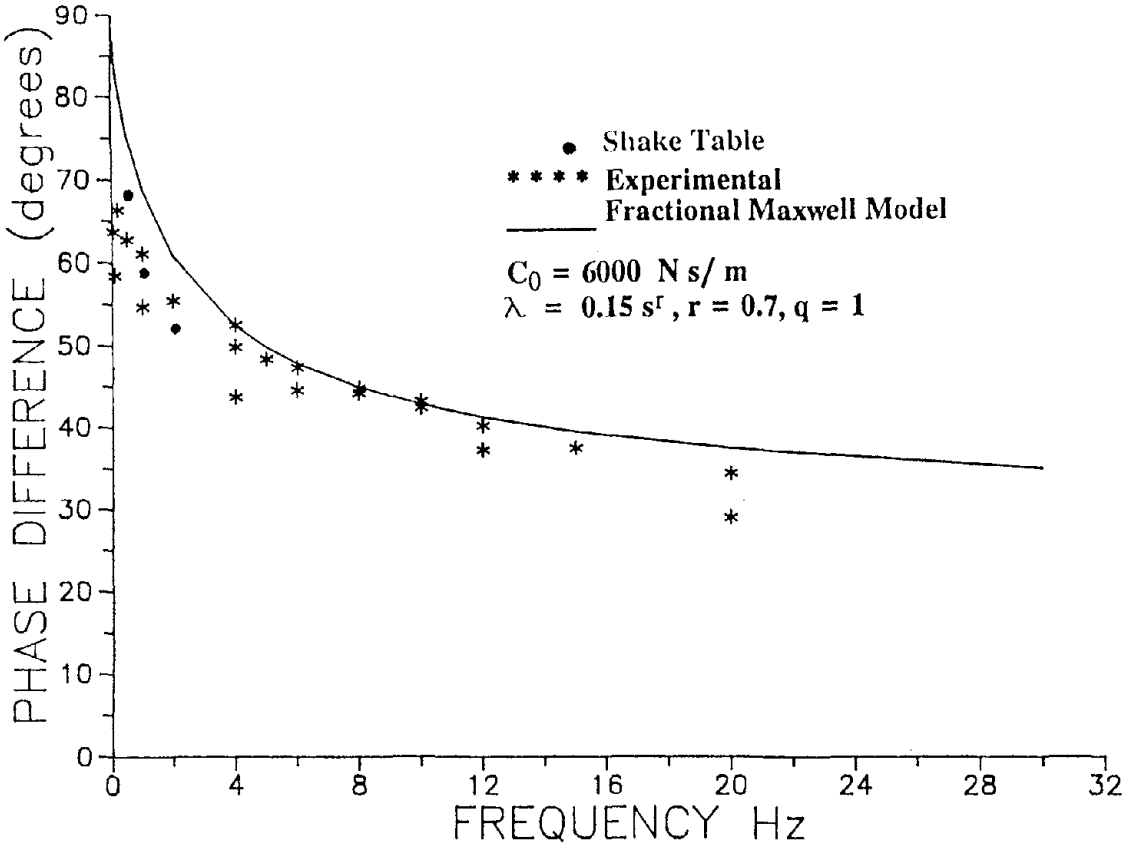

Figure 2-21 Fitting of Phase Difference of Tested Damper in Horizontal Motion by Fractional Maxwell Model.

SECTION 3

VERIFICATION OF MODEL

A model for the force-displacement relationship of viscous dampers has been developed and calibrated. The calibration was based on experimental data under conditions of steady-state motion. For verification, the predictions of the model are compared to experimental results under conditions of transient motion. This requires the development of numerical procedures for the solution of the constitutive relationship, i.e. the solution of equation 2-17 for the time history of force P when the time history of displacement U is known. Two numerical procedures are developed, one valid in the time domain and the other valid in the frequency domain.

3.1 Solution of Constitutive Relation in The Time Domain - G1FP Algorithm

Numerical procedures in the time domain are usually preferred so that nonlinearities can be included if necessary. For example, a time domain analysis procedure is required when viscous dampers are used in isolation systems which incorporate other nonlinear devices like sliding bearings, or in structures which undergo inelastic deformations.

Several algorithms for the numerical evaluation of fractional derivatives are presented by Oldham and Spanier, 1974. One of these algorithms, which is called the "G1-algorithm", is generated from the Grunwald definition of fractional derivative (equation 2-3) by omitting the $N\to\infty$ operation. However, in evaluating the fractional derivative of the force at time t, the value of the force at that time is needed which is unknown. Accordingly, the G1-algorithm has been modified to include an iterative procedure. Equation 2-17 is written (for the case of q=1) as

$$D^r[P(t)] = \frac{1}{\lambda}\left[\mu \frac{du}{dt} - P(t)\right] \qquad (3\text{-}1)$$

where the fractional derivative is given by

$$D^r[P(t)] = \frac{[\frac{t}{N}]^{-r}}{\Gamma(-r)} \sum_{j=0}^{N-1} \frac{\Gamma(j-r)}{\Gamma(j+1)} P(t-j\frac{t}{N}) \qquad (3\text{-}2)$$

The value P(t) is assumed and equation 3-2 is used to evaluate $D^r[P(t)]$. The calculated value is compared to the value calculated from equation 3-1 and iteration is employed with continuous updating of the value of P(t) until the difference between the two calculated values is within a prescribed tolerance. This algorithm we term the "G1FP-algorithm." To expedite the evaluation of the series in equation 3-2, the recursion

$$\frac{\Gamma(j-q)}{\Gamma(j+1)} = \frac{j-q-1}{j} \frac{\Gamma(j-q-1)}{\Gamma(j)} \qquad (3\text{-}3)$$

is used. This avoids explicit use of gamma functions.

The relative error in evaluating the fractional derivative of a function using the G1-algorithm has been determined by Oldham and Spanier, 1974 in selected cases of simple functions in the form of powers of the independent variable. The relative error, defined as the approximate value minus the exact value and divided by the exact value is

$$\epsilon \approx \frac{r^2}{2N} \qquad (3\text{-}4)$$

This equation may be used to establish the number of terms needed in the series of equation 3-2 for specified relative error ϵ. For example, when r=0.7 and ϵ=0.001, N should be larger than 245.

To demonstrate the accuracy of the G1FP-algorithm, an analytical solution of equation 2-17 is presented for the particular case of q=1, r=0.5 and $u=U_o \sin\omega t$. Applying Laplace transform to equation 2-17 we arrive at

$$L[P(t)] = L[\frac{1}{\pi^{1/2} t^{1/2}} - \frac{1}{\lambda} \exp(\frac{t}{\lambda^2}) \operatorname{erfc}(\frac{t^{1/2}}{\lambda})] L[\frac{du}{dt}] \qquad (3\text{-}5)$$

where $L[\ ]$ stands for the Laplace transform of the expression in the brackets and erfc is the complementary error function. Recognizing that equation 3-5 is a convolution, the force P(t) is determined to be

$$P(t)=(2\omega)^{1/2}U_o(\cos\omega t C_2+\sin\omega t\ S_2)$$

$$-\frac{U_o\omega}{\lambda}\cos\omega t\int_o^t \exp\left(\frac{\tau}{\lambda^2}\right)\operatorname{erfc}\left(\frac{\tau^{1/2}}{\lambda}\right)\cos\omega\tau d\tau$$

$$-\frac{U_o\omega}{\lambda}\sin\omega t\int_o^t \exp\left(\frac{\tau}{\lambda^2}\right)\operatorname{erfc}\left(\frac{\tau^{1/2}}{\lambda}\right)\sin\omega\tau d\tau \qquad (3\text{-}6)$$

where C_2 and S_2 are the Fresnel integrals (Abramowitz and Stegun, 1970)

$$C_2=\frac{1}{(2\pi)^{1/2}}\int_o^{\omega t}\frac{\cos z}{z^{1/2}}dz,\quad S_2=\frac{1}{(2\pi)^{1/2}}\int_o^{\omega t}\frac{\sin z}{z^{1/2}}dz \qquad (3\text{-}7)$$

Figure 3-1 compares the analytical solution for the time history of force P to the numerical solution (G1FP algorithm) for the case of a damper with r=0.5, $\lambda=0.3\ (\text{sec})^{0.5}$, C_o=15,000 Ns/m and for displacement with U_o=5.08mm and frequency $f=\omega/2\pi$ = 1 Hz and U_o=2.54mm and f=20Hz. The agreement between analytical and numerical results is very good.

3.2 Solution of Constitutive Relation in the Frequency Domain-DFT Algorithm

Numerical schemes in the frequency domain are very convenient to use but restricted to linear systems. Returning to equation 2-18 we recognize that the expression $K_1(\omega)+iK_2(\omega)$ represents the amplitude and phase angle of the steady-state force in the damper for a harmonic displacement input of unit amplitude. Accordingly, the time history of force is expressed as

$$P(t)=\frac{1}{2\pi}\int_{-\infty}^{\infty}[K_1(\omega)+iK_2(\omega)]\ \bar{u}(\omega)e^{i\omega t}d\omega \qquad (3\text{-}8)$$

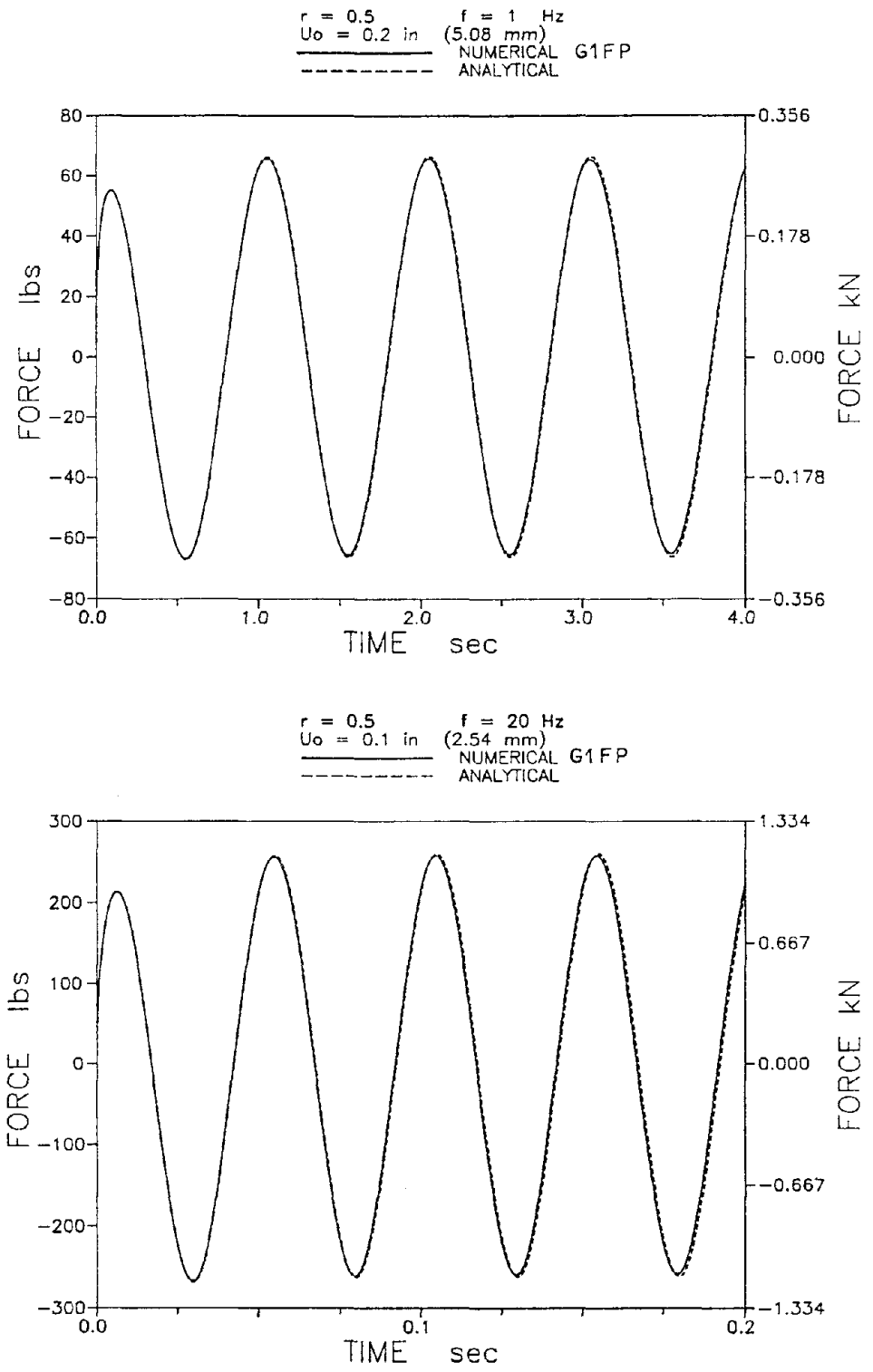

Figure 3-1 Comparison of Analytical Time History of Force in Damper Driven at Harmonic Motion to Numerical Results Obtained by the G1FP-Algorithm.

where $\bar{u}(\omega)$ represents the Fourier transform of the imposed motion. The computation of the force is thus easily obtained by the Discrete Fourier Transform (DFT) approach in combination with Fast Fourier Transform (FFT) algorithms (Veletsos and Ventura, 1985). A particular advantage of equation 3-8 is that it applies to all models of viscoelasticity, provided that parameters K_1 and K_2 are known. In contrast, the GlFP-algorithm (equations 3-1 and 3-2) applies to the specific case of the fractional derivative Maxwell model with q=1.

The DFT-algorithm has been employed in the calculation of the time history of force when input is the displacement history used in the experiments for the calibration of the model (see Table 2-I). In this respect, equation 3-8 has been used with u(t) being the measured displacement of the piston of the damper which was available in discretized form. Figures 3-2 compare the experimental force-displacement loops to the analytically determined loops. The agreement is excellent. It should be observed that the model predicts every detail of the experimental response including the transient part at the initiation of motion.

3.3 Verification Tests

The results shown in Figures 3-2 provide a verification of the developed fractional derivative Maxwell model for viscous dampers. However, in these tests the motion of the piston had a simple form and contained only a single frequency. Further tests were conducted with more complicated motion of the piston and the experimental results have been compared to predictions of the model. All tests were with motion in the vertical direction.

In one set of verification tests the motion was harmonic with time dependent frequency and amplitude. The displacement was specified as either

$$u=U_o \sin[\omega(t)\ t] \qquad (3\text{-}9)$$

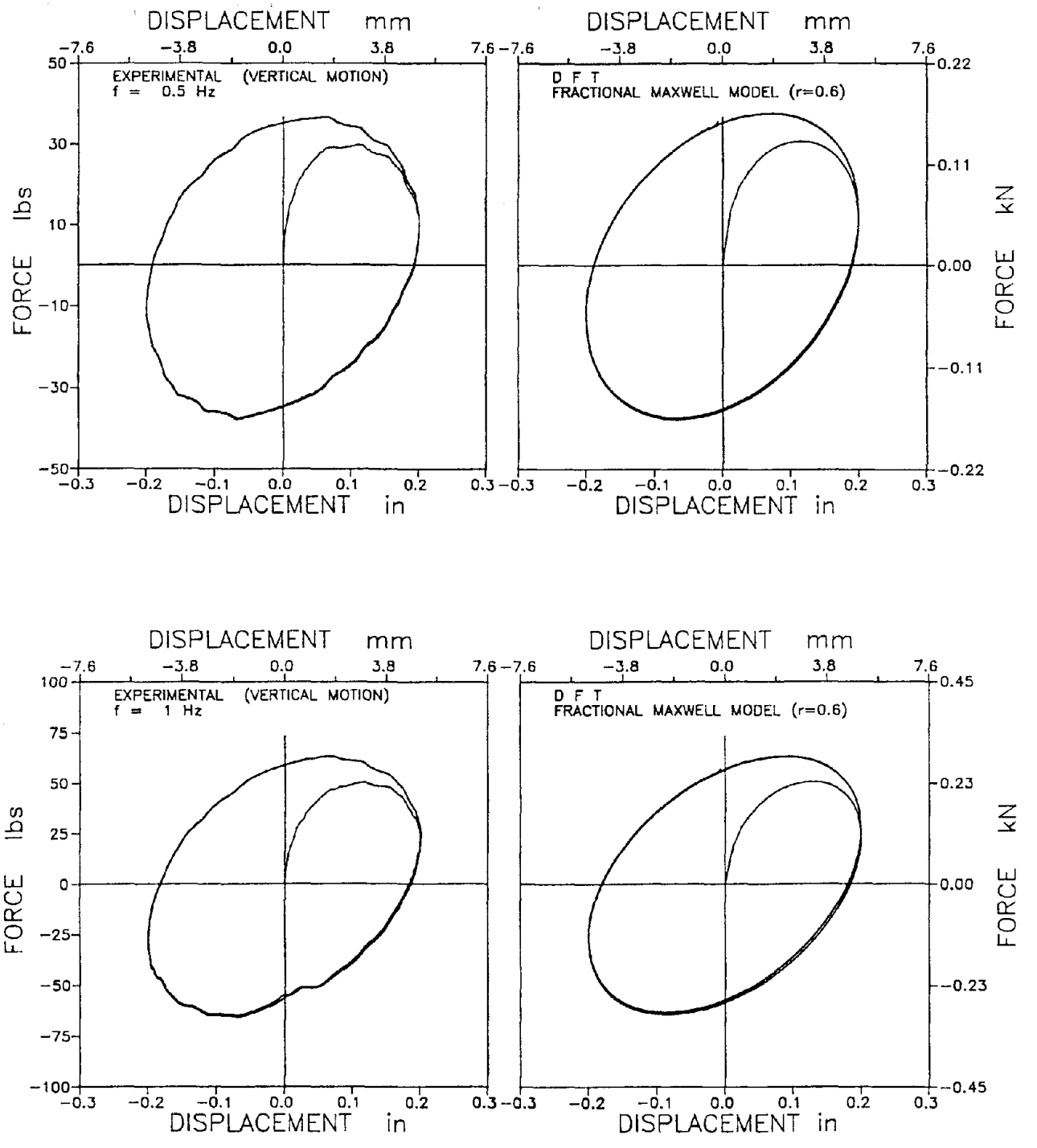

Figure 3-2 Comparison of Recorded Force-Displacement Loops of Damper for Vertical Motion to Loops Predicted by the Fractional Maxwell Model. Solution by the DFT Algorithm.

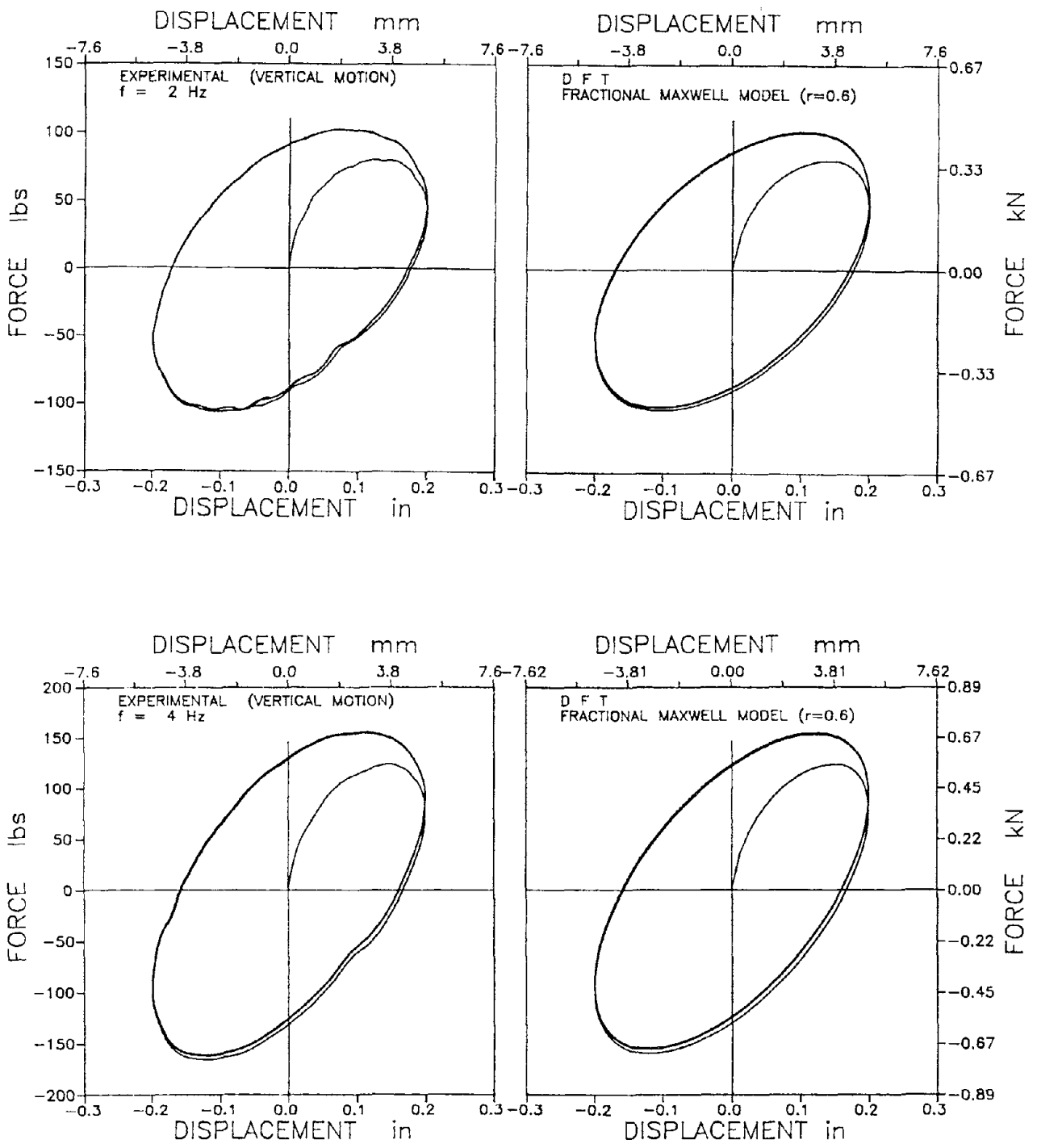

Figure 3-2 Continued.

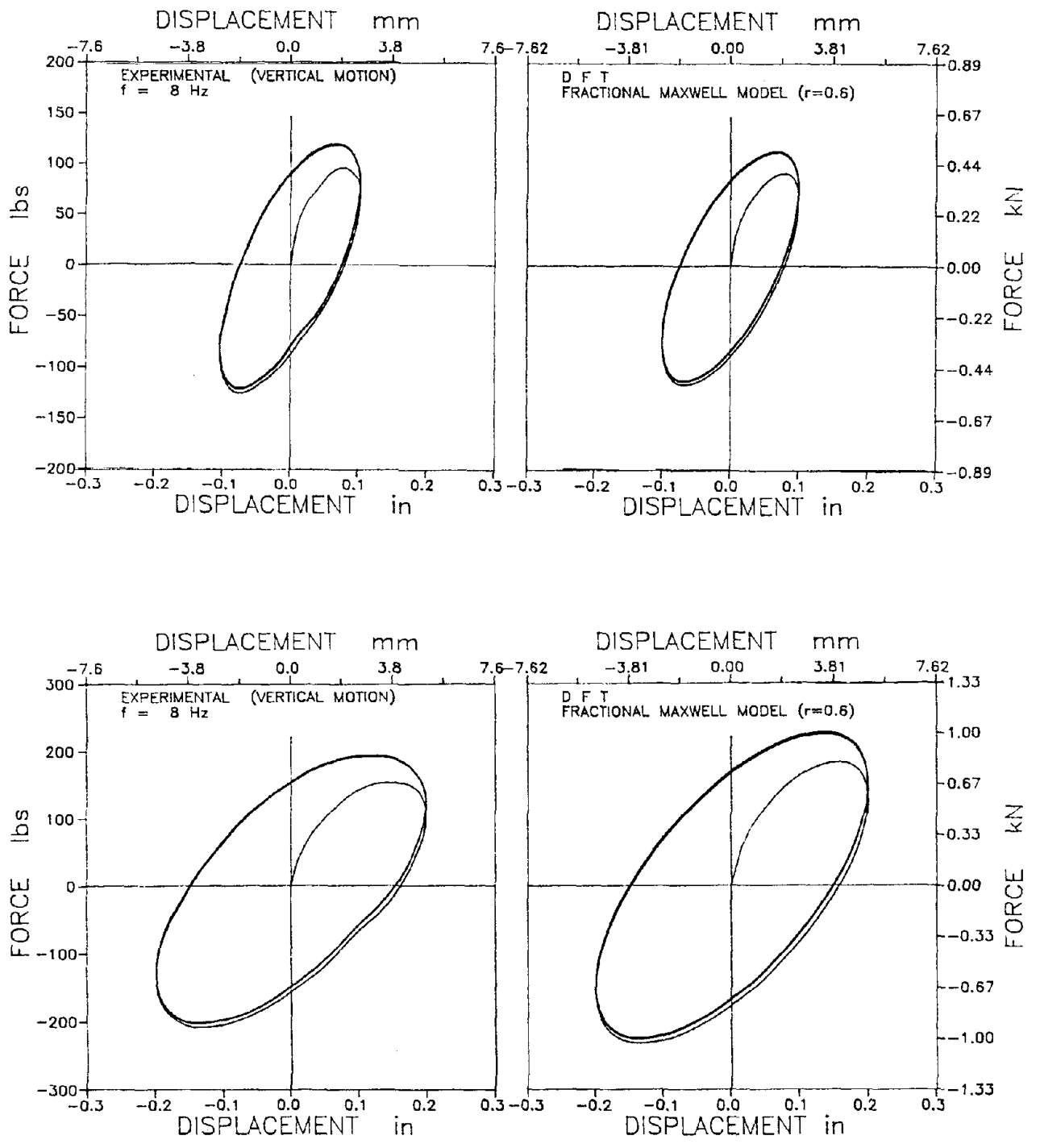

Figure 3-2 Continued.

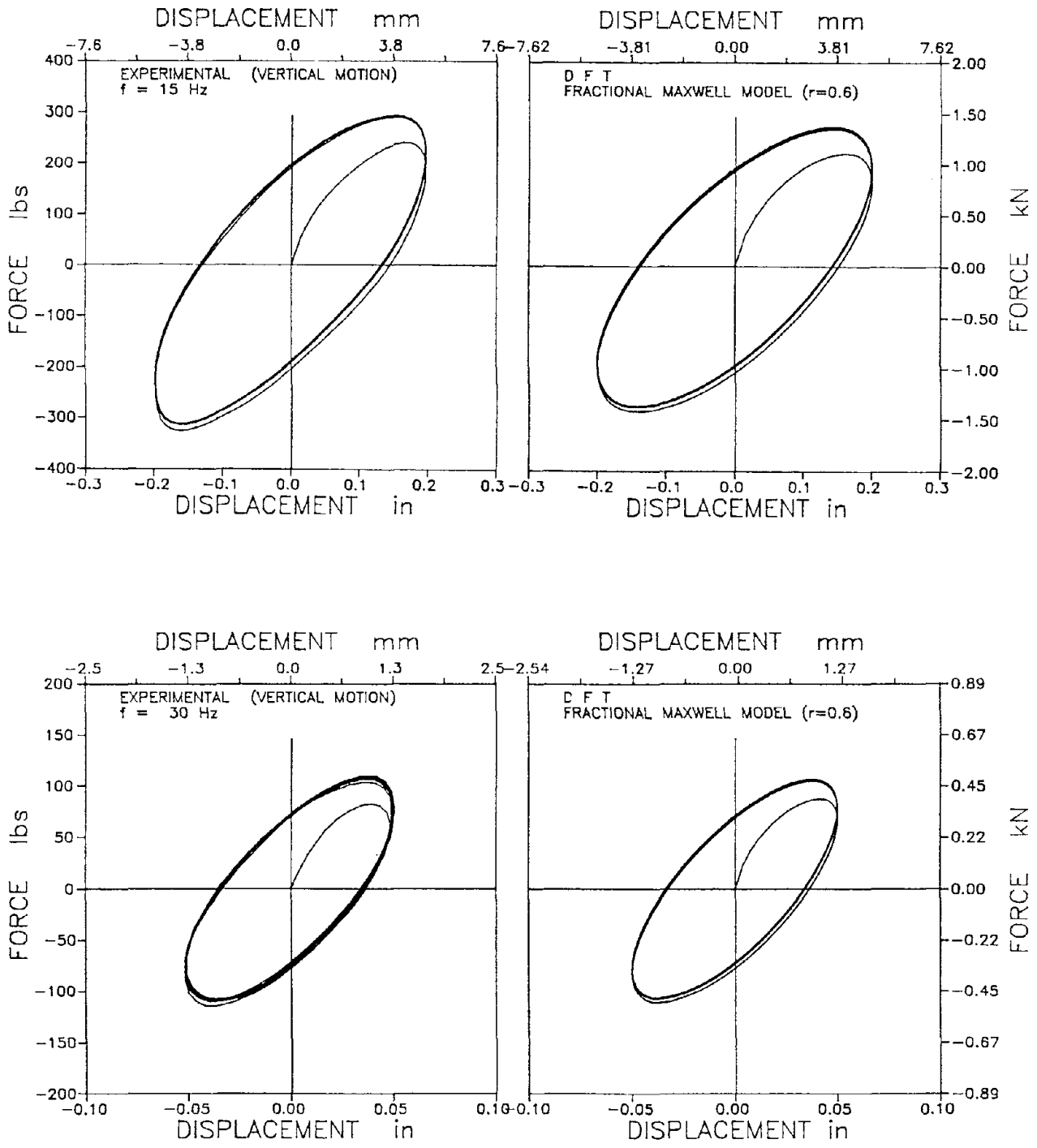

Figure 3-2 Continued.

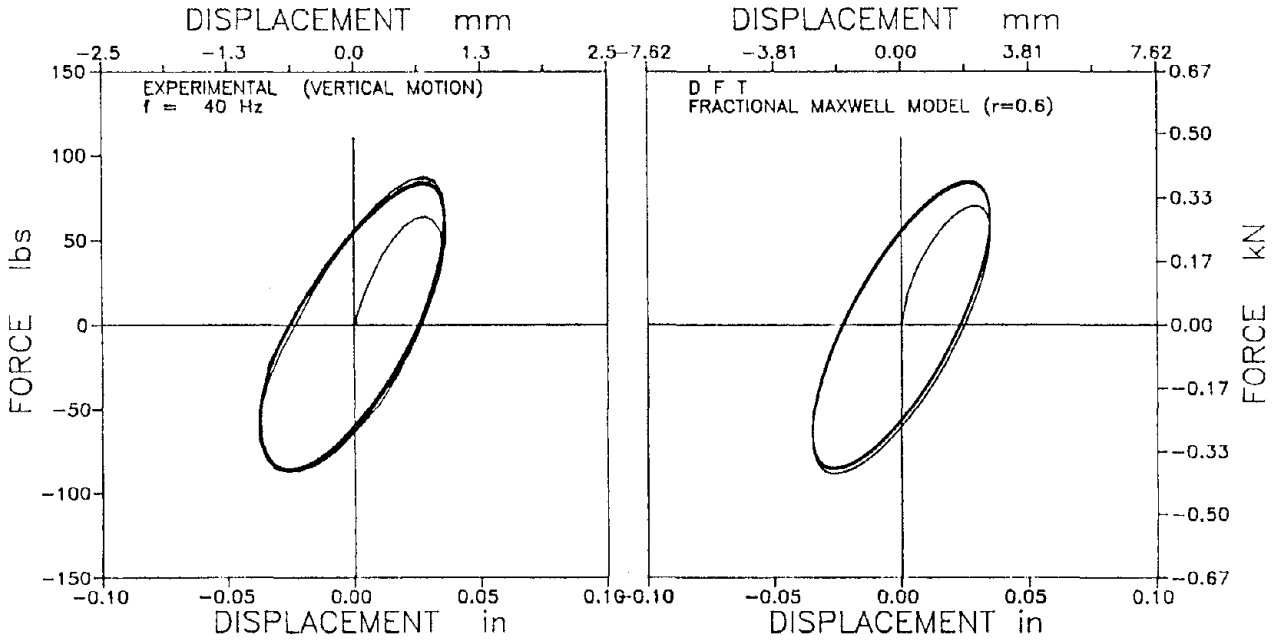

Figure 3-2 Continued.

or as

$$u=2U_o\frac{(t_m-t)}{t_m}\sin[\omega(t)\ t] \tag{3-10}$$

where

$$\omega(t) = \frac{ft}{2\pi\ t_m} \tag{3-11}$$

with U_o=2.54mm (0.1 in.), t_m=9 sec and f=20 Hz. The displacement histories were digitized and used as input to the actuator in the testing arrangement of Figure 2-6. The experiments were run for time t between 0 and 2 secs. In this time interval, the frequency of motion (equation 3-11) changes from 0 to 4.45 Hz. In this range of frequencies the properties of the damper change by several orders of magnitude (see Figures 2-8 to 2-11). Figures 3-3 and 3-4 show the experimental loops in the two tests together with the loops predicted by the model and calculated by the GIFP and DFT algorithms, respectively. The figure on top is for the constant amplitude motion (equation 3-9) and the figure at the bottom is for the variable amplitude motion (equation 3-10). The agreement between analytical and experimental results is very good.

In another test, the input motion was a four cycle beat described by

$$u=U_o\ (\sin\omega_1 t + \sin\omega_2 t) \tag{3-12}$$

with U_o=2.54mm (0.1 in.), ω_1= 4π r/s (2 Hz) and ω_2=5π r/s (2.5 Hz). The experimental loop together with the predicted loop (DFT algorithm) are shown in Figure 3-5. The agreement is very good.

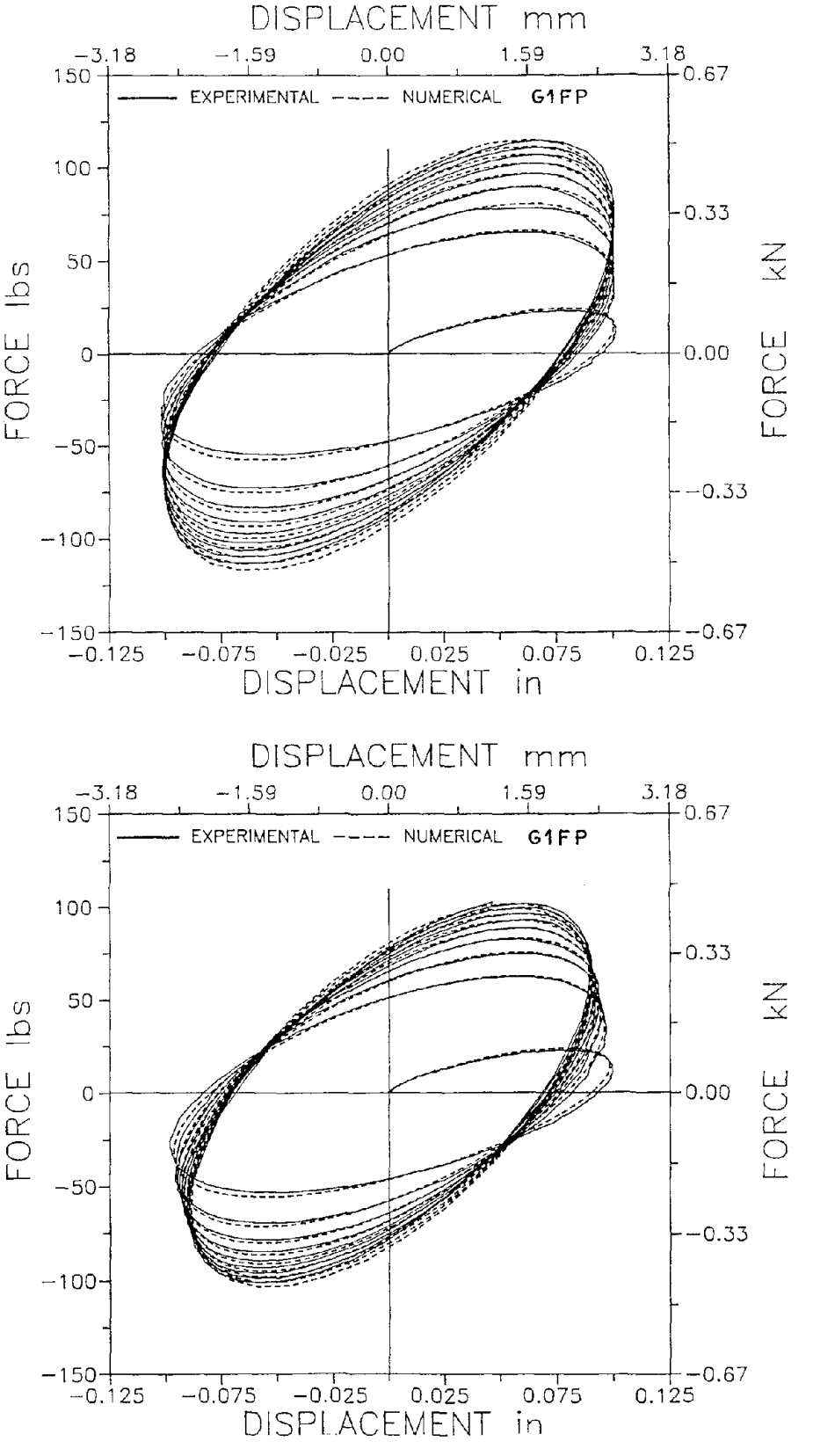

Figure 3-3 Recorded Force-Displacement Loop of Damper for Vertical Motion of Varying Frequency and Constant (Top) or Varying Amplitude (Bottom) and Comparison to Loop Predicted by Fractional Maxwell Model. Solution by G1FP-Algorithm.

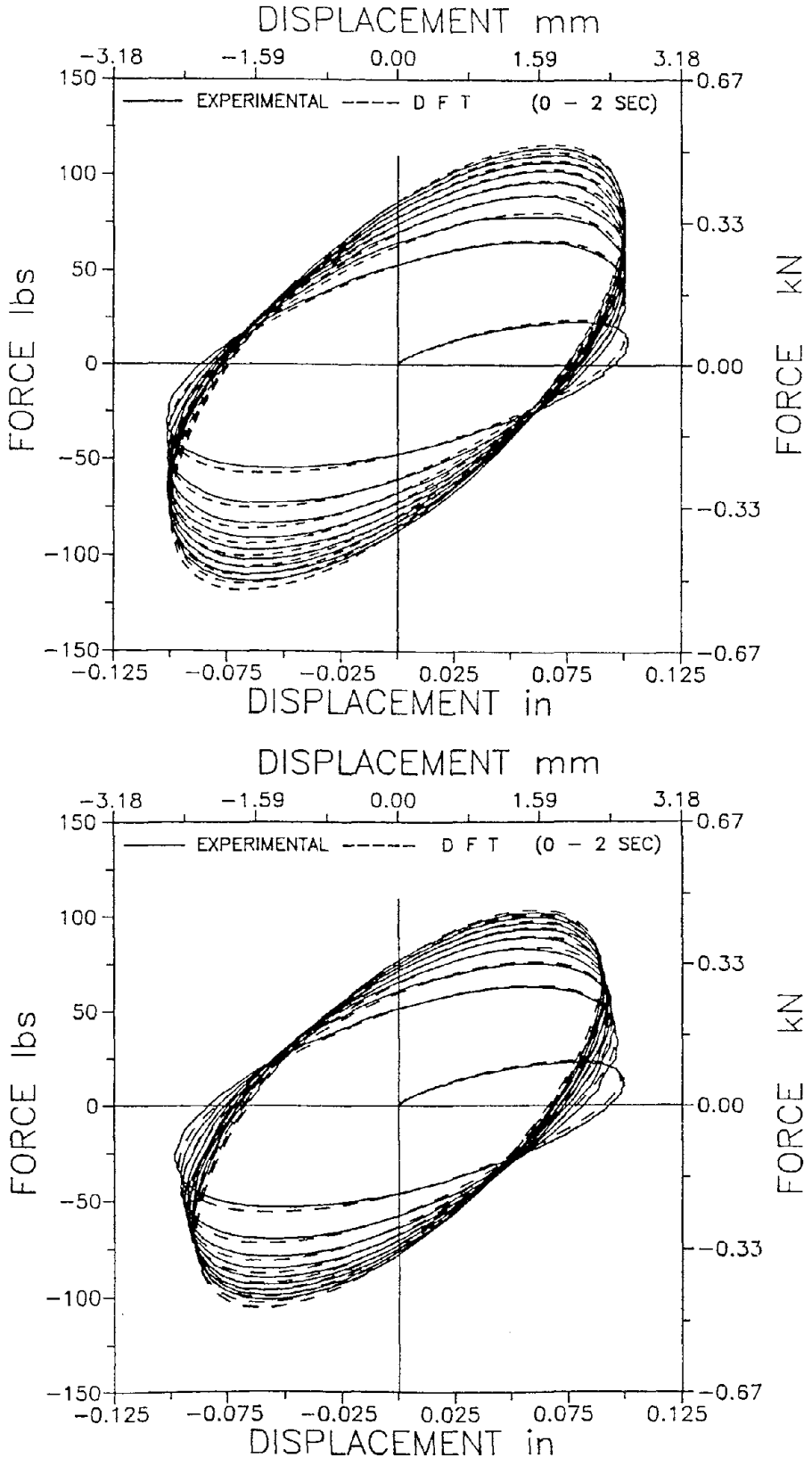

Figure 3-4 Recorded Force-Displacement Loop of Damper for Vertical Motion of Varying Frequency and Constant (Top) or Varying Amplitude (Bottom) and Comparison to Loop Predicted by Fractional Maxwell Model. Solution by DFT-Algorithm.

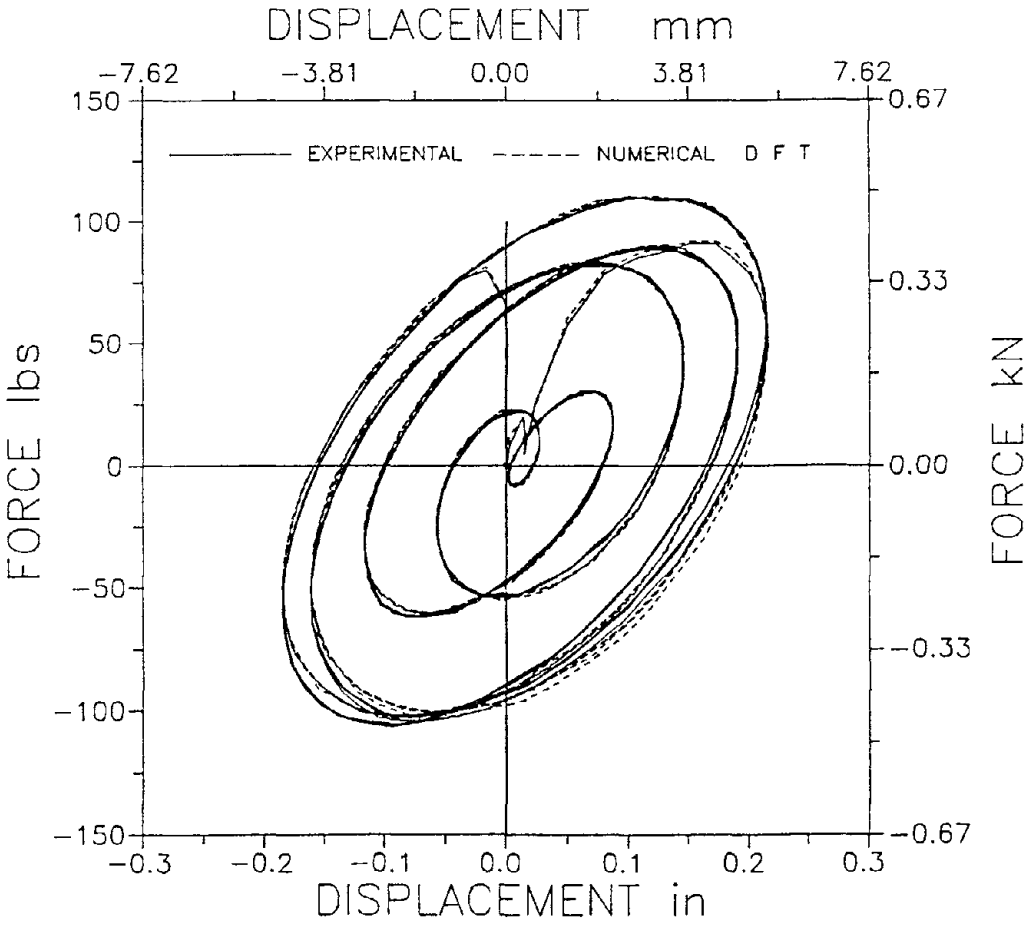

Figure 3-5 Recorded Force-Displacement Loop of Damper for Vertical 4-Cycle Beat Displacement and Comparison to Loop Predicted by Fractional Maxwell Model. Solution by DFT-Algorithm.

SECTION 4

VISCODAMPER OSCILLATOR

A viscodamper oscillator is defined as a single-degree-of-freedom (SDOF) spring-mass system with viscous dampers. It represents the simplest model of a vibration isolation system.

4.1 Frequency and Damping Ratio in Free Vibration

The equation of motion of a free vibrating viscodamper oscillator is

$$m\ddot{u}(t)+K\,u(t) + P(t) = 0 \tag{4-1}$$

$$P(t) + \lambda D^{r}[P(t)] = C_o \frac{du}{dt} \tag{4-2}$$

where m is the mass, K is the stiffness of spring, u(t) is the displacement and P(t) is the force from viscous dampers.

The eigenvalue problem of equations 4-1 and 4-2 is produced by applying Laplace transform and deriving the characteristic equation in terms of the Laplace transform parameter s

$$s^2 + \frac{2\xi_d\omega_o S}{1+\lambda s^r} + \omega_o{}^2 = 0 \tag{4-3}$$

where

$$\omega_o = \left(\frac{K}{m}\right)^{1/2} \tag{4-4}$$

$$\xi_d = \frac{C_o}{2(mK)^{1/2}} \tag{4-5}$$

In equations 4-4 and 4-5, ω_o is recognized is the frequency of free vibration of the oscillator when viscous dampers are not present and ξ_d is recognized as the damping ratio of an oscillator with constant viscous coefficient equal to C_o. Clearing the Laplace parameter from the denominator of equation 4-3,

$$\lambda s^{2+r} + s^2 + 2\xi_d \omega_o s + \lambda \omega_o{}^2 s^r + \omega_o{}^2 = 0 \tag{4-6}$$

The next step is to apply a transformation to equation 4-6 which produces a polynomial equation. In the particular case of r=0.6 (vertical vibration of viscous dampers) the transformation is

$$\sigma = s^{1/5} \tag{4-7}$$

The result is

$$\lambda \sigma^{13} + \sigma^{10} + 2\xi_d \omega_o \sigma^5 + \lambda \omega_o{}^2 \sigma^3 + \omega_o = 0 \tag{4-8}$$

The solution of equation 4-8 results in 13 eigenvalues. Raising these eigenvalues to the power of 5 we obtain the complex roots of equation 4-6. For an underdamped system (a system that has oscillatory behavior), the complex roots which correspond to the natural frequency of the system will appear as a conjugate pair

$$s = s_R \pm i\, s_I \tag{4-9}$$

from where the natural frequency ω_1 and damping ratio ξ_1 are derived

$$\omega_1 = (s_R{}^2 + s_I{}^2)^{1/2} \tag{4-10}$$

$$\xi_1 = \frac{s_R}{\omega_1} \tag{4-11}$$

To identify the complex roots that correspond to the natural frequency, their phase angle must be calculated and found to lie in the range of -180 to 180^{o}. Only one conjugate pair of roots can satisfy this condition. The remaining roots are not associated with frequenices but rather describe the nonoscillatory behavior of the system.

For the proof of equations 4-10 and 4-11 consider the SDOF viscous oscillator with frequency ω_1 and damping ratio ξ_1. Its characteristic equation in terms of the Fourier parameter ω is

$$\omega^2 - 2i\xi_1\omega_1\omega - \omega_1^2 = 0 \tag{4-12}$$

with roots

$$\omega = \pm \omega_1(1-\xi_1^2)^{1/2} + i\xi_1\omega_1 \tag{4-13}$$

Using the relation between Laplace and Fourier parameters, $s = -i\omega$,

$$s = \xi_1\omega_1 \mp i\,\omega_1\,(1-\xi_1^2)^{1/2} \tag{4-14}$$

By comparing equations 4-9 and 4-14, equations 4-10 and 4-11 are derived.

The procedure described above has been implemented in the case of a viscodamper oscillator with viscous dampers moving in the vertical direction. Parameters λ and r were 0.3 $(sec)^{0.6}$ and 0.6 as determined in the experiments. The frequency $f_1 = \omega_1/2\pi$ and damping ratio ξ_1 were calculated for a system with $f_o = \omega_o/2\pi$ in the range of 0.5 to 10 Hz and ξ_d (equation 4-5) in the range of 0.5 to 2.5. The results are plotted in Figure 4-1. The figure demonstrates that frequency f_1 is always larger than f_o. This, of course, is a result of the stiffening effect of viscous dampers.

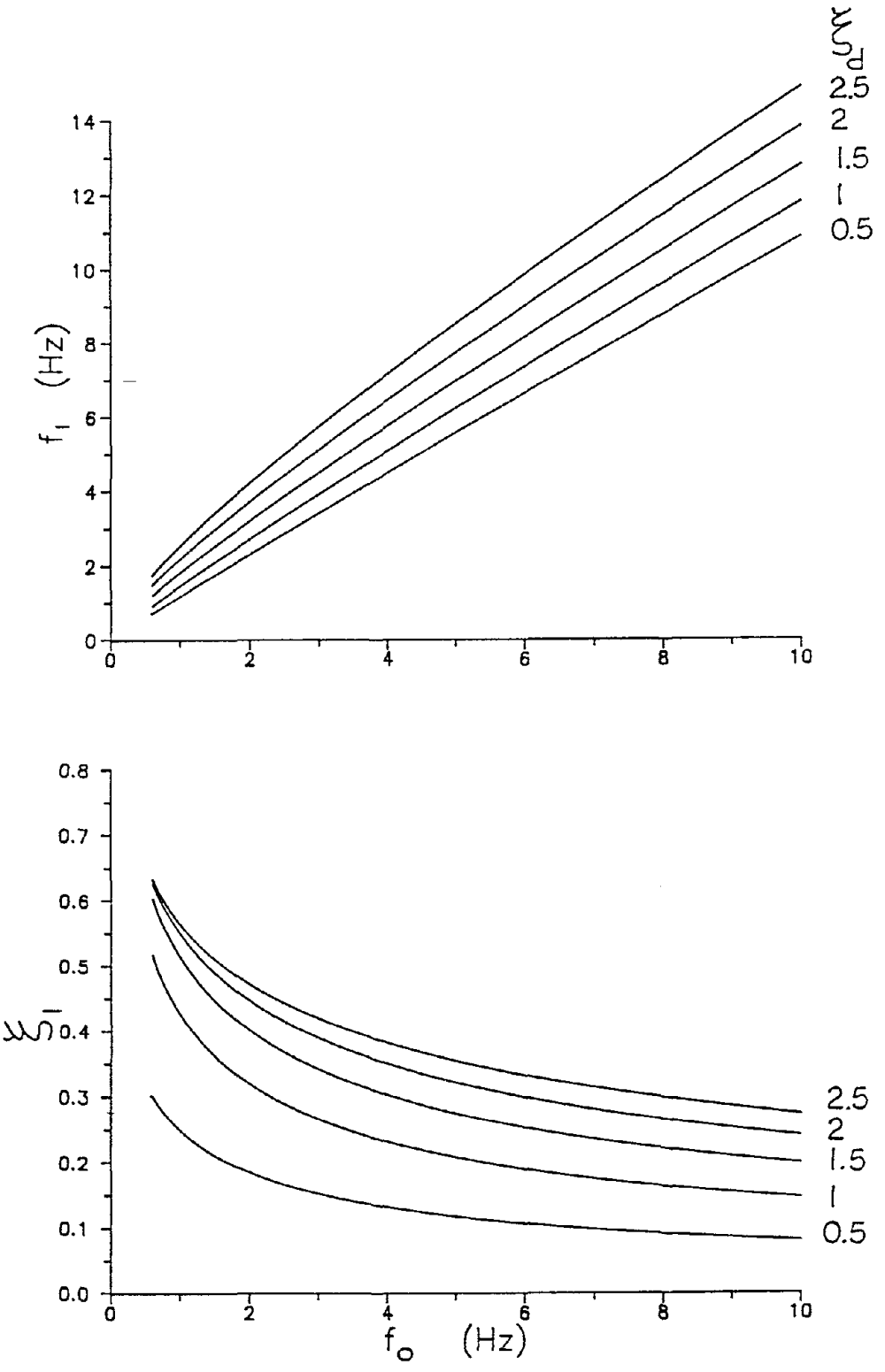

Figure 4-1 Frequency and Damping Ratio of Viscodamper Oscillator for $\lambda=0.3(\text{sec})^{0.6}$ and r=0.6.

Figure 4-1 may be used as a design tool for vibration isolation systems. Consider for example that a system with 60,000 Kg mass is to be supported by springs and viscous dampers for vibration isolation. A frequency of 5 Hz and damping ratio of about 0.25 are desired. From Figure 4-1 we determine that a design with f_o = 4 Hz and ξ_d = 1 will satisfy these requirements. Using equations 4-4 and 4-5, we determine K = 37899 kN/m and C_o = 3016 kNs/m. With these values known, springs and viscous dampers could be selected for the isolation system. It should be noted that the determined values for K and C_o are valid only for values of parameters λ and r equal to 0.3 $(sec)^{0.6}$ and 0.6, respectively. This means that viscous dampers of different size have identical parameters λ and r and differ only in the value of constant C_o. Commercially available viscous dampers of different sizes exhibit properties that have almost identical variation with frequency (GERB, 1986). This confirms the above hypothesis.

The calculation of the frequency and damping ratio of a viscodamper oscillator is a complex procedure. In this respect, the development of an approximate but simple procedure is of practical significance. For this we recall that under steady-state conditions, the force needed for maintaining harmonic motion of the damper with displacement u and velocity $\dot{u}$ is given by

$$P = K_1(\omega)\ u + C(\omega)\ \dot{u} \tag{4-15}$$

where ω is the frequency of motion and K_1 and C are the storage stiffness and damping coefficient of the damper. Accordingly, a new oscillator is defined whose equation of free vibration is

$$m\ddot{u} + C\ (\Omega)\ \dot{u} + [K+K_1(\Omega)]\ u = 0 \tag{4-16}$$

where Ω is an arbitrary frequency. This oscillator we term the <u>equivalent viscous oscillator</u>. More conveniently, equation 4-16 is written as

$$\ddot{u} + 2\xi_e\omega_e\dot{u} + \omega_e{}^2 u = 0 \tag{4-17}$$

where ω_e and ξ_e are the natural frequency and damping ratio of the equivalent viscous oscillator. These parameters are determined from the expressions for the storage stiffness and damping coefficient of viscous dampers which were presented in section 3,

$$\omega_e = \omega_o[1+ \frac{2\xi_d\lambda\Omega^{1+r}s}{\omega_o(1+\lambda^2\Omega^{2r}+2\lambda\Omega^r c)}]^{1/2} \tag{4-18}$$

$$\xi_e = \frac{\xi_d\omega_o(1+\lambda\Omega^r c)}{\omega_e(1+\lambda^2\Omega^{2r}+2\lambda\Omega^r c)} \tag{4-19}$$

where s and c stand for the sine and cosine of $r\pi/2$. When ω_e and ξ_e are evaluated at frequency $\Omega=\omega_e$, they represent approximations to the exact frequency ω_1 and damping ratio ξ_1 of the viscodamper oscillator. For the evaluation, an iterative procedure is required, starting from $\Omega=\omega_o$. Figure 4-2 compares the frequency and damping ratio of the viscodamper and equivalent viscous oscillators for the range of parameters with most interest in vibration isolation applications ($\xi_1 \leq 0.3$, $f_o \leq 10$ Hz). In Figure 4-2, $\lambda=0.3(\text{sec})^{0.6}$, $r=0.6$ and $f_e=\omega_e/2\pi$. The agreement between approximate and exact values is good. Some discrepancies are observed in the values of frequency when f_o is less than about 3 Hz and ξ_d is larger than 1.5. This combination results in unrealistic values of ξ_1 (exceeding unity).

The accuracy of the approximate procedure is further investigated for other values of parameters λ and r in Figure 4-3. Exact values of frequency f_1 and damping ratio ξ_1 (solid line) are compared to approximate values f_e and ξ_e (dashed line) for a system with $f_o=5$ Hz, $\xi_d=0.5$ and λ in the range of 0 to $1(\text{sec})^r$ where r=0, 0.3, 0.6 and 1. The case r=1 corresponds to the conventional Maxwell model, whereas the case r=0 corresponds to the simple linear dashpot model with damping constant equal to $C_o/(1+\lambda)$ where now λ is dimensionless.

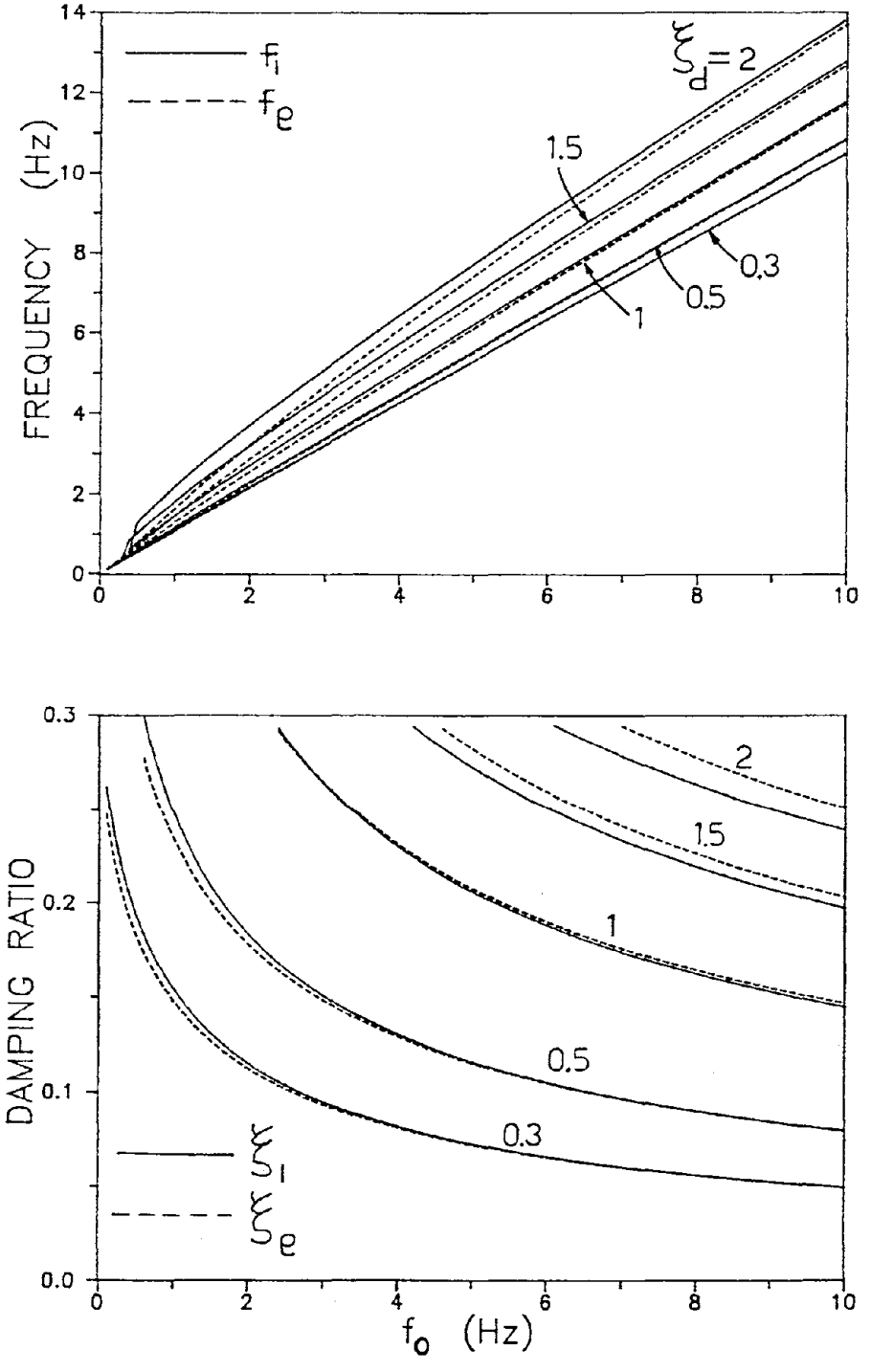

Figure 4-2 Comparison of Exact Frequency and Damping Ratio of Viscodamper Oscillator to Frequency and Damping Ratio of Equivalent Viscous Oscillator for $\lambda=0.3(\text{sec})^{0.6}$ and r=0.6.

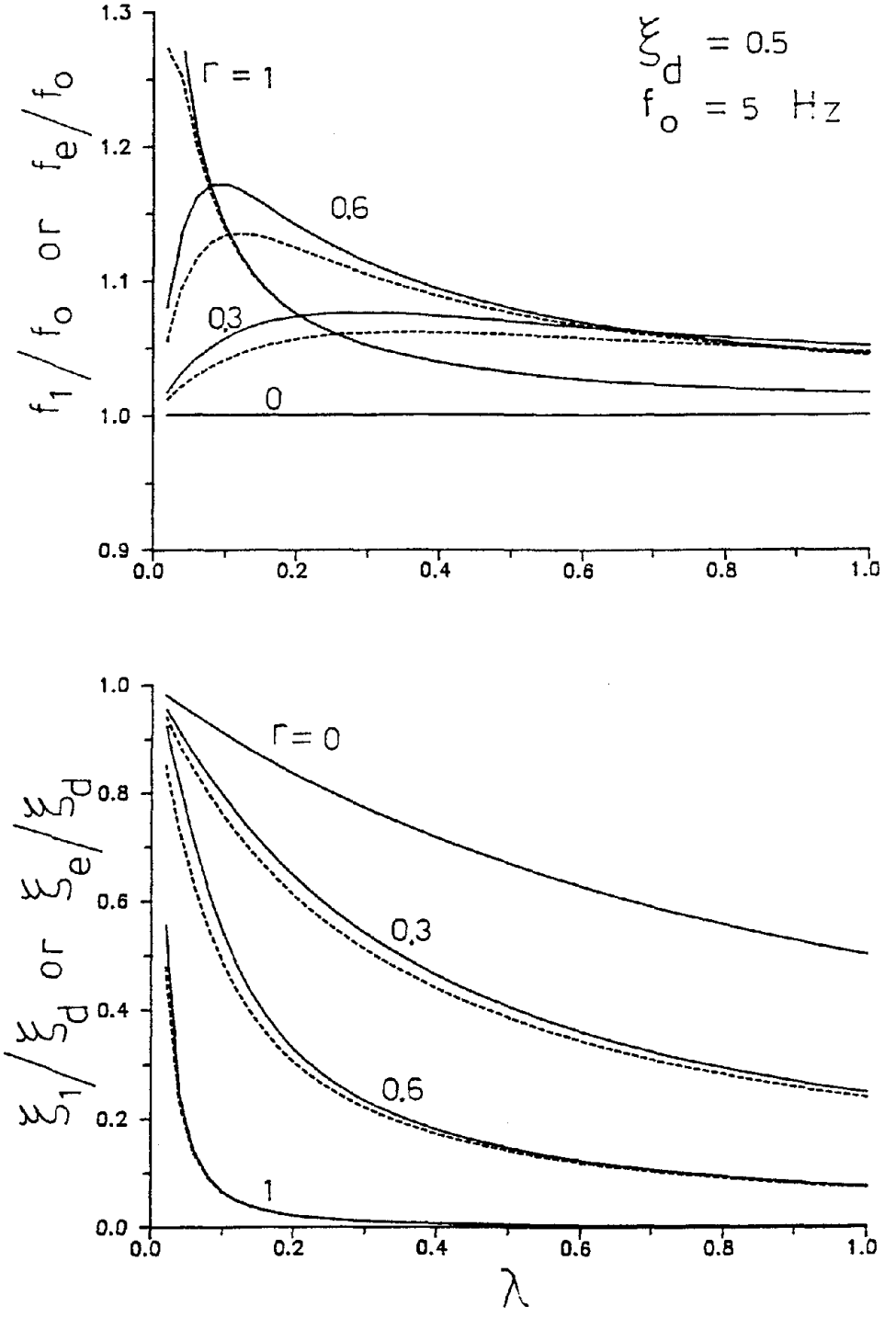

Figure 4-3 Comparison of Exact Frequency and Damping Ratio of Viscodamper Oscillator to Frequency and Damping Ratio of Equivalent Viscous Oscillator for other Values of λ and r.

Very good agreement between exact and approximate values is observed. The largest error in the approximate frequency is about 3% of the exact value, which corresponds to about 7% underestimation of the effective stiffness.

Concluding, procedures have been established for the determination and identification of the frequency and damping ratio of the viscodamper oscillator. Furthermore, a simple procedure has been presented for determining approximate values of these quantities.

4.2 Steady-State Harmonic Response of Viscodamper Oscillator

When the viscodamper oscillator is subjected to dynamic loading, the equation of motion is

$$m\ddot{u}(t) + K\,u(t) + P(t) = F(t) \tag{4-20}$$

where P(t) is given by equation 4-2. The frequency response function of the viscodamper oscillator is easily derived by employing Fourier transform to equation 4-20,

$$H(\omega) = \frac{\bar{u}(\omega)}{\bar{F}(\omega)} = \frac{1}{K}\left[1-\beta^2 + \frac{2i\xi_d\beta}{1+i^r\beta^r\nu}\right]^{-1} \tag{4-21}$$

where

$$\beta = \frac{\omega}{\omega_o} \tag{4-22}$$

$$\nu = \lambda\omega_o{}^r \tag{4-23}$$

and $\bar{u}(\omega)$, $\bar{F}(\omega)$ represent the Fourier amplitude of u(t) and F(t), respectively. It should be noted that equation 4-21 reduces to the equation for a SDOF viscous oscillator with natural frequency ω_o and damping ratio ξ_d when ν=0.

For a harmonic forcing function $F(t) = F_o \sin \omega t$, the steady-state displacement response is given by

$$u(t) = \frac{F_o}{K} D \sin(\omega t - \theta) \tag{4-24}$$

$$D = \left\{ \frac{(1+\beta^r \nu c)^2 + (\beta^r \nu s)^2}{(1-\beta^2)^2(1+\beta^r \nu c)^2 + [(1-\beta^2)\beta^r \nu s + 2\xi_d \beta]^2} \right\}^{1/2} \tag{4-25}$$

$$\tan\theta = \frac{2\xi_d \beta(1+\beta^r \nu c)}{(1-\beta^2)[(1+\beta^r \nu c)^2 + (\beta^r \nu s)^2] + 2\xi_d \beta^{1+r} \nu s} \tag{4-26}$$

In the above equations c and s stand for the cosine and sine of $r\pi/2$. In equations 4-24 to 4-26, D represents the dynamic magnification factor and θ represents the phase angle. They are the amplitude and phase of the complex frequency response function (equation 4-21), respectively. Equation 4-24 is, of course, valid in the limit of large time and provided that a sinusoidal force acting on the viscodamper oscillator produces a sinusoidal displacement after transients have died out. Analytic proof for this behavior is presented in Appendix A.

The maximum force exerted against the base of the oscillator by the spring and viscous damper upon division by the amplitude of the driving force, F_o, gives the absolute transmissibility

$$TR = \left\{ \frac{(1+\beta^r \nu c)^2 + (\beta^r \nu s)^2 + (2\xi_d \beta)^2 + 4\xi_d \beta^{1+r} \nu s}{(1-\beta^2)^2(1+\beta^r \nu c)^2 + [(1-\beta^2)\beta^r \nu s + 2\xi_d \beta]^2} \right\}^{1/2} \tag{4-27}$$

in which again s and c stand for sine and cosine of $r\pi/2$. The absolute transmissibility has been derived by the following procedure. The force exerted against the base is given by

$$F_T(t) = P(t) + K\, u(t) \tag{4-28}$$

Applying Fourier transform to equation 4-28 and using equation 4-21 we obtain

$$\frac{\bar{F}_T(\omega)}{\bar{F}(\omega)} = H(\omega)\left[K + \frac{i\omega C_o}{1+\lambda i^r \omega^r}\right] \tag{4-29}$$

The absolute transmissibility is the amplitude of the complex function on the right side of equation 4-29.

It may be noted that equations 4-25 to 4-27 reduce to those of a SDOF viscous oscillator with natural frequency ω_o and damping ratio ξ_d when ν=0.

Plots of the dynamic magnification factor, D, phase angle, θ, and transmissibility, TR, are shown in Figures 4-4 to 4-5 for a system with $f_o=\omega_o/2\pi$=5 Hz, ν=2.374 and r=0.6. The following significant features of the steady-state response of the viscodamper oscillator can be observed in Figures 4-4 to 4-5:

a. The peak value of the dynamic magnification factor occurs for values of β larger than unity, whereas in the SDOF viscous oscillator this peak occurs at values of β less than unity. This phenomenon is caused by the stiffening effect of the viscous damper.

b. At resonance, β=1, the phase angle θ is equal to $r\pi/2$.

c. The phase angle, θ, does not increase monotonically with increasing frequency ratio β. Rather, it exhibits a peak value, which is always less than π, at a value of β larger than unity. Beyond this value, θ decreases. Again, this result is caused by the stiffening effect of the viscous damper.

d. The curves of transmissibility do not pass through the same point as in the SDOF viscous oscillator. Damping ratio ξ_d tends to reduce the effectiveness of an isolation system for frequency ratio β greater than a

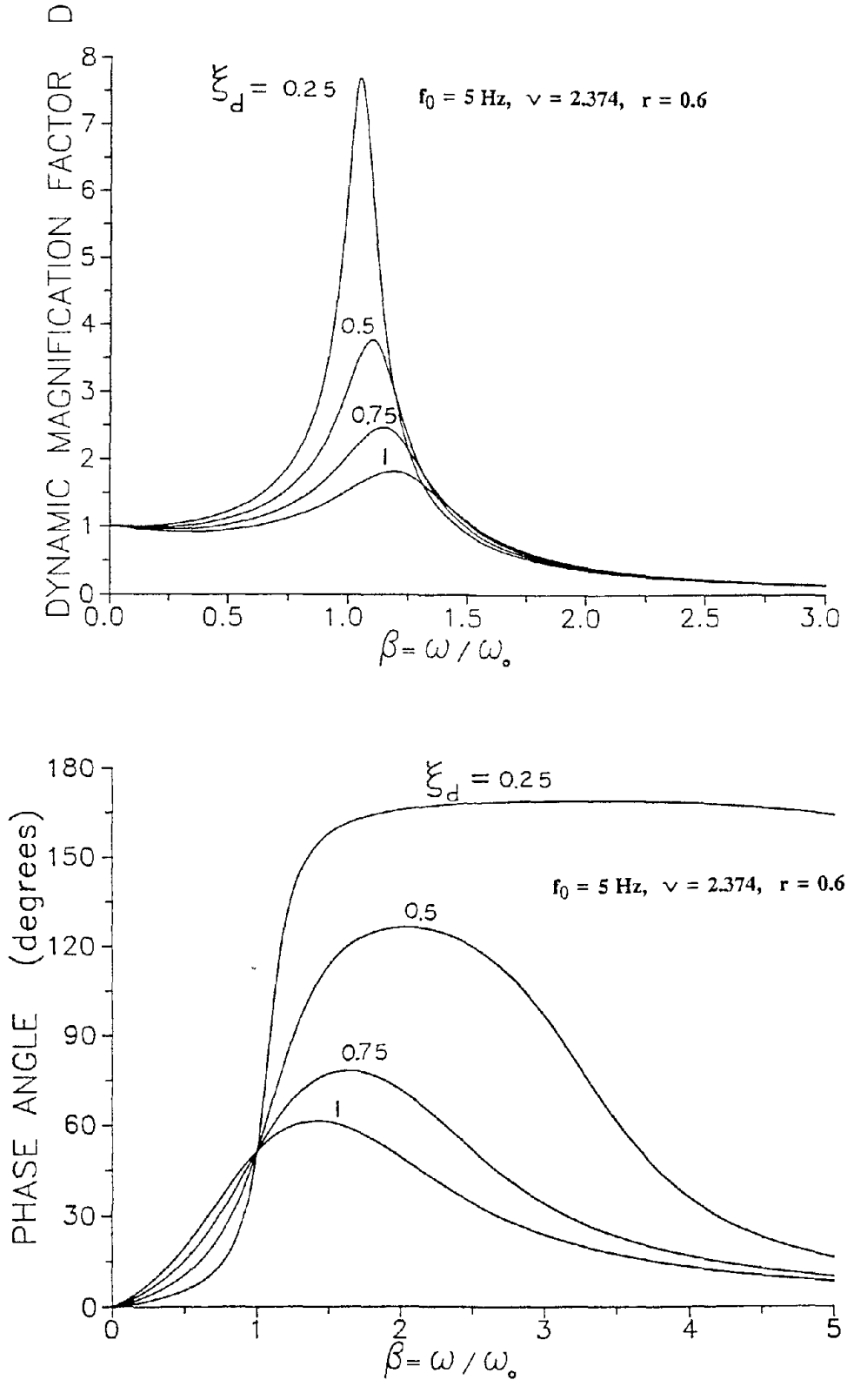

Figure 4-4 Dynamic Magnification Factor and Phase Angle Plot of Viscodamper Oscillator for Steady-State Harmonic Motion.

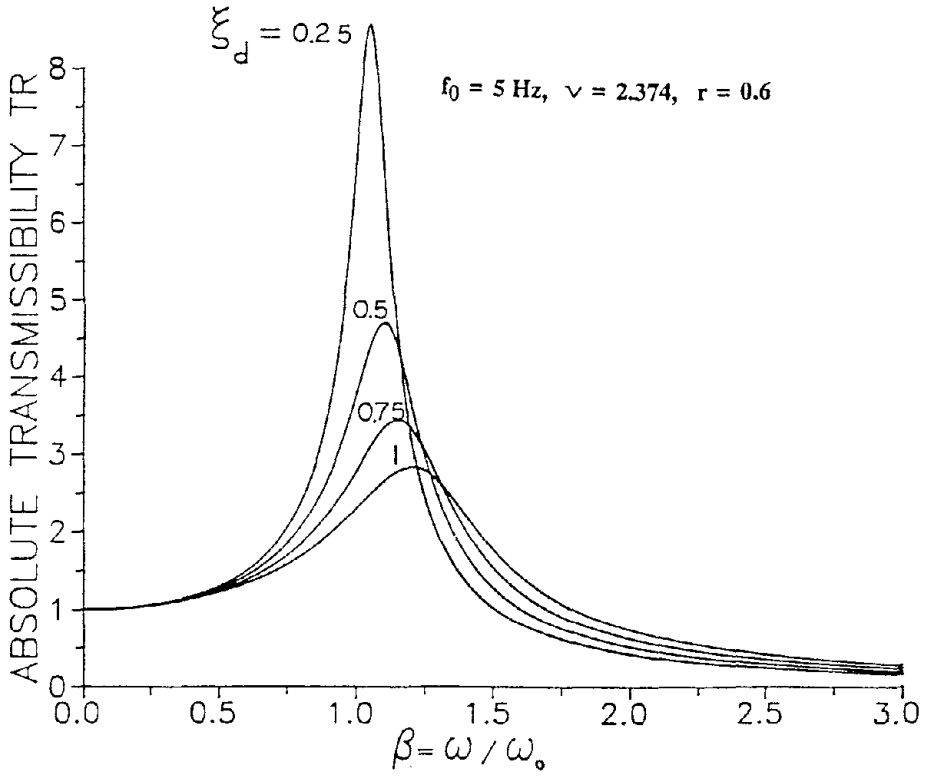

Figure 4-5 Absolute Transmissibility Plot of Viscodamper Oscillator for Steady-State Harmonic Motion.

certain value which, unlike the SDOF viscous oscillator, is not fixed but rather depends on the system's parameters.

The presented results on the harmonic steady-state response of the viscodamper oscillator may be used in constructing design charts for vibration isolation systems consisting of springs and viscous dampers.

4.3 Transient Response of Viscodamper Oscillator

Analytical solutions for the transient response of the viscodamper oscillator are extremely difficult even in the simplest cases of loading. For an example, the reader is refered to Appendix A for an analytic solution of the response to harmonic loading. Another case for which an analytic solution is possible is that of impulsive loading $F(t)=\delta(t)$. This case has been treated by Bagley and Torvik, 1983. Apparently, the most convenient method for deriving transient responses is by numerical procedures.

The response of the viscodamper oscillator to general dynamic loading is most conveniently determined by the DFT approach. Alternatively, time domain algorithms may be used, but they are computationally intensive. One such algorithm will be presented later in this report in conjunction with the analysis of a nonlinear isolation system. The time domain G1DP-algorithm presented in section 3 will be used later in this report in conjunction with the analysis of a nonlinear isolation system.

The response of the viscodamper oscillator to general dynamic loading and for zero initial conditions is derived by application of Fourier transform to equation 4-20

$$u(t)= \frac{1}{2\pi} \int_{-\infty}^{\infty} H(\omega)\ \bar{F}(\omega)\ e^{i\omega t}\ d\omega \qquad (4\text{-}30)$$

where $H(\omega)$ is the complex frequency response function (equation 4-21), and $\bar{F}(\omega)$ is the Fourier transform of load F(t). The application of the DFT approach is directly analogous to that of the SDOF viscous oscillator (Veletsos and Ventura, 1985).

The transient response of the viscodamper oscillator will be compared to the response of the equivalent SDOF viscous oscillator which was introduced earlier. This oscillator is defined as one whose response is essentially the same as that of the viscodamper oscillator. In the equivalent oscillator, the frequency dependency of the parameters of the viscous damper is neglected so that the equation of motion is

$$m\ddot{u} + C(\Omega)\dot{u} + [K+K_1(\Omega)]\ u = F(t) \qquad (4\text{-}31)$$

where $K_1(\Omega)$ and $C(\Omega)$ are the storage stiffness and damping coefficient of the viscous damper evaluated at frequency Ω. This frequency could be the natural frequency of the equivalent oscillator or it could be a frequency contained in the load F(t).

More conveniently, equation 4-31 is rewritten as

$$\ddot{u} + 2\xi_e\omega_e\dot{u} + \omega_e^2\ u = \frac{F(t)}{m} \qquad (4\text{-}32)$$

where ξ_e and ω_e are given by equations 4-18 and 4-19.

The validity of the equivalent oscillator is studied in two interesting applications of viscous dampers.

4.3.1 Impulsive Loading

Forging hammers is one application of viscous dampers in which impulsive loading is involved. Forging hammers are massive machines with mass equal to

about 60,000Kg. The ram of the machine has a mass of about 3,000Kg with an impact velocity of 5.5m/s. On inpact, the hammer response velocity is approximately 0.4 m/s. The load on the machine has a 5 to 15 msec duration and is approximately a half sine impulse.

A commonly used support system for forging hammers consists of helical steel springs and viscous dampers. This vibration isolation system substantially reduces the transmission of vibration to the surroundings and prevents settling and tilting of the hammer. Damping in the isolation system is large so that vibrations of the hammer are eliminated within a very short time interval. Typically, the isolation system is designed to give a vertical frequency of free vibration of about 5Hz with an effective damping ratio of about 0.25.

Figure 4-6 shows a time history of displacement of a hammer for a half since impulse load of 10 msec duration. The amplitude of the load is determined so that $\int F(t)dt/m=V_o=0.4$ m/sec. The response was evaluated by applying DFT to equation 4-30. The exact response of the viscodamper oscillator is compared to that of the equivalent viscous oscillator with parameters ω_e and ξ_e as given by equations 4-18 and 4-19. Ω was selected to be the natural frequency of the equivalent oscillator, $\Omega=\omega_e$. In evaluating ω_e and ξ_e, an iterative procedure is required, starting from $\Omega=\omega_o$. The parameters of the isolation system were selected to be $\omega_o=31.42$ rad/s ($f_o=\omega_o/2\pi=5$ Hz), $\lambda=0.3$ $(\text{sec})^r$, $r=0.6$ and $\xi_d=1.52$. The parameters of the equivalent oscillator were $\omega_e=41.56$ rad/s and $\xi_e=0.25$. The stiffening effect of viscous dampers is evident in the difference between frequencies ω_o and ω_e. Alternatively, one could use the exact frequency, ω_1, and damping ratio, ξ_1, rather than the approximate values. Using Figure 4-1, we get $\omega_1=43.97$ r/s and $\xi_1=0.27$. The response of the equivalent oscillator closely follows the exact response, capturing the correct content in frequency but underestimating the peak displacement. This is explained when considering that the peak displacement is reached in very short time, when the response exhibits strong low frequency components. In this short time, the viscodamper oscillator

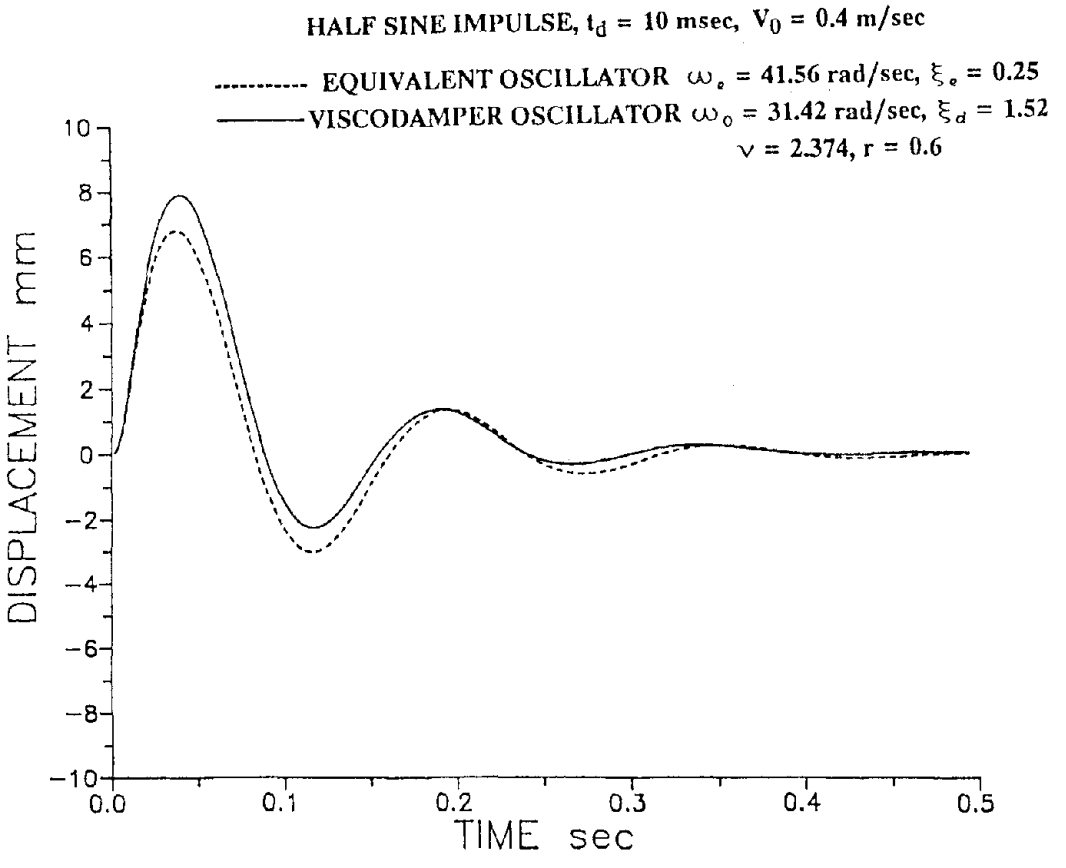

Figure 4-6 Comparison of Time Histories of Response of Viscodamper and Equivalent Viscous Oscillator When Subjected to Impulsive Loading.

exhibits a stiffness close to K, whereas the equivalent oscillator has a higher stiffness equal to $K+K_1(\Omega)$.

The role of viscous dampers in isolation systems for forging hammers is to provide energy dissipation so that vibrations are eliminated within a very short time interval. Figure 4-7 shows the time needed for the displacement to reduce to five percent of its peak value as a function of parameter ξ_d in three isolation systems for forging hammers. The equivalent viscous oscillator predicts results in good agreement with the exact.

The plots of Figure 4-7 represent a useful design tool. Consider for example that an isolation system for a 60,000 Kg forging hammer is to be designed for the impulsive loading shown in the figure. The design criterion is that vibration should be reduced to 5% of the peak value within 250 msec. From Figure 4-7 we determine that two possibilities exist: ω_o=62.83 r/s and ξ_d=1.12 or ω_o=31.42 r/s and ξ_d=1.42. The latter solution gives a total spring constant K=59 218 kN/m and a total damping coefficient C_o=5353 kNs/m (using equations 4-4 and 4-5).

4.3.2 Earthquake Loading

Applications of viscous dampers in which earthquake loading is involved are in seismic isolation of equipment and structures. One such application has been discussed in the introduction of this report.

The equation of motion of a seismically excited SDOF viscodamper oscillator is given by equation 4-20 with $F(t)=-m\ddot{u}_g(t)$. $\ddot{u}_g(t)$ is the ground acceleration and u(t) represents the relative displacement. Again, the solution is derived by application of the DFT approach. Figure 4-8 presents displacement response spectra of viscodamper oscillators for the 1940 El Centro earthquake (Imperial Valley, component SOOE, peak ground acceleration of 0.348g) and for the 1985 Mexico City earthquake (SCT building, component N90W, peak ground acceleration of 0.17g). The oscillators are defined by parameters $T_o=2\pi/\omega_o$,

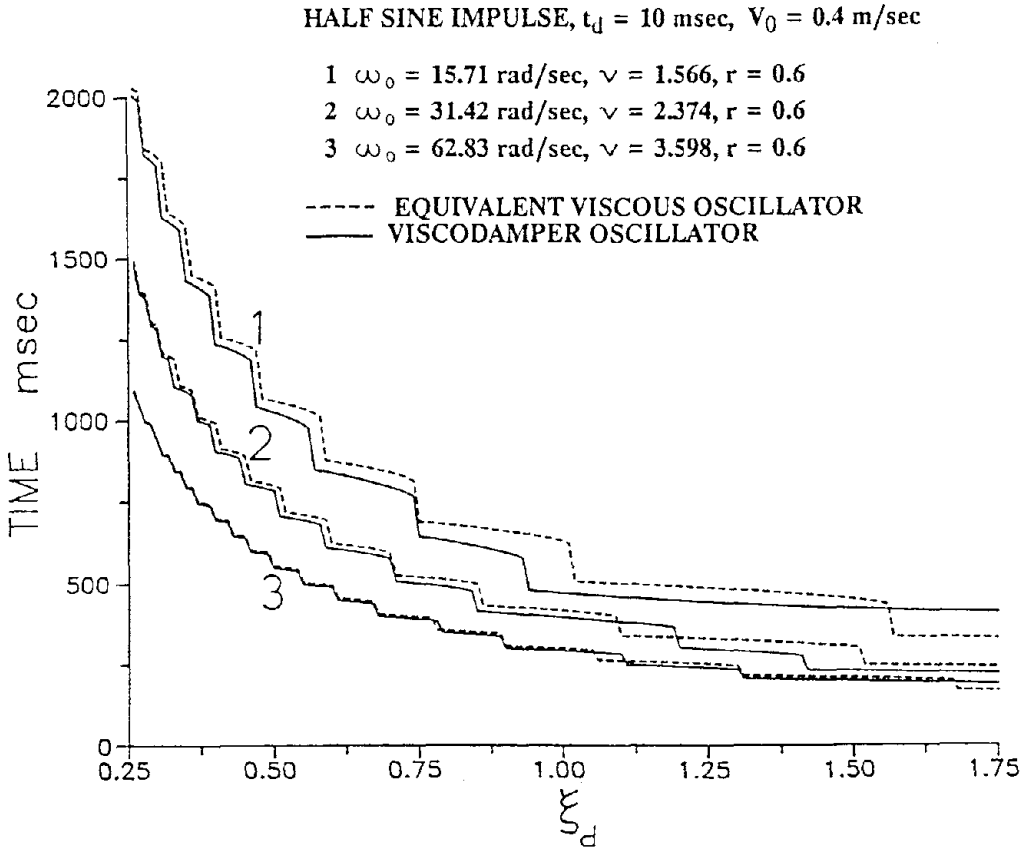

Figure 4-7 Time Needed for Displacement Response to Impulsive Loading to Reduce to Five Percent of Peak Value.

$\lambda=0.3(\text{sec})^r$, r=0.6 and equivalent damping ratio ξ_e, eguation 4-19, in which Ω is taken equal to ω_e. The equivalent viscous oscillator, defined by parameters ω_e and ξ_e, equations 4-18 and 4-19, gives results in very good agreement with the exact. It should be noted that each of the curves of Figure 4-8 are presented for a constant ξ_e. This means that parameter ξ_d varies as T_o varies, i.e. different size viscous dampers are needed to give constant ξ_e at different values of T_o. Furthermore, for fixed ξ_e and T_o the actual period of the system is less than T_o because of the stiffening effect of the viscous dampers.

Figures 4-9 and 4-10 present spectra of velocity and total acceleration for the same systems and excitations (these are spectra of actual velocity and acceleration, not of pseudovelocity and pseudoacceleration). To compute the time histories of relative velocity and relative acceleration, the complex frequency response functions of these quantities are used

$$\dot{u}(t) = \frac{1}{2\pi} \int_{-\infty}^{\infty} (i\omega)\, H\,(\omega)\, \bar{F}\,(\omega)\, e^{i\omega t}\, d\omega \qquad (4\text{-}33)$$

$$\ddot{u}(t) = \frac{1}{2\pi} \int_{-\infty}^{\infty} (-\omega^2)\, H\,(\omega)\, \bar{F}\,(\omega)\, e^{i\omega t}\, d\omega \qquad (4\text{-}34)$$

where $H(\omega)$ is the complex frequency response function for the relative displacement (equation 4-21). The total acceleration is computed as $\ddot{u}(t) + \ddot{u}_g(t)$. Figures 4-9 and 4-10 demonstrate very good agreement between the predictions of the equivalent viscous oscillator and the exact results.

Concluding the section, procedures have been presented for the exact analysis of the viscodamper oscillator. Approximate procedures, which are based on the concept of equivalent viscous oscillator, have been presented and shown to give results in good agreement with the exact.

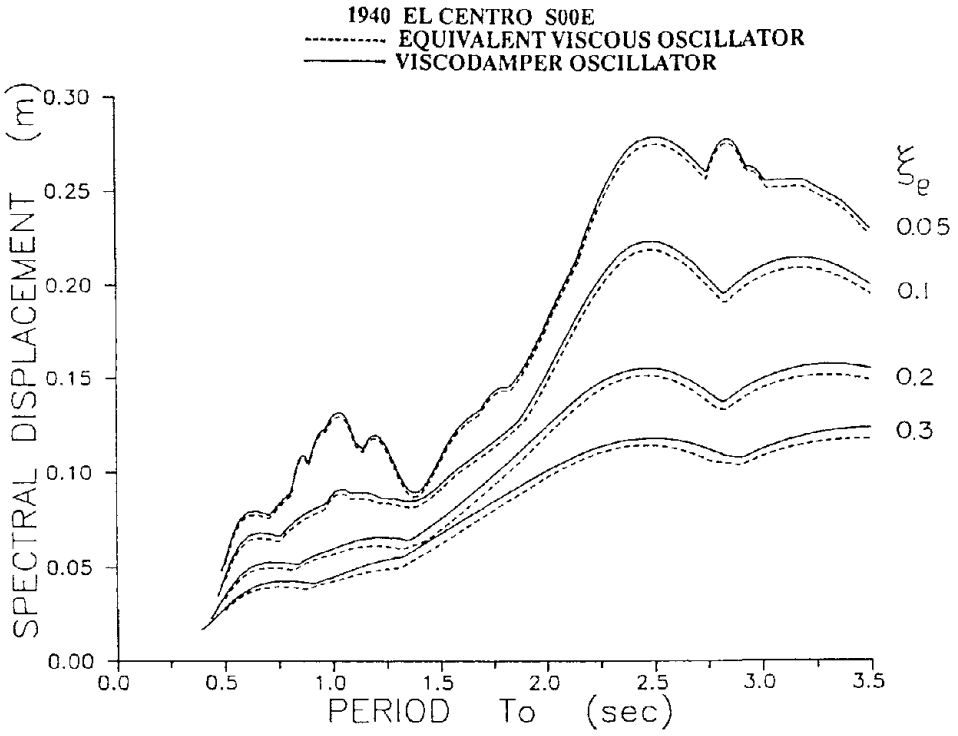

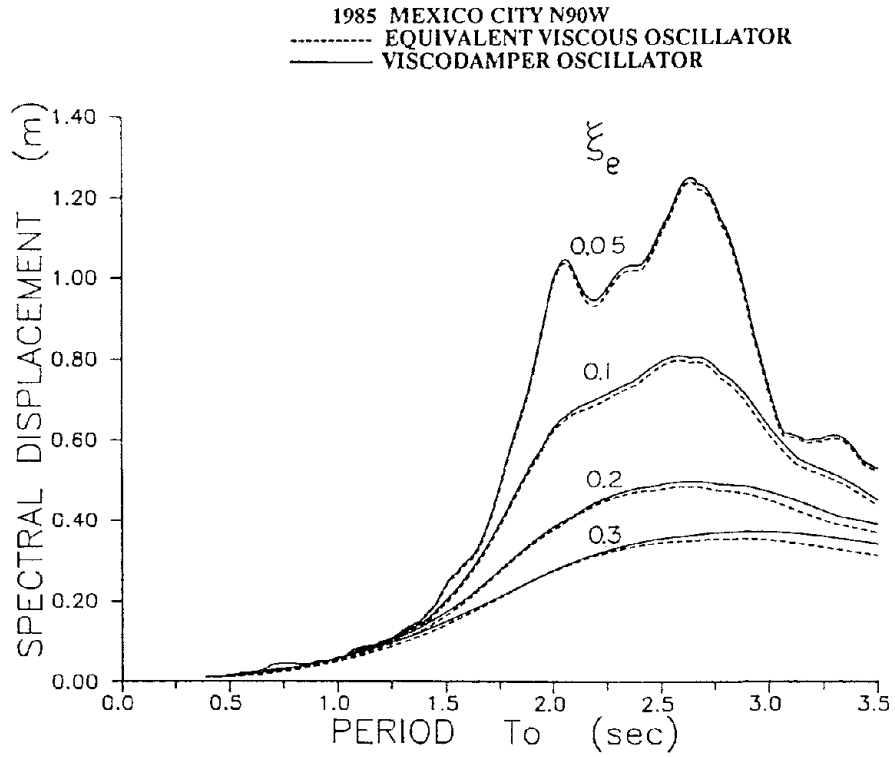

Figure 4-8 Comparison of Displacement Response Spectra of Viscodamper and Equivalent Viscous Oscillators for 1940 El Centro and 1985 Mexico City Earthquakes.

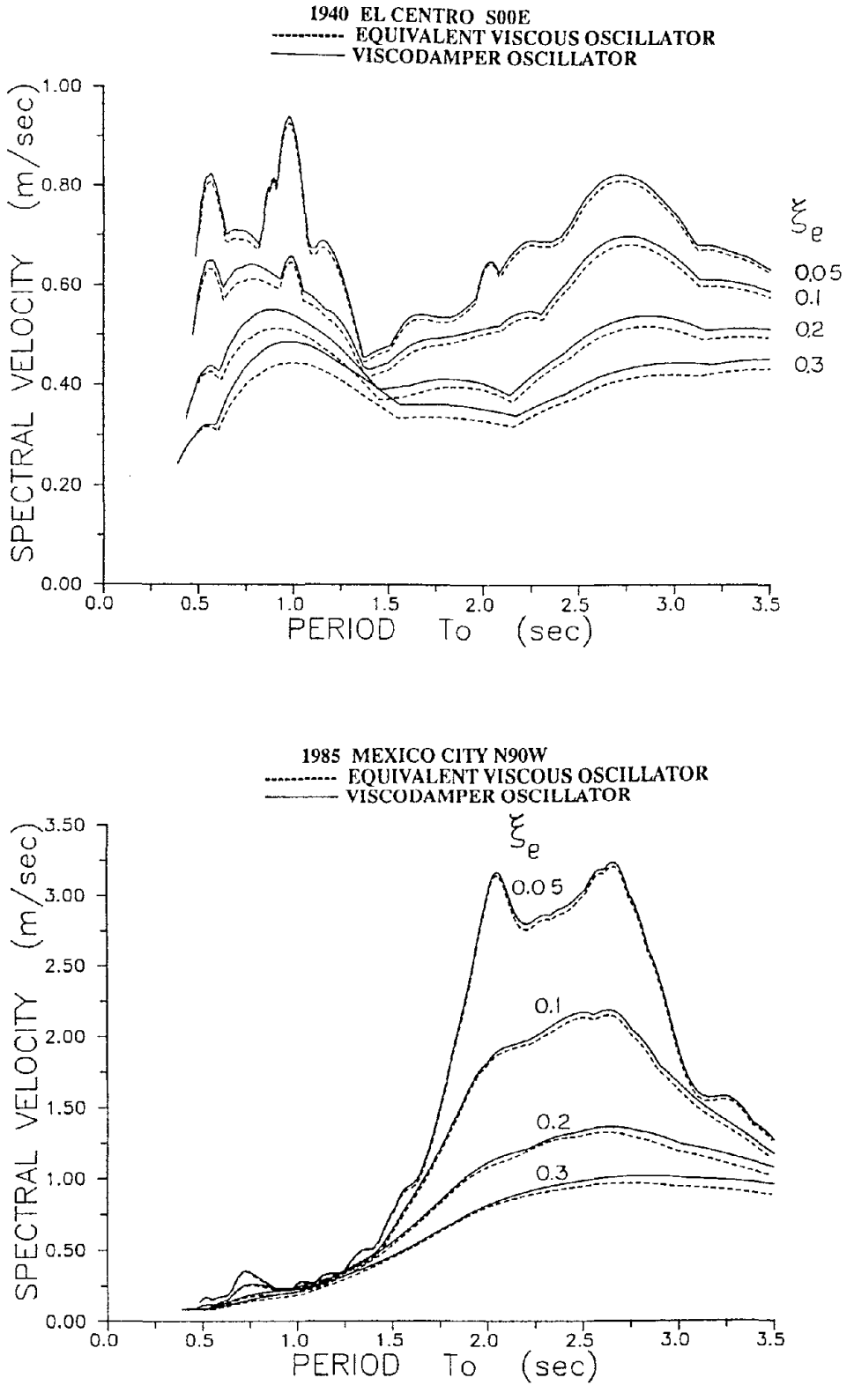

Figure 4-9 Comparison of Velocity Response Spectra of Viscodamper and Equivalent Viscous Oscillators for 1940 El Centro and 1985 Mexico City Earthquakes.

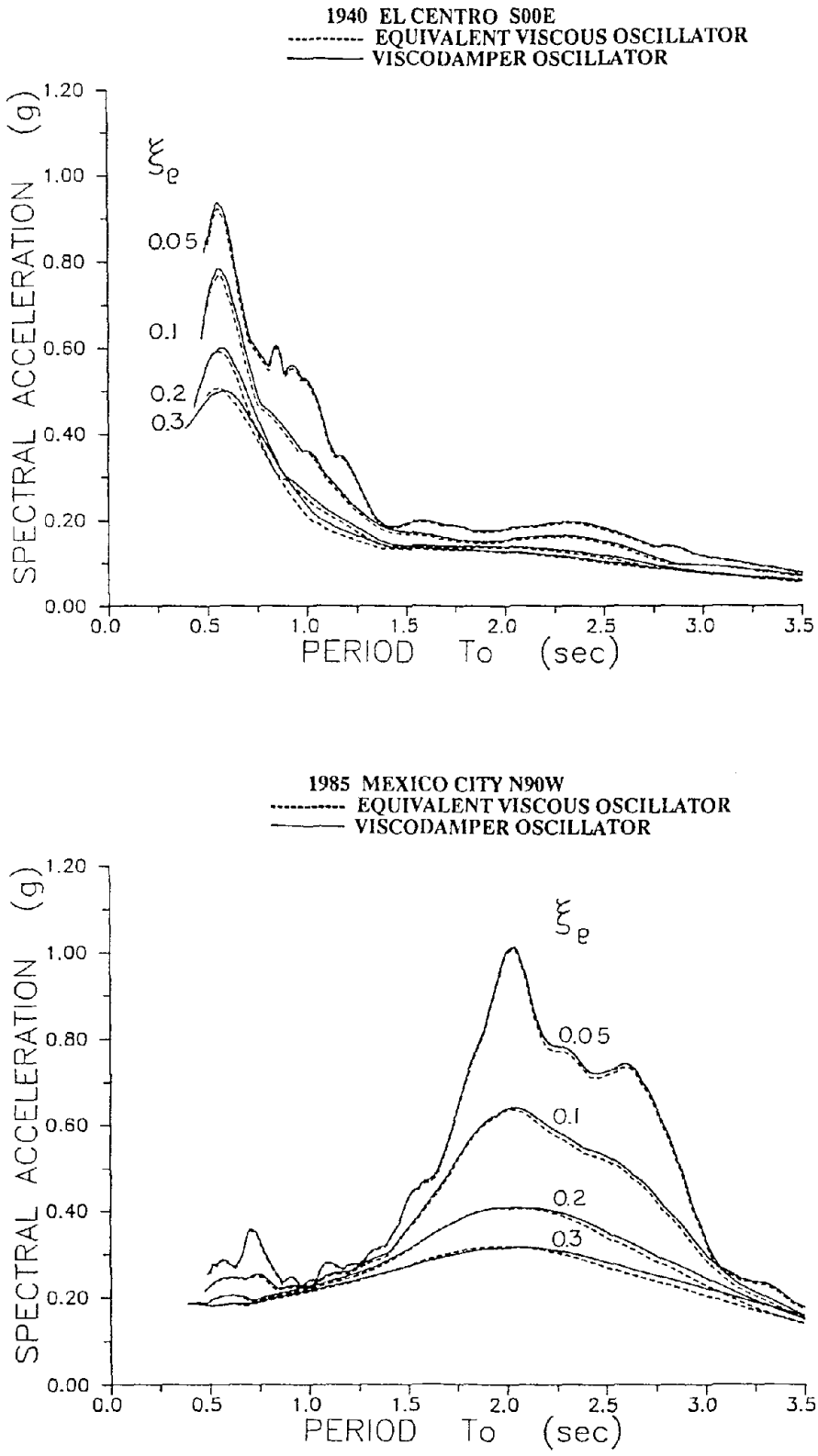

Figure 4-10 Comparison of Acceleration Response Spectra of Viscodamper and Equivalent Viscous Oscillators for 1940 El Centro and 1985 Mexico City Earthquakes.

SECTION 5

APPLICATION OF VISCOUS DAMPERS IN SLIDING ISOLATION SYSTEMS

Sliding isolation systems have been used for the seismic protection of structures. They are more stable and have lower bearing displacements than elastomeric isolation systems, at the expense however of higher structural accelerations. One such sliding system has been recently tested on a shake table using a six-story, quarter scale, 230KN (51.4 Kips) model structure (Constantinou et al, 1990a and 1990b). The isolation system consisted of Teflon sliding bearings and restoring force devices in the form of helical steel springs.

In the tested system, the helical springs had a spring constant of 470 N/mm (2.68 K/in.) and the coefficient of friction in the sliding bearings was dependent on the velocity of sliding. It varied between a minimum value and a maximum value which was mobilized at large velocity of sliding. The friction coefficient, μ, followed with good accuracy the relation

$$\mu = f_{max} - Df \cdot \exp(-a|V|) \qquad (5\text{-}1)$$

where f_{max} is the maximum value, $(f_{max} - Df)$ is the minimum value, V is the velocity of sliding and a is a constant. The parameters in equation 5-1 were f_{max} = 0.16 to 0.17, Df = 0.04 to 0.06 and a = 21.65 sec/m (0.55 sec/in.). They were determined experimentally.

The isolation system was specifically designed to have weak restoring force and strong frictional force, so that it has low sensitivity to the frequency content of the earthquake motion (Constantinou et al, 1990a and 1990b). This property has been confirmed in the experiments. While the strong frictional force/weak restoring force combination may be desirable in this respect, it may also result in large permanent displacements. The permanent displacement has the following upper limit

$$u_p < \frac{(f_{max} - Df)\ W}{K} \qquad (5\text{-}2)$$

where W is the weight carried by the bearings and K is the stiffness of the restoring force devices. For the tested system this upper limit is 39 mm (1.53 in.), which is about half the bearing displacement capacity. However, during the shake table tests the maximum permanent bearing displacement was only 4 mm (0.16 in.). This value is remarkably low and by far smaller than the limit of equation 5-2. This limit was derived assuming that no inertia forces act on the structure, and apparently the inertial forces "help" the isolation system to re-center itself.

In analyses of the response of the model structure prior to testing, it was observed that by including viscous damping into the isolation system (modeled by linear dashpots), the displacements and accelerations of the model were reduced. Accordingly, it was decided to add viscous dampers to the isolation system. By adding four of the tested dampers (Figure 1-1), it was estimated that the damping ratio in the fundamental mode would be about 0.1. This, of course, was based on the assumption that viscous dampers could be modeled as linear dashpots. In the shake table testing it was observed that indeed the viscous dampers were effective in reducing the peak to peak displacement of the isolation system. However, it was clear in the experimental results that the dampers were not simple linear dashpots. This prompted the authors to conduct component tests on the dampers which led to the developed fractional derivative model.

5.1 Test Program and Results

The model structure has been described in detail in Constantinou et al, 1990b. Four viscous dampers identical to the tested one (Figure 1-1) were added to the isolation system. The sliding bearings did not allow any vertical movement so that the dampers were only effective in the horizontal direction. The model structure was subjected to four earthquake signals on the shake table. These earthquakes were:

1. San Fernando earthquake (Pacoima Dam) of February 9, 1971. Component S16E, peak ground acceleration (PGA) = 1.17g. This record was scaled to a peak table acceleration (PTA) of 0.73 g.

2. Miyagiken-Oki earthquake of June 12, 1978 (Tohoku Univ., Sendai, Japan). Component EW, PGA = 0.16g. The record was scaled to PTA = 0.42g.

3. Tokachi-Oki earthquake, Japan (Hachinohe) of May 16, 1968. Component NS, PGA-23g. The acceleration of this record was not scaled (PTA = 0.22g).

4. Mexico City earthquake of September 19, 1985 (SCT Building station). Component N90W, PGA = 0.17g. The record was scaled to PTA = 0.21 g.

All records were time scaled by a factor of 2 to satisfy similitude requirements of the quarter scale model.

Figures 5-1 to 5-4 present experimental results in the four cases of input on the base (bearing) displacement time history, structure shear over weight ratio time history, 6th floor displacement with respect to base time history and base shear over weight ratio versus bearing displacement loop. The structure shear is the shear force at the first story, whereas the base shear is the shear force at the bearing level. The weight is 230 kN (51.4 Kips). The results are presented in units of inches as they were measured. For comparison, Figures 5-5 to 5-8 present experimental results for the same input and model structure but without the four viscous dampers. It is apparent that the addition of viscous dampers resulted in large permanent displacements.

Table 5-I compares experimental results in the two sets of tests. The peak to peak displacement is the distance between the positive peak and negative peak position of the bearing. The viscous dampers were effective in reducing this peak to peak displacement in all cases. Particularly in the Mexico City earthquake, this reduction is substantial (about 35%). The good performance in this case is due to the low frequency response of the system in which the dampers exhibit high damping coefficient and low storage stiffness. Otherwise, the response of the two systems is about the same, except for the permanent

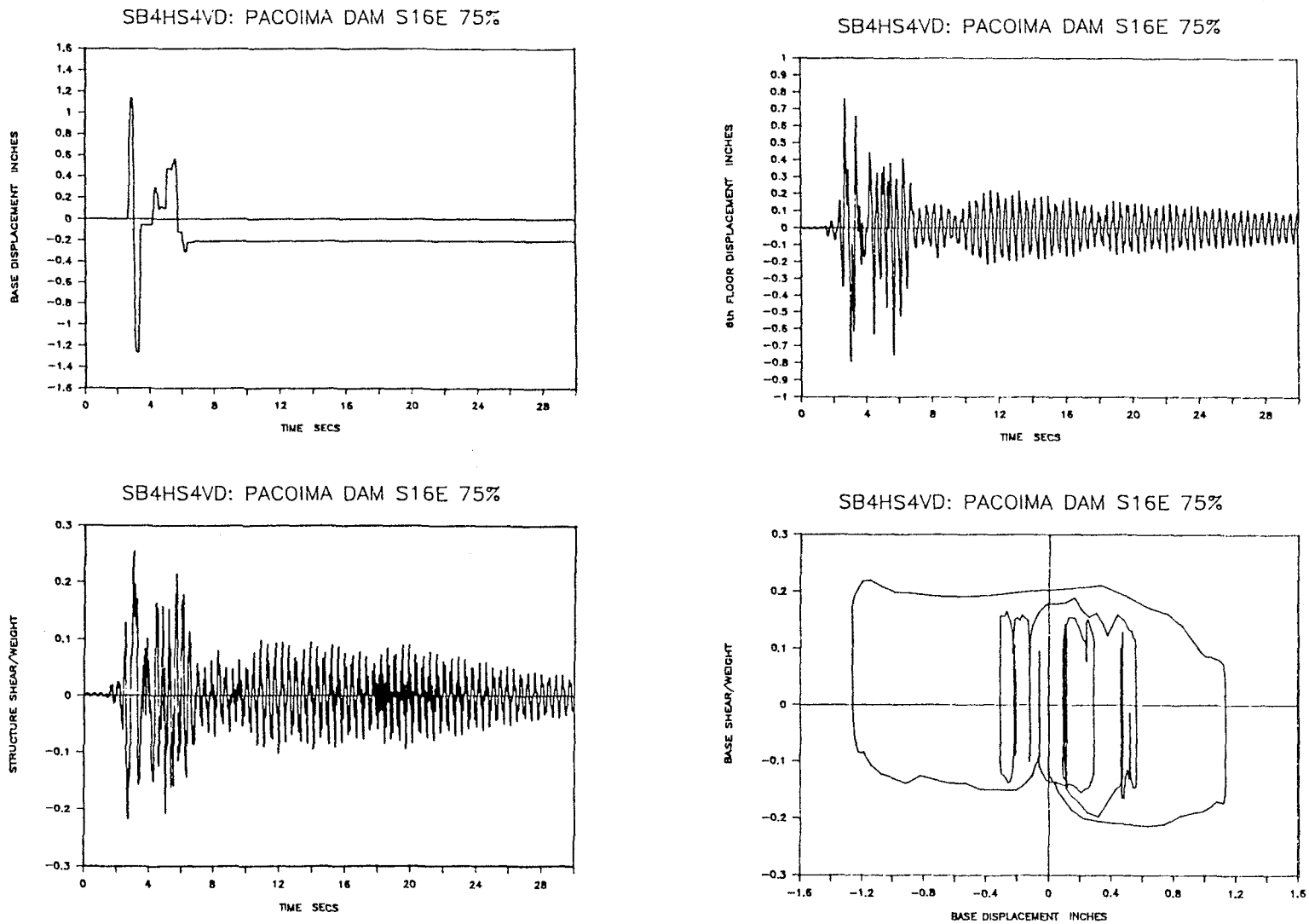

Figure 5-1 Experimental Time Histories of Base Displacement, Structure Shear and 6th Floor Displacement with Respect to Base and Base Shear-Displacement Loop in Sliding System with Viscous Dampers for Pacoima Dam Input (0.73g peak table acceleration).

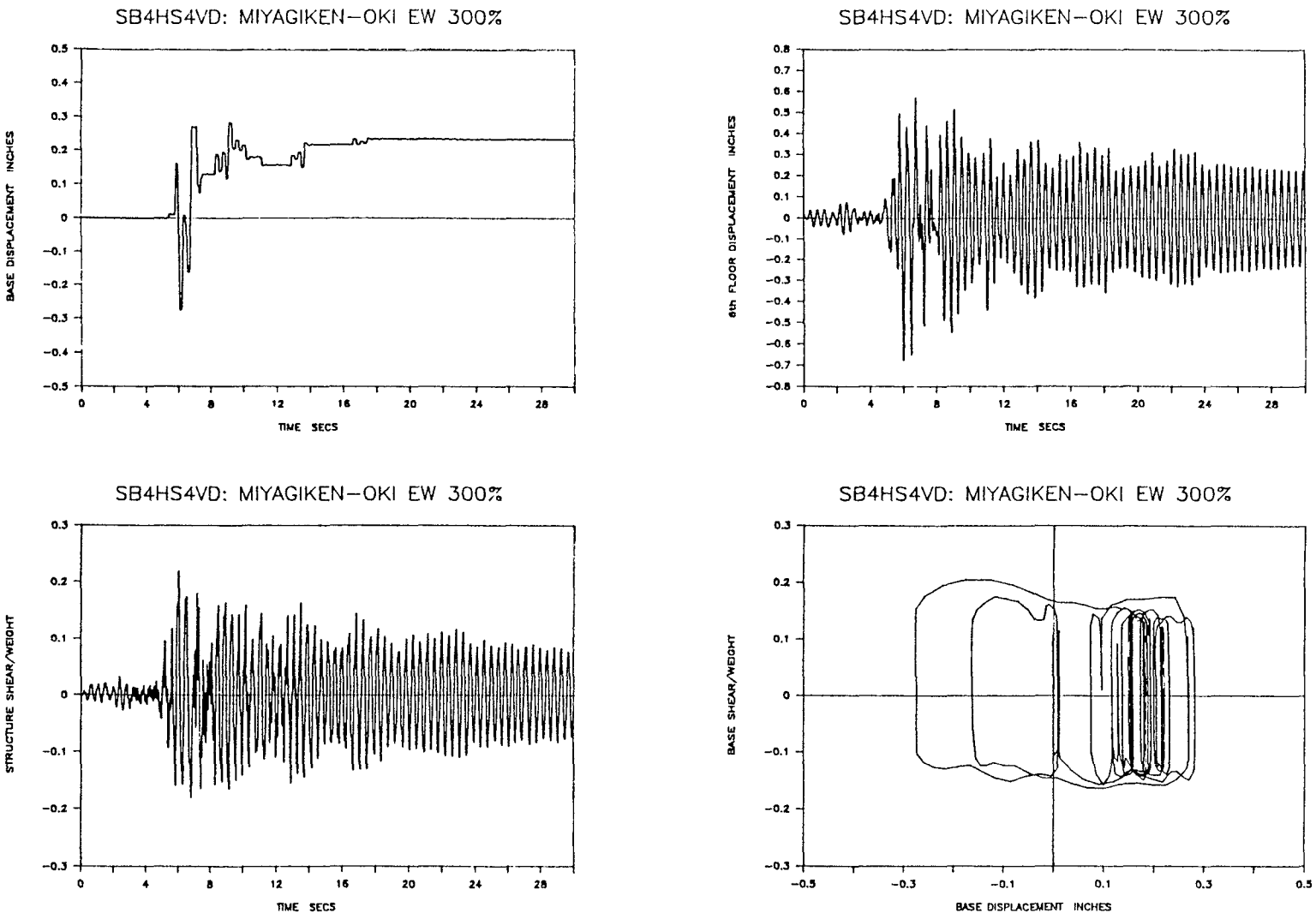

Figure 5-2 Experimental Time Histories of Base Displacement, Structure Shear and 6th Floor Displacement with Respect to Base and Base Shear-Displacement Loop in Sliding System with Viscous Dampers for Miyagiken-Oki Input (0.42 g peak table acceleration).

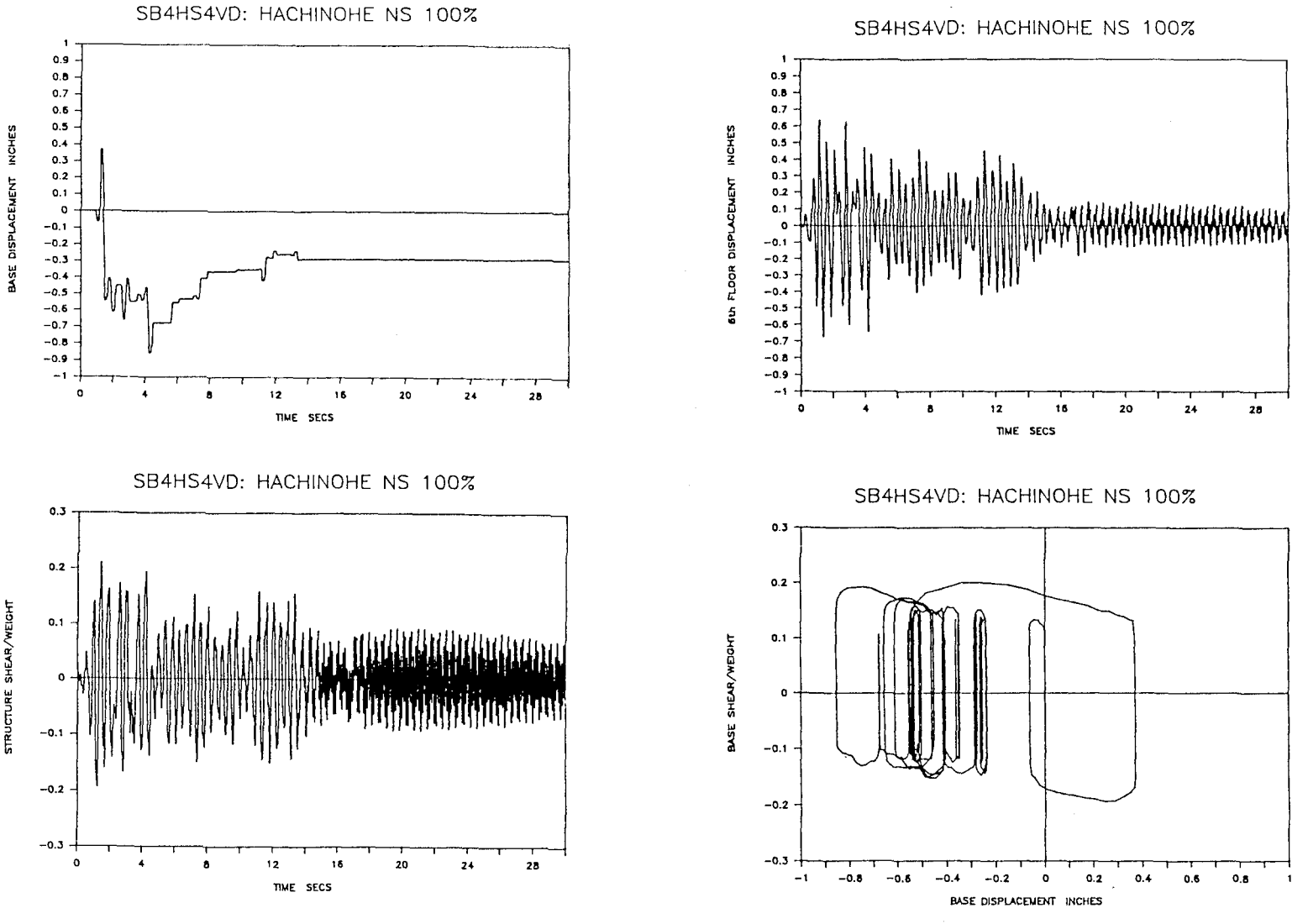

Figure 5-3 Experimental Time Histories of Base Displacement, Structure Shear and 6th Floor Displacement with Respect to Base and Base Shear-Displacement Loop in Sliding System with Viscous Dampers for Hachinohe Input (0.22 g peak table acceleration).

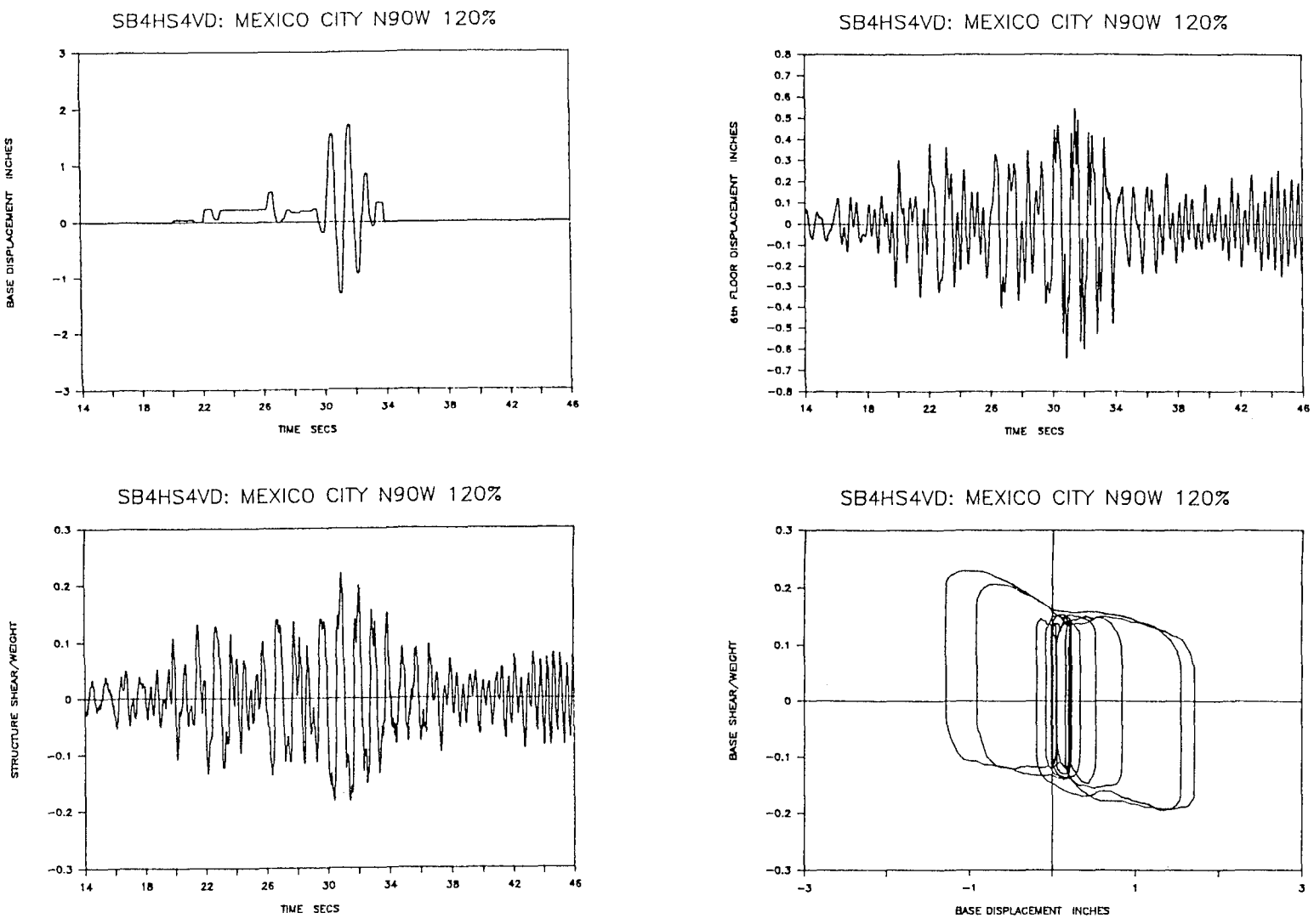

Figure 5-4 Experimental Time Histories of Base Displacement, Structure Shear and 6th Floor Displacement with Respect to Base and Base Shear-Displacement Loop in Sliding System with Viscous Dampers for Mexico City Input (0.21 g peak table acceleration).

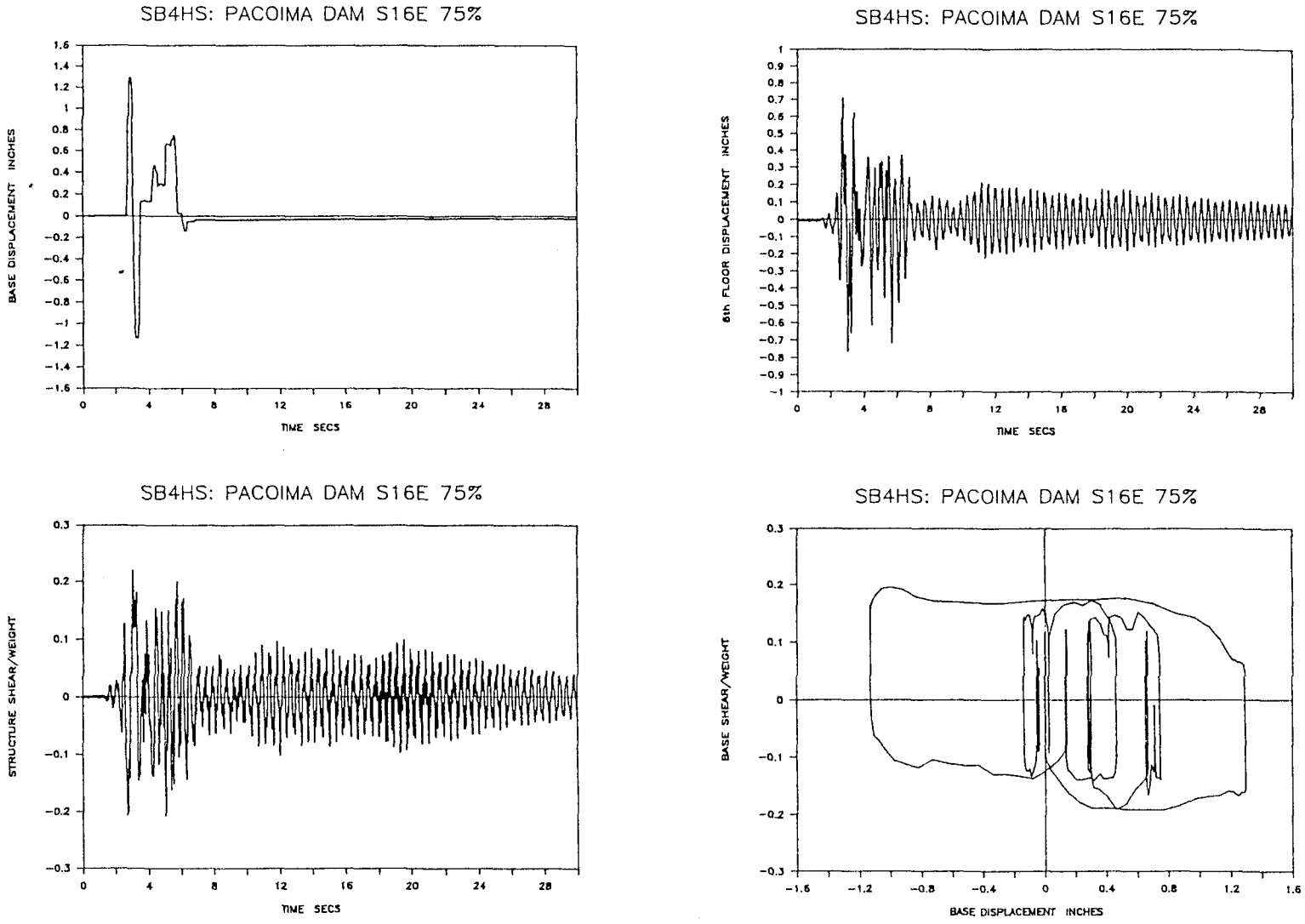

Figure 5-5 Experimental Time Histories of Base Displacement, Structure Shear and 6th Floor Displacement with Respect to Base and Base Shear-Displacement Loop in Sliding System without Viscous Dampers for Pacoima Dam Input (0.73g peak table acceleration).

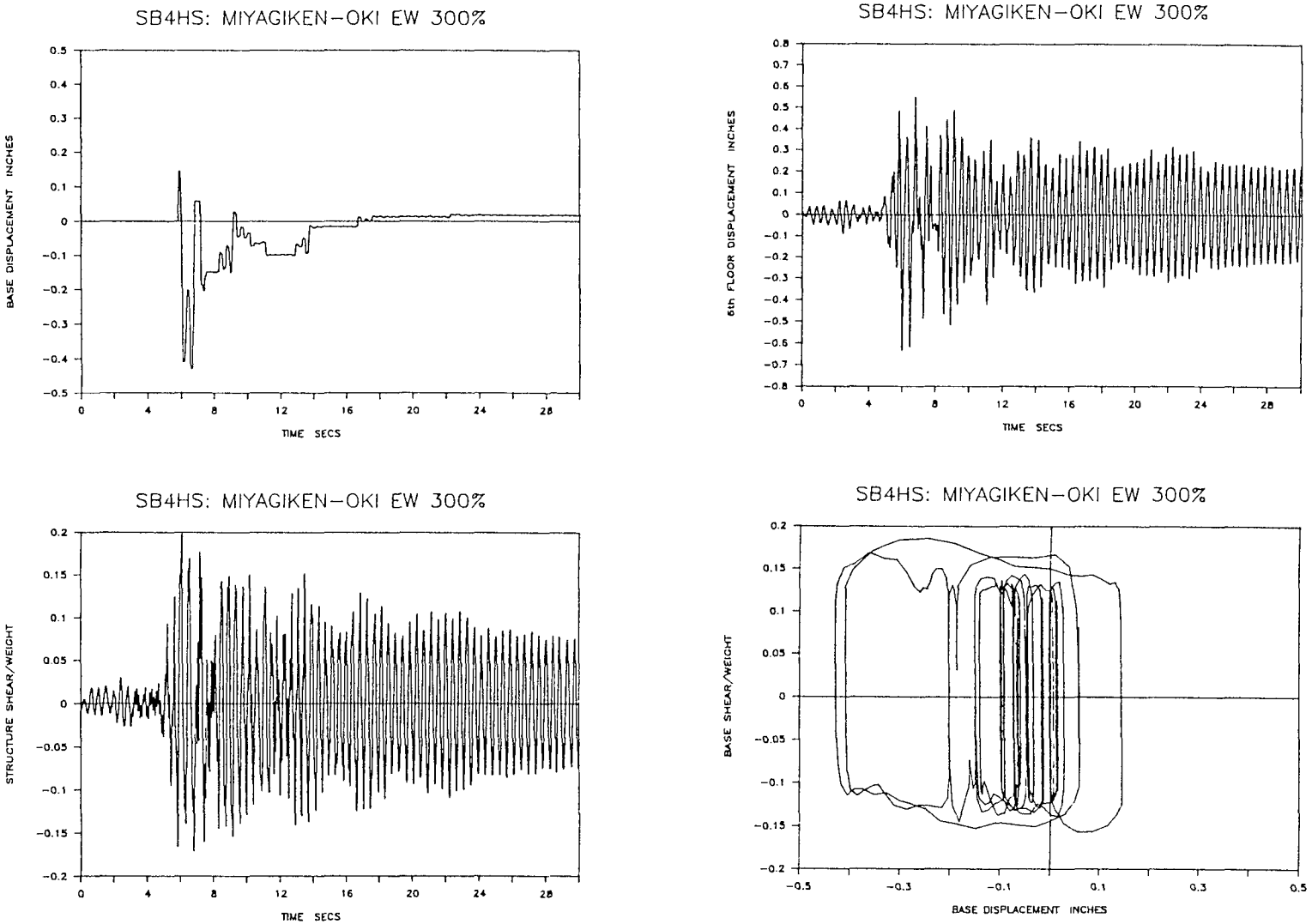

Figure 5-6 Experimental Time Histories of Base Displacement, Structure Shear and 6th Floor Displacement with Respect to Base and Base Shear-Displacement Loop in Sliding System without Viscous Dampers for Miyagiken-Oki Input (0.42 g peak table acceleration).

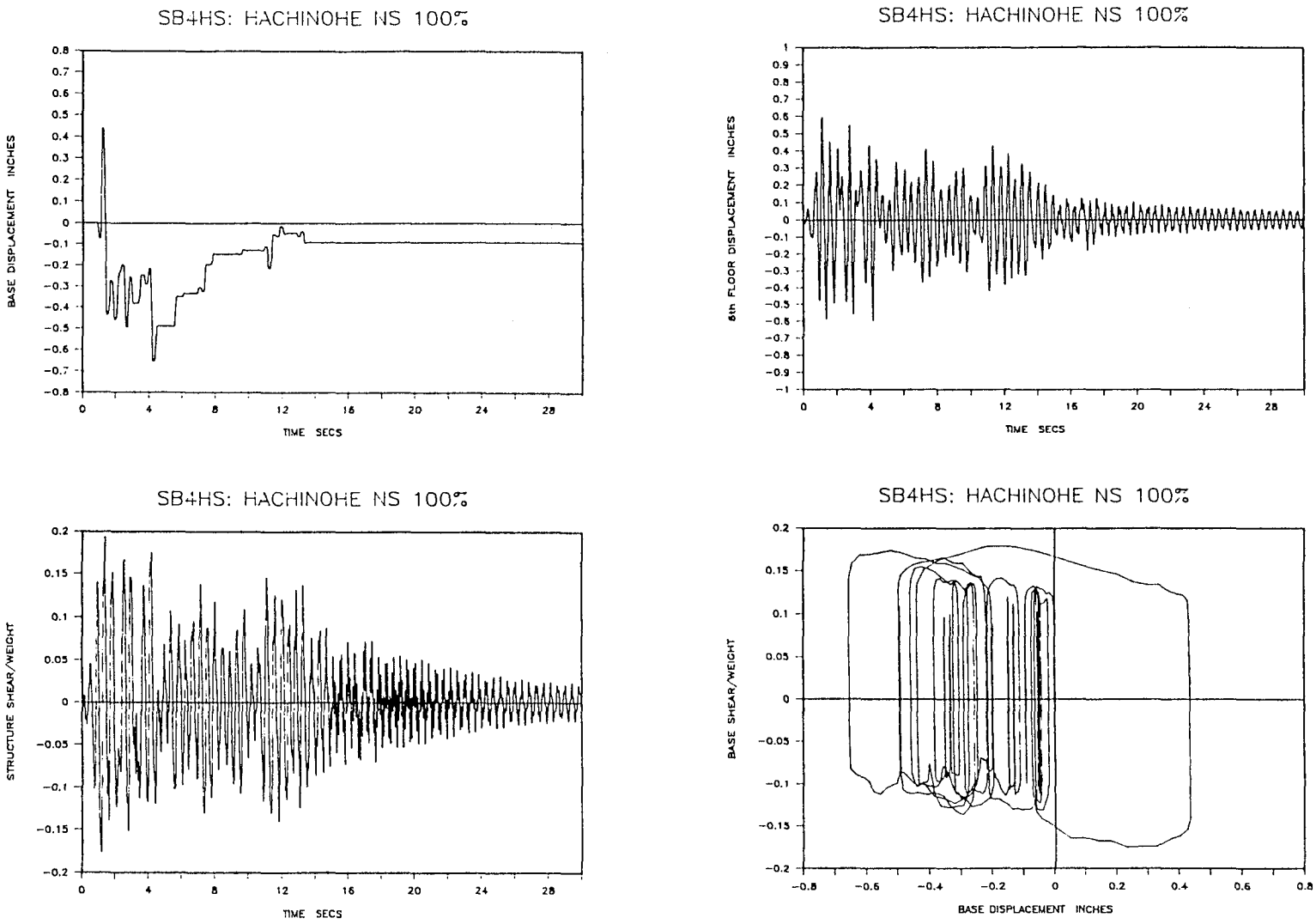

Figure 5-7 Experimental Time Histories of Base Displacement, Structure Shear and 6th Floor Displacement with Respect to Base and Base Shear-Displacement Loop in Sliding System without Viscous Dampers for Hachinohe Input (0.22 g peak table acceleration).

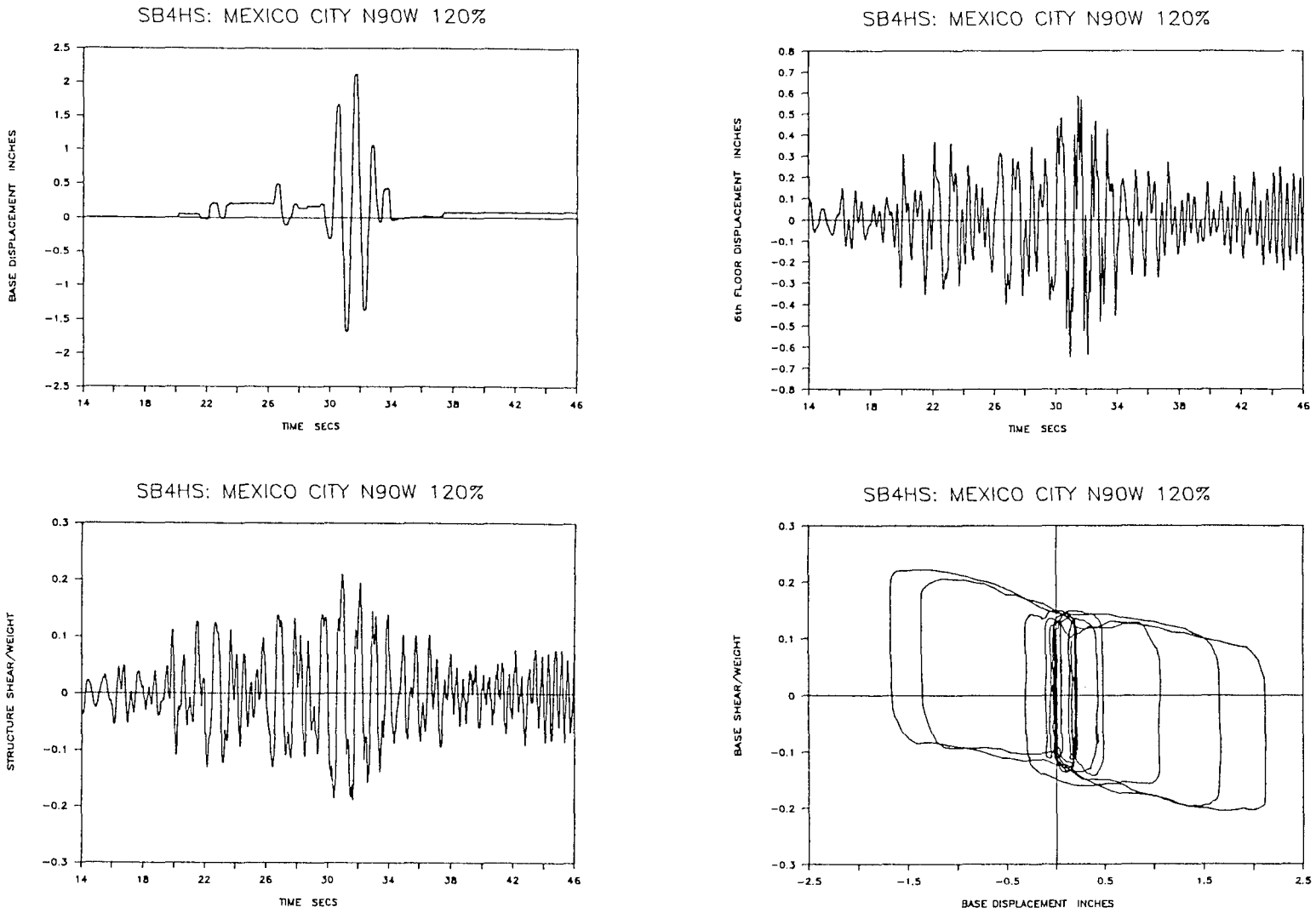

Figure 5-8 Experimental Time Histories of Base Displacement, Structure Shear and 6th Floor Displacement with Respect to Base and Base Shear-Displacement Loop in Sliding System without Viscous Dampers for Mexico City Input (0.21 g peak table acceleration).

TABLE 5-I: Comparison of Experimental Results (1 in. = 25.4 mm)

Excitation	Isolation Condition+	Pk. Table Accel. (g)	Peak to Peak Bearing Displ. (in.)	Permanent Displ. (in.)	Pk. Interstory Drift* (in.)	Pk. Model Accel.* (g)	Base Shear/ Weight	Structure Shear/ Weight
Pacoima S16E	SB4HS	0.73	2.585	0.024	0.191(3)	1.00(6)	0.196	0.220
Miyagiken-Oki	SB4HS	0.42	0.611	0.018	0.143(3)	0.82(3)	0.186	0.198
Hachinohe	SB4HS	0.22	1.175	0.092	0.130(3)	0.65(6)	0.179	0.193
Mexico City	SB4HS	0.21	4.056	0.085	0.149(2)	0.51(6)	0.223	0.220
Pacoima S16E	SB4HS4VD	0.73	2.398	0.206	0.194(3)	0.98(6)	0.221	0.255
Miyagiken-Oki	SB4HS4VD	0.42	0.549	0.234	0.154(3)	0.87(3)	0.206	0.219
Hachinohe	SB4HS4VD	0.22	1.098	0.286	0.150(2)	0.71(6)	0.201	0.212
Mexico City	SB4HS4VD	0.21	2.690	0.000	0.151(3)	0.49(6)	0.231	0.221

+ SB4HS: System without viscous dampers
SB4HS4VD: System with four viscous dampers

* Quantity in parenthesis is story or floor at which maximum was recorded

displacement. Other then the case of Mexico City motion, the permanent displacement in the system with viscous dampers is much larger than that in the system without viscous dampers. The dampers appear to counteract the combined effect of inertia and restoring (spring) forces which tend to re-center the isolation system.

The experiments demonstrated that viscous dampers are not useful in sliding isolation systems because of the possibility of occurrence of large permanent displacements.

5.2 Analytical Prediction of Response

The shake table tests provided a good opportunity to verify the developed fractional derivative model and to test the validity of the G1FP-algorithm for analysis in the time domain.

For the analysis of the tested model structure, a lumped mass model with degrees of freedom being the floor and base displacements was used. The equations of motion are

$$[M]\ \{\ddot{U}\} + [C]\ \{\dot{U}\} + [K]\ \{U\} = -\ [M]\ \{1\}\ (\ddot{U}_b + \ddot{U}_g) \tag{5-3}$$

$$\sum_{i=1}^{6} m_i(\ddot{U}_i + \ddot{U}_b + \ddot{U}_g) + m_b(\ddot{U}_b + \ddot{U}_g) + F_f + F_r + P(t) = 0 \tag{5-4}$$

Equation (5-3) is the equation of motion of the six story superstructure with [M], [C] and [K] being the mass, damping and stiffness matrices, respectively. Equation (5-4) is that of dynamic equilibrium of the entire structure in the horizontal direction. {U} is the vector of floor displacements with respect to the base, U_b is the base displacement with respect to the table and U_g is the table displacement. A dot denotes differentiation with respect to time. m_i and m_b (i = 1 to 6) are the floor and base masses. Matrices [K] and [C] were constructed analytically using analytically determined modal shapes and frequencies and experimentally determined damping factors (see Constantinou et al, 1990a for details).

F_f and F_r are the frictional and restoring forces, respectively, at the isolation interface. The frictional force is given by:

$$F_f = [\mu(\dot{U}_b)\cos\delta - \text{sgn}(\dot{U}_b)\sin\delta]W\,Z \tag{5-5}$$

where sgn stands for the signum function and $\mu(\dot{U}_b)$ is the coefficient of sliding friction of the Teflon bearings, which depends on the velocity of sliding, $\dot{U}_b$, in accordance to equation 5-1. δ is the accidental average inclination of the sliding interfaces which was determined to be between 0.15 and 0.35 degrees.

Variable Z in equation 5-5 is used to account for the conditions of separation and reattachment (Constantinou et al, 1990c) and is governed by the following differential equation:

$$Y\,\dot{Z} + \gamma\,|\dot{U}_b|Z|Z| + \beta\dot{U}_b Z^2 - \dot{U}_b = 0 \tag{5-6}$$

in which Y = 0.127 mm (0.005 in.) and $\beta + \gamma = 1$.
The restoring force is given by:

$$F_r = \begin{cases} K_1 U_b & ,|U_b| \leq D_1 \\ (K_1 - K_2)\,D_1\,\text{sgn}(U_b) + K_2 U_b & ,|U_b| > D_1 \end{cases} \tag{5-7}$$

in which K_1 is the initial low value of the spring stiffness, valid for displacements less than the limit D_1 and K_2 is the stiffness beyond the limit D_1. Equation (5-7) describes the force in an elastic bilinear spring. For the tested system, K_1 = 270 N/mm (1.54 Kip/in.), K_2 = 470 N/mm (2.68 Kip/in.) and D_1 = 12.7 mm (0.5 in.). Furthermore, P(t) in equation 5-4 is the force from four viscous dampers which is described by

$$P(t) + \lambda D^{r}[P(t)] = C_o \dot{U}_b \qquad (5\text{-}8)$$

with $r = 0.7$, $\lambda = 0.15\ (\text{sec})^{0.7}$ and $C_o = 24$ Ns/mm (136.71 lb-s/in.)

In solving equations 5-3 to 5-8, force P(t) was brought to the right side of equation 5-4 and treated as load. The equations were reduced to a system of first order differential equations and integrated using Gears method for stiff differential equations (Gear, 1971). In each time step, which was extremely small, the force P(t) was assumed constant and equal to the value calculated at the previous integration step. At the end of each step, equation 5-8 was solved by employing the G1FP-algorithm (section 3.1) and the value of P(t) was calculated.

Figure 5-9 compares the recorded and analytically determined time histories of the base (bearing) displacement of the system without (top figure) and with four viscous dampers (bottom figure) for the Mexico City motion (PTA = 0.21g). The agreement between the experimental and analytical results is good.

Figure 5-10 compares the experimental and analytical time histories of the base displacement for the Japanese Miyagiken-Oki motion (PTA = 0.42g). Again, the agreement between experimental and analytical results is good. It is very interesting to note that the analytical solution correctly predicts the significant permanent displacement in the case of the system with viscous dampers. This permanent displacement could not be accurately predicted by the simple equivalent viscous damper model (see section 4). Figure 5-11 compares the experimental response to that predicted by the equivalent viscous damper model. The details of the displacement history are predicted well but the permanent displacement is underestimated.

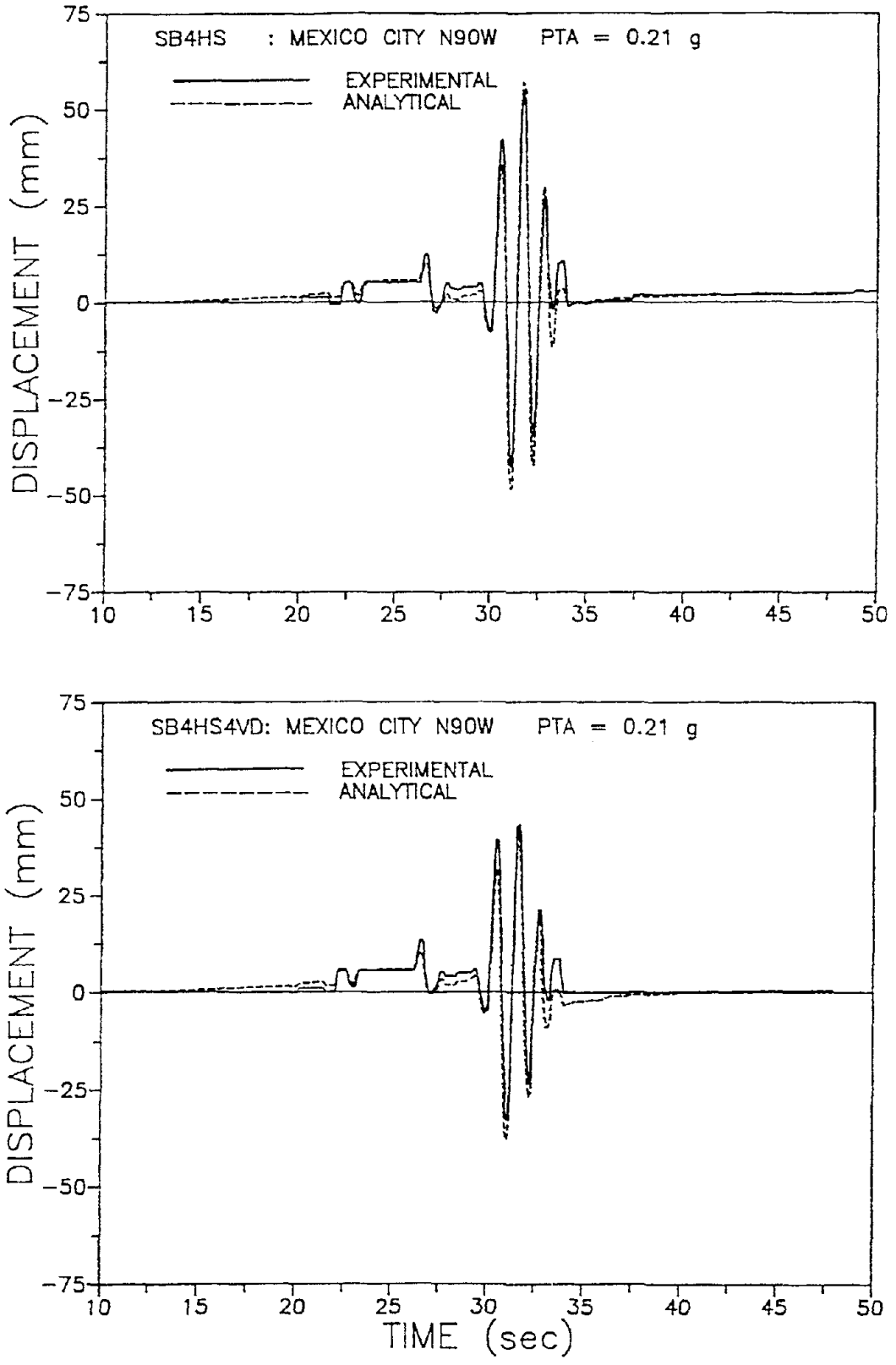

Figure 5-9 Comparison of Recorded and Analytically Predicted Histories of Displacement of Sliding Isolation System Without (Top) and With (Bottom) Viscous Dampers for Mexico City Input.

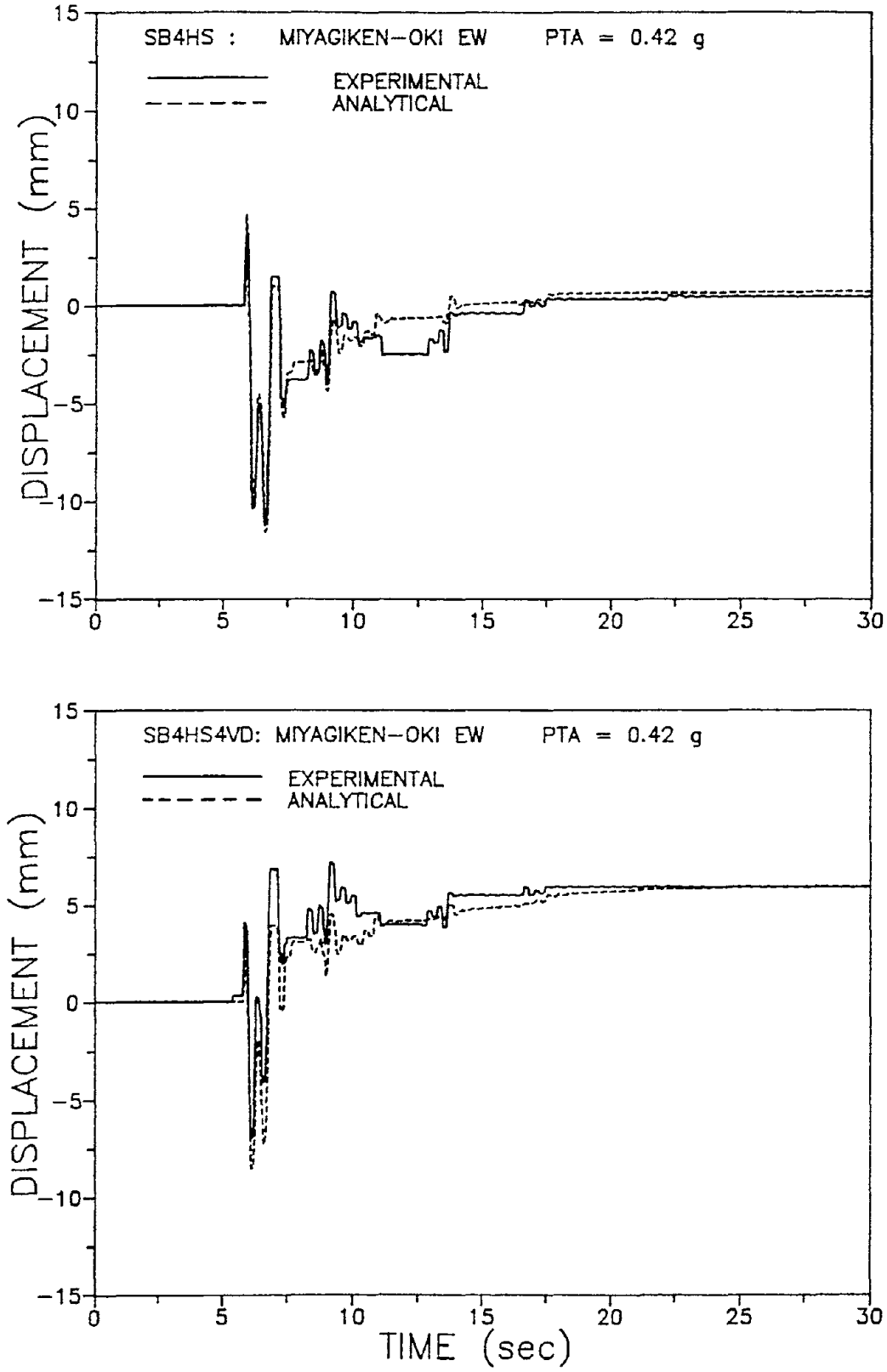

Figure 5-10 Comparison of Recorded and Analytically Predicted Histories of Displacement of Sliding Isolation System Without (Top) and With (Bottom) Viscous Dampers for Miyagiken-Oki Input.

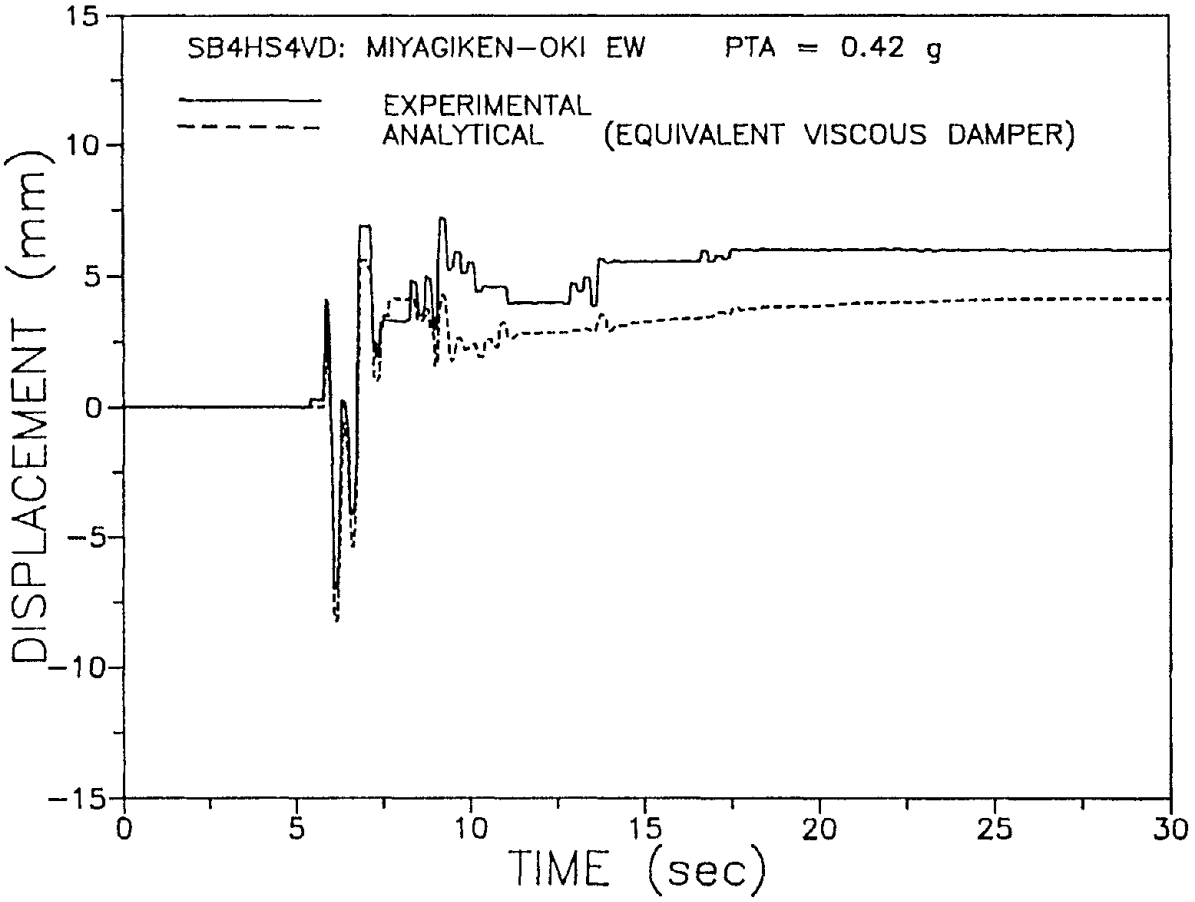

Figure 5-11 Comparison of Recorded History of Displacement of Sliding Isolation System with Viscous Dampers to Analytically Predicted Response by the Equivalent Viscous Damper Model. Compare to Fig. 5-10.

SECTION 6

CONCLUSIONS

The fractional derivative Maxwell model has been found to fit the viscoelastic properties of a type of viscous damper consisting of a piston moving in a highly viscous gel. This damper is used in vibration isolation systems for pipeworks and industrial machines and in seismic isolation systems for structures.

Experiments were conducted for the calibration and verification of the developed model. The model could predict the experimental results with very good accuracy and over a wide range of frequencies.

A SDOF viscodamper oscillator, consisting of a mass, a linear spring and a fractional derivative Maxwell element is used in the representation of an isolation system. The problem of determination of the frequency and damping ratio of the viscodamper oscillator is formulated. The steady-state response of the oscillator is shown to always exist and is derived analytically. Furthermore, the evaluation of the response of the oscillator to general dynamic loading is presented within the context of Fourier analysis.

An equivalent SDOF viscous oscillator is defined whose response is essentially the same as that of the viscodamper isolator. The equivalent oscillator has the combined stiffness of the spring and storage stiffness of the fractional Maxwell element and the damping coefficient of the fractional Maxwell elements. The storage stiffness and damping coefficient are evaluated at the fundamental frequency of the oscillator. The equivalent oscillator is found to predict well the dynamic response of the SDOF viscodamper oscillator when subjected to general dynamic loading.

Numerical procedures for the analysis of the viscodamper oscillator are presented. Most convenient is the analysis in the frequency domain by the DFT approach in combination with FFT algorithms. For this, the complex frequency response function of the oscillator has been derived. For the analysis in the time domain, an algorithm termed "GlFP" is presented.

Finally, shake table tests of a large isolated model structure equipped with a sliding isolation system and enhanced by viscous dampers were conducted. While the test demonstrated the good ability of the dampers to reduce peak displacements, it was also found that they had an undesirable effect on the permanent displacement of the isolation system. The developed numerical analysis procedures in the time domain were employed in the analysis of the tested model and found to predict accurately the recorded response.

SECTION 7

REFERENCES

Abramowitz, M. and Stegun, I.A. (1970). Handbook of Mathematic Functions. Dover Publications, Inc. New York.

Bagley, R.L. and Torvic, P.J. (1983). "Fractional Calculus - A Different Approach to the Analysis of Viscoelastically Damped Structures." AIAA Journal, 21(5), 741-748.

Bird, B., Armstrong, R. and Hassager, O. (1987). Dynamics of Polymeric Liquids. J. Wiley, New York.

Constantinou, M.C., Mokha, A. and Reinhorn, A.M. (1990a). "Study of a Sliding Bearing and Helical Steel Spring Isolation System." J. Structural Engineering, ASCE, to appear.

Constantinou, M.C., Mokha, A. and Reinhorn, A.M. (1990b). "Experimental and Analytical Study of a Combined Sliding Disc Bearing and Helical Steel Spring Isolation System." Report NCEER-90-0019, National Center for Earthquake Engineering Research, Buffalo, NY.

Constantinou, M.C., Mokha, A. and Reinhorn, A.M. (1990c). "Teflon Bearings in Base Isolation II: Modeling." J. Structural Engineering, ASCE, 116(2), 455-474.

Gear, C.W. (1971). "The Automatic Integration of Ordinary Differential Equations." Numerical Mathematics, Communications of ACM, 14(3), 176-190.

Gemant, A. (1936). "A Method of Analyzing Experimental Results Obtained from Elasto-viscous Bodies." Physics, 7, 311-317.

GERB Vibration Control (1986). "Pipework Dampers. Technical Report," Westmont, Illinois.

Higashino, M., Aizawa, S. and Hayamizu, Y. (1988). "The Study of Base Isolation System for Actual Use." Proc. 9th World Conference on Earthquake Engineering, Tokyo, Japan, V705-V710.

Huffmann, G. (1985). "Full Base Isolation for Earthquake Protection by Helical Springs and Viscodampers." Nuclear Engineering and Design, 84, 331-338.

Koh, C.G. and Kelly, J.M. (1990). "Application of Fractional Derivatives to Seismic Analysis of Base-isolated Models." Earthquake Engineering and Structural Dynamics, 19, 229-241.

Oldham, K.B. and Spanier, J. (1974). The Fractional Calculus. Mathematics in Science and Engineering, Vol. III. Academic Press.

Schwahn, K.J., Reinsch, K.H. and Weber, F.M. (1988). "Description of the Features of Viscous Dampers on the Basis of Equivalent Rheological Models, Presented for Pipework Dampers." Proc. Pressure, Vessel and Piping Conference, Seismic Engineering, Vol. 127, American Society of Mechanical Engineers, 477-484.

Veletsos, A.S. and Ventura, C.E. (1985). "Dynamic Analysis of Structures by the DFT Method." J. Structural Engineering, ASCE, 111(2), 2625-2642.

APPENDIX A

EXISTENCE OF STEADY-STATE RESPONSE

We consider the viscodamper oscillator with homogeneous initial conditions and subjected to harmonic loading. The equation of motion is

$$m\ddot{U}(t) + KU(t) + P(t) = F_o \sin\omega t \tag{A.1}$$

$$P(t) + \lambda D^r[P(t)] = C_o \dot{U}(t) \tag{A.2}$$

We apply the method of Laplace transform to find

$$[\lambda s^{2+r} + s^2 + 2\,\xi_d\omega_o s + \lambda\omega_o{}^2 s^r + \omega_o{}^2]\; U(s) = \frac{F_o\omega}{m}\,\frac{1 + \lambda s^r}{s^2+\omega^2} \tag{A.3}$$

where $U(s)$ is the Laplace transform of $U(t)$ and ω_o and ξ_d are given by equations 4-4 and 4-5. In equation A.3 we recognize on the left side the expression in the characteristic equation 4-6. Let the smallest common denominator of fraction r and unity be n(e.g. for r = 0.6, n = 5). Equation A.3 may be written as

$$U(s) = \frac{F_o\omega}{m} \cdot \frac{1 + \lambda s^r}{s^2+\omega^2} \cdot \sum_{j=1}^{J} \frac{A_j}{s^{1/n} - \lambda_j} \tag{A.4}$$

where λ_j are the eigenvalues of the polynominal equation corresponding to equation 4.6 (for r = 0.6, equation 4.8). Furthermore, J is an integer equal to (2 + r)n and A_j are constants). The eigenvalues are derived by the procedure described in Section 4. It should be noted that equation A.4 is identical in form to that studied by Bagley and Torvik, 1983.

The inverse transform is

$$U(t) = L^{-1}[U(s)] = \frac{1}{2\pi i}\int_{\gamma-i\infty}^{\gamma+i\infty} e^{st}\, U(s)\, ds \tag{A.5}$$

Figure A-1 shows the closed contour for the integration. All singularities of function U(s) are to the left of segment 1 of the contour. The radii of contours 2 and 6 are increased indefinitely and segments 3 and 5 are extended indefinitely in the negative real direction. The contribution to the closed loop integral from segments 2 and 6 is zero. Furthermore, in direct similarity to the problem studied by Bagley and Torvik, 1983, the contribution from segment 4 (branch point of function $s^{1/n}$) goes to zero as the radius of the contour goes to zero. For the evaluation of integral A.5 (integral along contour 1) it remains to evaluate the contributions from poles $s = \lambda_j^n$, j = 1 to J, poles $s = \pm i\omega$ and the branch cut of functions $s^{1/n}$ (negative real axis, segments 3 and 5).

$$U(t) = \frac{1}{2\pi i}\int_{\gamma-i\infty}^{\gamma+i\infty} e^{st}U(s)\,ds = -\frac{1}{2\pi i}\int_{3,5} e^{st}U(s)\,ds + \sum_{j=1}^{J} R_j + R_\omega + R_{-\omega} \tag{A.6}$$

where R_j are the contributions from the residues of poles $s = \lambda_j^n$ and $R_{\pm\omega}$ are the contributions from the poles $s = \pm i\omega$. All poles are of first order. By application of the residue theorem we obtain

$$\sum_{j=1}^{J} R_j = \sum_{j=1}^{J} \frac{A_j F_o \omega n \lambda_j^{n-1}(1 + \lambda\lambda_j^{nr})}{\lambda_j^{2n} + \omega^2} \exp(\lambda_j^n t) \tag{A.7}$$

$$R_\omega = \frac{F_o\omega[1+\lambda(i\omega)^r]}{2i\omega m} e^{i\omega t} \sum_{j=1}^{J} \frac{A_j}{(i\omega)^{1/n} - \lambda_j} \tag{A.8}$$

$$R_{-\omega} = \frac{F_o\omega[1+\lambda(-i\omega)^r]}{-2i\omega m} e^{i\omega t} \sum_{j=1}^{J} \frac{A_j}{(-i\omega)^{1/n} - \lambda_j} \tag{A.9}$$

The integral along segments 3 and 5 (branch cut) was evaluated by Bagley and Torvik, 1983

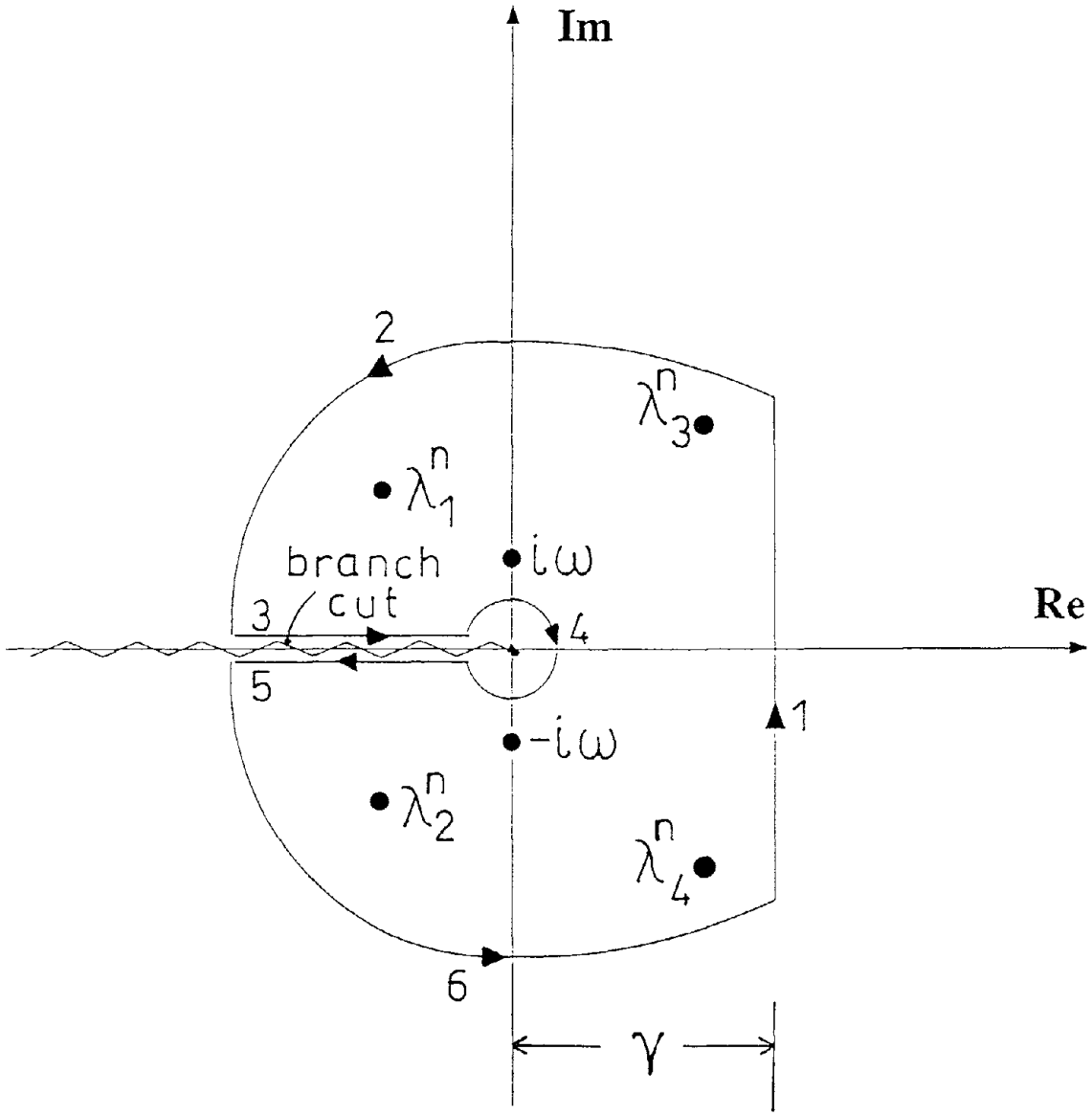

Figure A-1 Contour of Integration in Complex Plane.

$$\frac{1}{2\pi i}\int_{3,5} e^{st}\,U(s)ds = -\frac{1}{\pi}\,\mathrm{Im}\Big\{\int_{o}^{\infty} U(ze^{-i\pi})\,e^{-zt}dz\Big\} \qquad (A.10)$$

where U is given by equation A.4 with s replaced by $ze^{-i\pi}$. Im stands for the imaginary part.

We observe that the response consists of part $R_{\omega} + R_{-\omega}$ which is a sinusoid of frequency ω and two other parts described by equations A.7 and A.10. Steady-state response exists only when these two parts vanish in the limit of large times. The part described by equation A.7 is a sum of exponentially decaying sinusoids provided that λ_j^n appear in complex conjugate pairs. In general, this is the case except in certain cases in which λ_j^n is a real and negative quantity. For example when r = 0.6, n = 5 and J = 13, eigenvalues λ_j are derived from the solution of equation 4-8 and thirteen values of $s = \lambda_j^n$ (n = 5) are obtained. They appear as six conjugate pairs and one negative real quantity. Note that eignevalues λ_j are found in the $s^{1/n}$ or σ (equation 4-7) plane and then transformed to the s plane. The real negative eigenvalue maps on the Riemann surfaces associated with the branch cut in the integration contour (Figure A-1). The residue of this pole does not contribute to the response of the system. Accordingly, the part given by equation A.7 is exponentially decaying with time.

The part given by equation A.10 is easily recognized as one decaying faster than the integral $\int_{o}^{\infty} \exp(-zt)\,dz$ as t tends to infinity. This integral is equal to $-t^{-1}$ for fixed t, so that the integral of equation A.10 is asymptotic to $t^{-(1+a)}$ where $a > 0$. Accordingly, this part also decays with time. Therefore, in the limit of large times only the parts given by equations A.8 and A.9 survive. These parts describe the steady-state response of the system. This response is sinusoidal of frequency ω.

NATIONAL CENTER FOR EARTHQUAKE ENGINEERING RESEARCH
LIST OF TECHNICAL REPORTS

The National Center for Earthquake Engineering Research (NCEER) publishes technical reports on a variety of subjects related to earthquake engineering written by authors funded through NCEER. These reports are available from both NCEER's Publications Department and the National Technical Information Service (NTIS). Requests for reports should be directed to the Publications Department, National Center for Earthquake Engineering Research, State University of New York at Buffalo, Red Jacket Quadrangle, Buffalo, New York 14261. Reports can also be requested through NTIS, 5285 Port Royal Road, Springfield, Virginia 22161. NTIS accession numbers are shown in parenthesis, if available.

NCEER-87-0001 "First-Year Program in Research, Education and Technology Transfer," 3/5/87, (PB88-134275/AS).

NCEER-87-0002 "Experimental Evaluation of Instantaneous Optimal Algorithms for Structural Control," by R.C. Lin, T.T. Soong and A.M. Reinhorn, 4/20/87, (PB88-134341/AS).

NCEER-87-0003 "Experimentation Using the Earthquake Simulation Facilities at University at Buffalo," by A.M. Reinhorn and R.L. Ketter, to be published.

NCEER-87-0004 "The System Characteristics and Performance of a Shaking Table," by J.S. Hwang, K.C. Chang and G.C. Lee, 6/1/87, (PB88-134259/AS). This report is available only through NTIS (see address given above).

NCEER-87-0005 "A Finite Element Formulation for Nonlinear Viscoplastic Material Using a Q Model," by O. Gyebi and G. Dasgupta, 11/2/87, (PB88-213764/AS).

NCEER-87-0006 "Symbolic Manipulation Program (SMP) - Algebraic Codes for Two and Three Dimensional Finite Element Formulations," by X. Lee and G. Dasgupta, 11/9/87, (PB88-219522/AS).

NCEER-87-0007 "Instantaneous Optimal Control Laws for Tall Buildings Under Seismic Excitations," by J.N. Yang, A. Akbarpour and P. Ghaemmaghami, 6/10/87, (PB88-134333/AS).

NCEER-87-0008 "IDARC: Inelastic Damage Analysis of Reinforced Concrete Frame - Shear-Wall Structures," by Y.J. Park, A.M. Reinhorn and S.K. Kunnath, 7/20/87, (PB88-134325/AS).

NCEER-87-0009 "Liquefaction Potential for New York State: A Preliminary Report on Sites in Manhattan and Buffalo," by M. Budhu, V. Vijayakumar, R.F. Giese and L. Baumgras, 8/31/87, (PB88-163704/AS). This report is available only through NTIS (see address given above).

NCEER-87-0010 "Vertical and Torsional Vibration of Foundations in Inhomogeneous Media," by A.S. Veletsos and K.W. Dotson, 6/1/87, (PB88-134291/AS).

NCEER-87-0011 "Seismic Probabilistic Risk Assessment and Seismic Margins Studies for Nuclear Power Plants," by Howard H.M. Hwang, 6/15/87, (PB88-134267/AS).

NCEER-87-0012 "Parametric Studies of Frequency Response of Secondary Systems Under Ground-Acceleration Excitations," by Y. Yong and Y.K. Lin, 6/10/87, (PB88-134309/AS).

NCEER-87-0013 "Frequency Response of Secondary Systems Under Seismic Excitation," by J.A. HoLung, J. Cai and Y.K. Lin, 7/31/87, (PB88-134317/AS).

NCEER-87-0014 "Modelling Earthquake Ground Motions in Seismically Active Regions Using Parametric Time Series Methods," by G.W. Ellis and A.S. Cakmak, 8/25/87, (PB88-134283/AS).

NCEER-87-0015 "Detection and Assessment of Seismic Structural Damage," by E. DiPasquale and A.S. Cakmak, 8/25/87, (PB88-163712/AS).

NCEER-87-0016 "Pipeline Experiment at Parkfield, California," by J. Isenberg and E. Richardson, 9/15/87, (PB88-163720/AS). This report is available only through NTIS (see address given above).

NCEER-87-0017 "Digital Simulation of Seismic Ground Motion," by M. Shinozuka, G. Deodatis and T. Harada, 8/31/87, (PB88-155197/AS). This report is available only through NTIS (see address given above).

NCEER-87-0018 "Practical Considerations for Structural Control: System Uncertainty, System Time Delay and Truncation of Small Control Forces," J.N. Yang and A. Akbarpour, 8/10/87, (PB88-163738/AS).

NCEER-87-0019 "Modal Analysis of Nonclassically Damped Structural Systems Using Canonical Transformation," by J.N. Yang, S. Sarkani and F.X. Long, 9/27/87, (PB88-187851/AS).

NCEER-87-0020 "A Nonstationary Solution in Random Vibration Theory," by J.R. Red-Horse and P.D. Spanos, 11/3/87, (PB88-163746/AS).

NCEER-87-0021 "Horizontal Impedances for Radially Inhomogeneous Viscoelastic Soil Layers," by A.S. Veletsos and K.W. Dotson, 10/15/87, (PB88-150859/AS).

NCEER-87-0022 "Seismic Damage Assessment of Reinforced Concrete Members," by Y.S. Chung, C. Meyer and M. Shinozuka, 10/9/87, (PB88-150867/AS). This report is available only through NTIS (see address given above).

NCEER-87-0023 "Active Structural Control in Civil Engineering," by T.T. Soong, 11/11/87, (PB88-187778/AS).

NCEER-87-0024 Vertical and Torsional Impedances for Radially Inhomogeneous Viscoelastic Soil Layers," by K.W. Dotson and A.S. Veletsos, 12/87, (PB88-187786/AS).

NCEER-87-0025 "Proceedings from the Symposium on Seismic Hazards, Ground Motions, Soil-Liquefaction and Engineering Practice in Eastern North America," October 20-22, 1987, edited by K.H. Jacob, 12/87, (PB88-188115/AS).

NCEER-87-0026 "Report on the Whittier-Narrows, California, Earthquake of October 1, 1987," by J. Pantelic and A. Reinhorn, 11/87, (PB88-187752/AS). This report is available only through NTIS (see address given above).

NCEER-87-0027 "Design of a Modular Program for Transient Nonlinear Analysis of Large 3-D Building Structures," by S. Srivastav and J.F. Abel, 12/30/87, (PB88-187950/AS).

NCEER-87-0028 "Second-Year Program in Research, Education and Technology Transfer," 3/8/88, (PB88-219480/AS).

NCEER-88-0001 "Workshop on Seismic Computer Analysis and Design of Buildings With Interactive Graphics," by W. McGuire, J.F. Abel and C.H. Conley, 1/18/88, (PB88-187760/AS).

NCEER-88-0002 "Optimal Control of Nonlinear Flexible Structures," by J.N. Yang, F.X. Long and D. Wong, 1/22/88, (PB88-213772/AS).

NCEER-88-0003 "Substructuring Techniques in the Time Domain for Primary-Secondary Structural Systems," by G.D. Manolis and G. Juhn, 2/10/88, (PB88-213780/AS).

NCEER-88-0004 "Iterative Seismic Analysis of Primary-Secondary Systems," by A. Singhal, L.D. Lutes and P.D. Spanos, 2/23/88, (PB88-213798/AS).

NCEER-88-0005 "Stochastic Finite Element Expansion for Random Media," by P.D. Spanos and R. Ghanem, 3/14/88, (PB88-213806/AS).

NCEER-88-0006 "Combining Structural Optimization and Structural Control," by F.Y. Cheng and C.P. Pantelides, 1/10/88, (PB88-213814/AS).

NCEER-88-0007 "Seismic Performance Assessment of Code-Designed Structures," by H.H-M. Hwang, J-W. Jaw and H-J. Shau, 3/20/88, (PB88-219423/AS).

NCEER-88-0008 "Reliability Analysis of Code-Designed Structures Under Natural Hazards," by H.H-M. Hwang, H. Ushiba and M. Shinozuka, 2/29/88, (PB88-229471/AS).

NCEER-88-0009 "Seismic Fragility Analysis of Shear Wall Structures," by J-W Jaw and H.H-M. Hwang, 4/30/88, (PB89-102867/AS).

NCEER-88-0010 "Base Isolation of a Multi-Story Building Under a Harmonic Ground Motion - A Comparison of Performances of Various Systems," by F-G Fan, G. Ahmadi and I.G. Tadjbakhsh, 5/18/88, (PB89-122238/AS).

NCEER-88-0011 "Seismic Floor Response Spectra for a Combined System by Green's Functions," by F.M. Lavelle, L.A. Bergman and P.D. Spanos, 5/1/88, (PB89-102875/AS).

NCEER-88-0012 "A New Solution Technique for Randomly Excited Hysteretic Structures," by G.Q. Cai and Y.K. Lin, 5/16/88, (PB89-102883/AS).

NCEER-88-0013 "A Study of Radiation Damping and Soil-Structure Interaction Effects in the Centrifuge," by K. Weissman, supervised by J.H. Prevost, 5/24/88, (PB89-144703/AS).

NCEER-88-0014 "Parameter Identification and Implementation of a Kinematic Plasticity Model for Frictional Soils," by J.H. Prevost and D.V. Griffiths, to be published.

NCEER-88-0015 "Two- and Three- Dimensional Dynamic Finite Element Analyses of the Long Valley Dam," by D.V. Griffiths and J.H. Prevost, 6/17/88, (PB89-144711/AS).

NCEER-88-0016 "Damage Assessment of Reinforced Concrete Structures in Eastern United States," by A.M. Reinhorn, M.J. Seidel, S.K. Kunnath and Y.J. Park, 6/15/88, (PB89-122220/AS).

NCEER-88-0017 "Dynamic Compliance of Vertically Loaded Strip Foundations in Multilayered Viscoelastic Soils," by S. Ahmad and A.S.M. Israil, 6/17/88, (PB89-102891/AS).

NCEER-88-0018 "An Experimental Study of Seismic Structural Response With Added Viscoelastic Dampers," by R.C. Lin, Z. Liang, T.T. Soong and R.H. Zhang, 6/30/88, (PB89-122212/AS).

NCEER-88-0019 "Experimental Investigation of Primary - Secondary System Interaction," by G.D. Manolis, G. Juhn and A.M. Reinhorn, 5/27/88, (PB89-122204/AS).

NCEER-88-0020 "A Response Spectrum Approach For Analysis of Nonclassically Damped Structures," by J.N. Yang, S. Sarkani and F.X. Long, 4/22/88, (PB89-102909/AS).

NCEER-88-0021 "Seismic Interaction of Structures and Soils: Stochastic Approach," by A.S. Veletsos and A.M. Prasad, 7/21/88, (PB89-122196/AS).

NCEER-88-0022 "Identification of the Serviceability Limit State and Detection of Seismic Structural Damage," by E. DiPasquale and A.S. Cakmak, 6/15/88, (PB89-122188/AS).

NCEER-88-0023 "Multi-Hazard Risk Analysis: Case of a Simple Offshore Structure," by B.K. Bhartia and E.H. Vanmarcke, 7/21/88, (PB89-145213/AS).

NCEER-88-0024 "Automated Seismic Design of Reinforced Concrete Buildings," by Y.S. Chung, C. Meyer and M. Shinozuka, 7/5/88, (PB89-122170/AS).

NCEER-88-0025 "Experimental Study of Active Control of MDOF Structures Under Seismic Excitations," by L.L. Chung, R.C. Lin, T.T. Soong and A.M. Reinhorn, 7/10/88, (PB89-122600/AS).

NCEER-88-0026 "Earthquake Simulation Tests of a Low-Rise Metal Structure," by J.S. Hwang, K.C. Chang, G.C. Lee and R.L. Ketter, 8/1/88, (PB89-102917/AS).

NCEER-88-0027 "Systems Study of Urban Response and Reconstruction Due to Catastrophic Earthquakes," by F. Kozin and H.K. Zhou, 9/22/88, (PB90-162348/AS).

NCEER-88-0028 "Seismic Fragility Analysis of Plane Frame Structures," by H.H-M. Hwang and Y.K. Low, 7/31/88, (PB89-131445/AS).

NCEER-88-0029 "Response Analysis of Stochastic Structures," by A. Kardara, C. Bucher and M. Shinozuka, 9/22/88, (PB89-174429/AS).

NCEER-88-0030 "Nonnormal Accelerations Due to Yielding in a Primary Structure," by D.C.K. Chen and L.D. Lutes, 9/19/88, (PB89-131437/AS).

NCEER-88-0031 "Design Approaches for Soil-Structure Interaction," by A.S. Veletsos, A.M. Prasad and Y. Tang, 12/30/88, (PB89-174437/AS).

NCEER-88-0032 "A Re-evaluation of Design Spectra for Seismic Damage Control," by C.J. Turkstra and A.G. Tallin, 11/7/88, (PB89-145221/AS).

NCEER-88-0033 "The Behavior and Design of Noncontact Lap Splices Subjected to Repeated Inelastic Tensile Loading," by V.E. Sagan, P. Gergely and R.N. White, 12/8/88, (PB89-163737/AS).

NCEER-88-0034 "Seismic Response of Pile Foundations," by S.M. Mamoon, P.K. Banerjee and S. Ahmad, 11/1/88, (PB89-145239/AS).

NCEER-88-0035 "Modeling of R/C Building Structures With Flexible Floor Diaphragms (IDARC2)," by A.M. Reinhorn, S.K. Kunnath and N. Panahshahi, 9/7/88, (PB89-207153/AS).

NCEER-88-0036 "Solution of the Dam-Reservoir Interaction Problem Using a Combination of FEM, BEM with Particular Integrals, Modal Analysis, and Substructuring," by C-S. Tsai, G.C. Lee and R.L. Ketter, 12/31/88, (PB89-207146/AS).

NCEER-88-0037 "Optimal Placement of Actuators for Structural Control," by F.Y. Cheng and C.P. Pantelides, 8/15/88, (PB89-162846/AS).

NCEER-88-0038 "Teflon Bearings in Aseismic Base Isolation: Experimental Studies and Mathematical Modeling," by A. Mokha, M.C. Constantinou and A.M. Reinhorn, 12/5/88, (PB89-218457/AS).

NCEER-88-0039 "Seismic Behavior of Flat Slab High-Rise Buildings in the New York City Area," by P. Weidlinger and M. Ettouney, 10/15/88, (PB90-145681/AS).

NCEER-88-0040 "Evaluation of the Earthquake Resistance of Existing Buildings in New York City," by P. Weidlinger and M. Ettouney, 10/15/88, to be published.

NCEER-88-0041 "Small-Scale Modeling Techniques for Reinforced Concrete Structures Subjected to Seismic Loads," by W. Kim, A. El-Attar and R.N. White, 11/22/88, (PB89-189625/AS).

NCEER-88-0042 "Modeling Strong Ground Motion from Multiple Event Earthquakes," by G.W. Ellis and A.S. Cakmak, 10/15/88, (PB89-174445/AS).

NCEER-88-0043 "Nonstationary Models of Seismic Ground Acceleration," by M. Grigoriu, S.E. Ruiz and E. Rosenblueth, 7/15/88, (PB89-189617/AS).

NCEER-88-0044 "SARCF User's Guide: Seismic Analysis of Reinforced Concrete Frames," by Y.S. Chung, C. Meyer and M. Shinozuka, 11/9/88, (PB89-174452/AS).

NCEER-88-0045 "First Expert Panel Meeting on Disaster Research and Planning," edited by J. Pantelic and J. Stoyle, 9/15/88, (PB89-174460/AS).

NCEER-88-0046 "Preliminary Studies of the Effect of Degrading Infill Walls on the Nonlinear Seismic Response of Steel Frames," by C.Z. Chrysostomou, P. Gergely and J.F. Abel, 12/19/88, (PB89-208383/AS).

NCEER-88-0047 "Reinforced Concrete Frame Component Testing Facility - Design, Construction, Instrumentation and Operation," by S.P. Pessiki, C. Conley, T. Bond, P. Gergely and R.N. White, 12/16/88, (PB89-174478/AS).

NCEER-89-0001 "Effects of Protective Cushion and Soil Compliancy on the Response of Equipment Within a Seismically Excited Building," by J.A. HoLung, 2/16/89, (PB89-207179/AS).

NCEER-89-0002 "Statistical Evaluation of Response Modification Factors for Reinforced Concrete Structures," by H.H-M. Hwang and J-W. Jaw, 2/17/89, (PB89-207187/AS).

NCEER-89-0003 "Hysteretic Columns Under Random Excitation," by G-Q. Cai and Y.K. Lin, 1/9/89, (PB89-196513/AS).

NCEER-89-0004 "Experimental Study of 'Elephant Foot Bulge' Instability of Thin-Walled Metal Tanks," by Z-H. Jia and R.L. Ketter, 2/22/89, (PB89-207195/AS).

NCEER-89-0005 "Experiment on Performance of Buried Pipelines Across San Andreas Fault," by J. Isenberg, E. Richardson and T.D. O'Rourke, 3/10/89, (PB89-218440/AS).

NCEER-89-0006 "A Knowledge-Based Approach to Structural Design of Earthquake-Resistant Buildings," by M. Subramani, P. Gergely, C.H. Conley, J.F. Abel and A.H. Zaghw, 1/15/89, (PB89-218465/AS).

NCEER-89-0007 "Liquefaction Hazards and Their Effects on Buried Pipelines," by T.D. O'Rourke and P.A. Lane, 2/1/89, (PB89-218481).

NCEER-89-0008 "Fundamentals of System Identification in Structural Dynamics," by H. Imai, C-B. Yun, O. Maruyama and M. Shinozuka, 1/26/89, (PB89-207211/AS).

NCEER-89-0009 "Effects of the 1985 Michoacan Earthquake on Water Systems and Other Buried Lifelines in Mexico," by A.G. Ayala and M.J. O'Rourke, 3/8/89, (PB89-207229/AS).

NCEER-89-R010 "NCEER Bibliography of Earthquake Education Materials," by K.E.K. Ross, Second Revision, 9/1/89, (PB90-125352/AS).

NCEER-89-0011 "Inelastic Three-Dimensional Response Analysis of Reinforced Concrete Building Structures (IDARC-3D), Part I - Modeling," by S.K. Kunnath and A.M. Reinhorn, 4/17/89, (PB90-114612/AS).

NCEER-89-0012 "Recommended Modifications to ATC-14," by C.D. Poland and J.O. Malley, 4/12/89, (PB90-108648/AS).

NCEER-89-0013 "Repair and Strengthening of Beam-to-Column Connections Subjected to Earthquake Loading," by M. Corazao and A.J. Durrani, 2/28/89, (PB90-109885/AS).

NCEER-89-0014 "Program EXKAL2 for Identification of Structural Dynamic Systems," by O. Maruyama, C-B. Yun, M. Hoshiya and M. Shinozuka, 5/19/89, (PB90-109877/AS).

NCEER-89-0015 "Response of Frames With Bolted Semi-Rigid Connections, Part I - Experimental Study and Analytical Predictions," by P.J. DiCorso, A.M. Reinhorn, J.R. Dickerson, J.B. Radziminski and W.L. Harper, 6/1/89, to be published.

NCEER-89-0016 "ARMA Monte Carlo Simulation in Probabilistic Structural Analysis," by P.D. Spanos and M.P. Mignolet, 7/10/89, (PB90-109893/AS).

NCEER-89-P017 "Preliminary Proceedings from the Conference on Disaster Preparedness - The Place of Earthquake Education in Our Schools," Edited by K.E.K. Ross, 6/23/89.

NCEER-89-0017 "Proceedings from the Conference on Disaster Preparedness - The Place of Earthquake Education in Our Schools," Edited by K.E.K. Ross, 12/31/89, (PB90-207895).

NCEER-89-0018 "Multidimensional Models of Hysteretic Material Behavior for Vibration Analysis of Shape Memory Energy Absorbing Devices, by E.J. Graesser and F.A. Cozzarelli, 6/7/89, (PB90-164146/AS).

NCEER-89-0019 "Nonlinear Dynamic Analysis of Three-Dimensional Base Isolated Structures (3D-BASIS)," by S. Nagarajaiah, A.M. Reinhorn and M.C. Constantinou, 8/3/89, (PB90-161936/AS).

NCEER-89-0020 "Structural Control Considering Time-Rate of Control Forces and Control Rate Constraints," by F.Y. Cheng and C.P. Pantelides, 8/3/89, (PB90-120445/AS).

NCEER-89-0021 "Subsurface Conditions of Memphis and Shelby County," by K.W. Ng, T-S. Chang and H-H.M. Hwang, 7/26/89, (PB90-120437/AS).

NCEER-89-0022 "Seismic Wave Propagation Effects on Straight Jointed Buried Pipelines," by K. Elhmadi and M.J. O'Rourke, 8/24/89, (PB90-162322/AS).

NCEER-89-0023 "Workshop on Serviceability Analysis of Water Delivery Systems," edited by M. Grigoriu, 3/6/89, (PB90-127424/AS).

NCEER-89-0024 "Shaking Table Study of a 1/5 Scale Steel Frame Composed of Tapered Members," by K.C. Chang, J.S. Hwang and G.C. Lee, 9/18/89, (PB90-160169/AS).

NCEER-89-0025 "DYNA1D: A Computer Program for Nonlinear Seismic Site Response Analysis - Technical Documentation," by Jean H. Prevost, 9/14/89, (PB90-161944/AS).

NCEER-89-0026 "1:4 Scale Model Studies of Active Tendon Systems and Active Mass Dampers for Aseismic Protection," by A.M. Reinhorn, T.T. Soong, R.C. Lin, Y.P. Yang, Y. Fukao, H. Abe and M. Nakai, 9/15/89, (PB90-173246/AS).

NCEER-89-0027 "Scattering of Waves by Inclusions in a Nonhomogeneous Elastic Half Space Solved by Boundary Element Methods," by P.K. Hadley, A. Askar and A.S. Cakmak, 6/15/89, (PB90-145699/AS).

NCEER-89-0028 "Statistical Evaluation of Deflection Amplification Factors for Reinforced Concrete Structures," by H.H.M. Hwang, J-W. Jaw and A.L. Ch'ng, 8/31/89, (PB90-164633/AS).

NCEER-89-0029 "Bedrock Accelerations in Memphis Area Due to Large New Madrid Earthquakes," by H.H.M. Hwang, C.H.S. Chen and G. Yu, 11/7/89, (PB90-162330/AS).

NCEER-89-0030 "Seismic Behavior and Response Sensitivity of Secondary Structural Systems," by Y.Q. Chen and T.T. Soong, 10/23/89, (PB90-164658/AS).

NCEER-89-0031 "Random Vibration and Reliability Analysis of Primary-Secondary Structural Systems," by Y. Ibrahim, M. Grigoriu and T.T. Soong, 11/10/89, (PB90-161951/AS).

NCEER-89-0032 "Proceedings from the Second U.S. - Japan Workshop on Liquefaction, Large Ground Deformation and Their Effects on Lifelines, September 26-29, 1989," Edited by T.D. O'Rourke and M. Hamada, 12/1/89, (PB90-209388/AS).

NCEER-89-0033 "Deterministic Model for Seismic Damage Evaluation of Reinforced Concrete Structures," by J.M. Bracci, A.M. Reinhorn, J.B. Mander and S.K. Kunnath, 9/27/89.

NCEER-89-0034 "On the Relation Between Local and Global Damage Indices," by E. DiPasquale and A.S. Cakmak, 8/15/89, (PB90-173865).

NCEER-89-0035 "Cyclic Undrained Behavior of Nonplastic and Low Plasticity Silts," by A.J. Walker and H.E. Stewart, 7/26/89, (PB90-183518/AS).

NCEER-89-0036 "Liquefaction Potential of Surficial Deposits in the City of Buffalo, New York," by M. Budhu, R. Giese and L. Baumgrass, 1/17/89, (PB90-208455/AS).

NCEER-89-0037 "A Determinstic Assessment of Effects of Ground Motion Incoherence," by A.S. Veletsos and Y. Tang, 7/15/89, (PB90-164294/AS).

NCEER-89-0038 "Workshop on Ground Motion Parameters for Seismic Hazard Mapping," July 17-18, 1989, edited by R.V. Whitman, 12/1/89, (PB90-173923/AS).

NCEER-89-0039 "Seismic Effects on Elevated Transit Lines of the New York City Transit Authority," by C.J. Costantino, C.A. Miller and E. Heymsfield, 12/26/89, (PB90-207887/AS).

NCEER-89-0040 "Centrifugal Modeling of Dynamic Soil-Structure Interaction," by K. Weissman, Supervised by J.H. Prevost, 5/10/89, (PB90-207879/AS).

NCEER-89-0041 "Linearized Identification of Buildings With Cores for Seismic Vulnerability Assessment," by I-K. Ho and A.E. Aktan, 11/1/89.

NCEER-90-0001 "Geotechnical and Lifeline Aspects of the October 17, 1989 Loma Prieta Earthquake in San Francisco," by T.D. O'Rourke, H.E. Stewart, F.T. Blackburn and T.S. Dickerman, 1/90, (PB90-208596/AS).

NCEER-90-0002 "Nonnormal Secondary Response Due to Yielding in a Primary Structure," by D.C.K. Chen and L.D. Lutes, 2/28/90.

NCEER-90-0003 "Earthquake Education Materials for Grades K-12," by K.E.K. Ross, 4/16/90.

NCEER-90-0004 "Catalog of Strong Motion Stations in Eastern North America," by R.W. Busby, 4/3/90.

NCEER-90-0005 "NCEER Strong-Motion Data Base: A User Manuel for the GeoBase Release (Version 1.0 for the Sun3)," by P. Friberg and K. Jacob, 3/31/90.

NCEER-90-0006 "Seismic Hazard Along a Crude Oil Pipeline in the Event of an 1811-1812 Type New Madrid Earthquake," by H.H.M. Hwang and C-H.S. Chen, 4/16/90.

NCEER-90-0007 "Site-Specific Response Spectra for Memphis Sheahan Pumping Station," by H.H.M. Hwang and C.S. Lee, 5/15/90.

NCEER-90-0008 "Pilot Study on Seismic Vulnerability of Crude Oil Transmission Systems," by T. Ariman, R. Dobry, M. Grigoriu, F. Kozin, M. O'Rourke, T. O'Rourke and M. Shinozuka, 5/25/90.

NCEER-90-0009 "A Program to Generate Site Dependent Time Histories: EQGEN," by G.W. Ellis, M. Srinivasan and A.S. Cakmak, 1/30/90.

NCEER-90-0010 "Active Isolation for Seismic Protection of Operating Rooms," by M.E. Talbott, Supervised by M. Shinozuka, 6/8/9.

NCEER-90-0011 "Program LINEARID for Identification of Linear Structural Dynamic Systems," by C-B. Yun and M. Shinozuka, 6/25/90.

NCEER-90-0012 "Two-Dimensional Two-Phase Elasto-Plastic Seismic Response of Earth Dams," by A.N. Yiagos, Supervised by J.H. Prevost, 6/20/90.

NCEER-90-0013 "Secondary Systems in Base-Isolated Structures: Experimental Investigation, Stochastic Response and Stochastic Sensitivity," by G.D. Manolis, G. Juhn, M.C. Constantinou and A.M. Reinhorn, 7/1/90.

NCEER-90-0014 "Seismic Behavior of Lightly-Reinforced Concrete Column and Beam-Column Joint Details," by S.P. Pessiki, C.H. Conley, P. Gergely and R.N. White, 8/22/90.

NCEER-90-0015 "Two Hybrid Control Systems for Building Structures Under Strong Earthquakes," by J.N. Yang and A. Danielians, 6/29/90.

NCEER-90-0016 "Instantaneous Optimal Control with Acceleration and Velocity Feedback," by J.N. Yang and Z. Li, 6/29/90.

NCEER-90-0017 "Reconnaissance Report on the Northern Iran Earthquake of June 21, 1990," by M. Mehrain, 10/4/90.

NCEER-90-0018 "Evaluation of Liquefaction Potential in Memphis and Shelby County," by T.S. Chang, P.S. Tang, C.S. Lee and H. Hwang, 8/10/90.

NCEER-90-0019 "Experimental and Analytical Study of a Combined Sliding Disc Bearing and Helical Steel Spring Isolation System," by M.C. Constantinou, A.S. Mokha and A.M. Reinhorn, 10/4/90.

NCEER-90-0020 "Experimental Study and Analytical Prediction of Earthquake Response of a Sliding Isolation System with a Spherical Surface," by A.S. Mokha, M.C. Constantinou and A.M. Reinhorn, 10/11/90.

NCEER-90-0021 "Dynamic Interaction Factors for Floating Pile Groups," by G. Gazetas, K. Fan, A. Kaynia and E. Kausel, 9/10/90.

NCEER-90-0022 "Evaluation of Seismic Damage Indices for Reinforced Concrete Structures," by S. Rodríguez-Gómez and A.S. Cakmak, 9/30/90.

NCEER-90-0023 "Study of Site Response at a Selected Memphis Site," by H. Desai, S. Ahmad, G. Gazetas and M.R. Oh, 10/11/90.

NCEER-90-0024 "A User's Guide to Strongmo: Version 1.0 of NCEER's Strong-Motion Data Access Tool for PCs and Terminals," by P.A. Friberg and C.A.T. Susch, 11/15/90.

NCEER-90-0025 "A Three-Dimensional Analytical Study of Spatial Variability of Seismic Ground Motions," by L-L. Hong and A.H.-S. Ang, 10/30/90.

NCEER-90-0026 "MUMOID User's Guide - A Program for the Identification of Modal Parameters," by S. Rodríguez-Gómez and E. DiPasquale, 9/30/90.

NCEER-90-0027 "SARCF-II User's Guide - Seismic Analysis of Reinforced Concrete Frames," by S. Rodríguez-Gómez, Y.S. Chung and C. Meyer, 9/30/90.

NCEER-90-0028 "Viscous Dampers: Testing, Modeling and Application in Vibration and Seismic Isolation," by N. Makris and M.C. Constantinou, 12/20/90.